

AD-A085 724

LOCKHEED MISSILES AND SPACE CO INC PALO ALTO CA PALO --ETC F/6 4/1
FLUORESCENCE EXPERIMENT AND AURORAL DATA EVALUATION TO IMPROVE --ETC(U)
FEB 79 J B KUMER, T C JAMES DNA001-78-C-0082

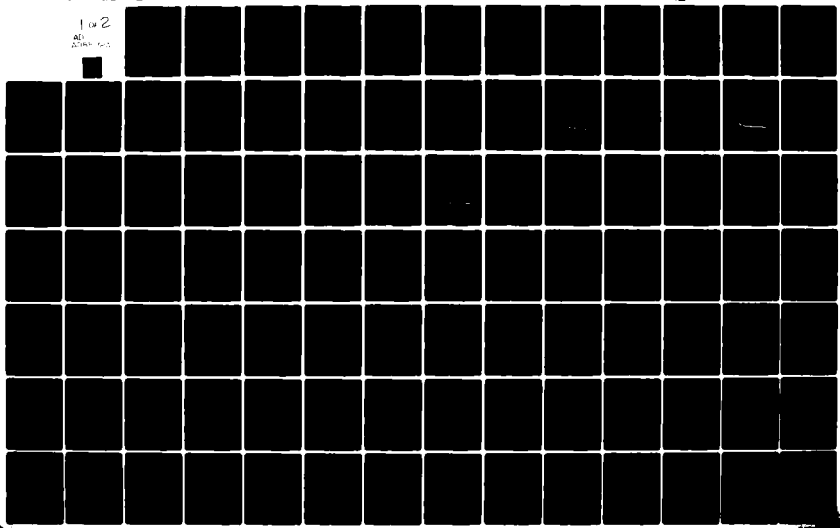
UNCLASSIFIED

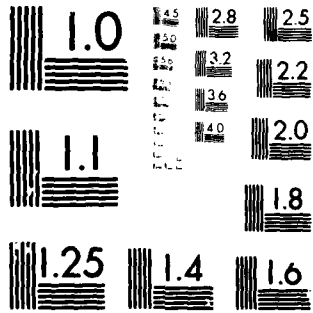
LMSC/D673384

DNA-4906F

NL

1 of 2
AD
2025-10-10





MICROCOPY RESOLUTION TEST CHART
NATIONAL BUREAU OF STANDARDS-1963-A

LEVEL III

AD-E 300 789

12
P.S.

DNA 4906F

ADA 085724

**FLUORESCENCE EXPERIMENT AND AURORAL
DATA EVALUATION TO IMPROVE PREDICTION
OF NUCLEAR ATMOSPHERIC INFRARED
BACKGROUND**

J. B. Kumer

T. C. James

Lockheed Missiles and Space Co., Inc.

3251 Hanover Street

Palo Alto, California 94304

28 February 1979

Final Report for Period 2 February 1978—28 February 1979

CONTRACT No. DNA 001-78-C-0082

APPROVED FOR PUBLIC RELEASE;
DISTRIBUTION UNLIMITED.

THIS WORK SPONSORED BY THE DEFENSE NUCLEAR AGENCY
UNDER RDT&E RMSS CODE B322078484 S99QAXHI00248 H2590D.

FILE COPY

Prepared for

Director

DEFENSE NUCLEAR AGENCY

Washington, D. C. 20305

DTIC
ELECTE
S JUN 20 1980 D
D

Destroy this report when it is no longer
needed. Do not return to sender.

PLEASE NOTIFY THE DEFENSE NUCLEAR AGENCY,
ATTN: STTI, WASHINGTON, D.C. 20305, IF
YOUR ADDRESS IS INCORRECT, IF YOU WISH TO
BE DELETED FROM THE DISTRIBUTION LIST, OR
IF THE ADDRESSEE IS NO LONGER EMPLOYED BY
YOUR ORGANIZATION.



UNCLASSIFIED

SECURITY CLASSIFICATION OF THIS PAGE (When Data Entered)

REPORT DOCUMENTATION PAGE		READ INSTRUCTIONS BEFORE COMPLETING FORM
1. REPORT NUMBER DNA 4906F ✓	2. GOVT ACCESSION NO. AD-4085 724	3. RECIPIENT'S CATALOG NUMBER
4. TITLE (and Subtitle) FLUORESCENCE EXPERIMENT AND AURORAL DATA EVALUATION TO IMPROVE PREDICTION OF NUCLEAR ATMOSPHERIC INFRARED BACKGROUND		5. TYPE OF REPORT & PERIOD COVERED Final Report for Period 2 Feb 78—28 Feb 79
		6. PERFORMING ORG. REPORT NUMBER LMSC D673384 ✓
7. AUTHOR(s) J. B. Kumer T. C. James		8. CONTRACT OR GRANT NUMBER(s) DNA 001-78-C-0082 سون
9. PERFORMING ORGANIZATION NAME AND ADDRESS Lockheed Missiles and Space Co., Inc. ✓ 3251 Hanover Street Palo Alto, California 94304		10. PROGRAM ELEMENT, PROJECT, TASK AREA & WORK UNIT NUMBERS Subtask S99QAXHI002-48
11. CONTROLLING OFFICE NAME AND ADDRESS Director Defense Nuclear Agency Washington, D.C. 20305		12. REPORT DATE 28 February 1979
		13. NUMBER OF PAGES 116
14. MONITORING AGENCY NAME & ADDRESS (if different from Controlling Office)		15. SECURITY CLASS (of this report) UNCLASSIFIED
		15a. DECLASSIFICATION/DOWNGRADING SCHEDULE
16. DISTRIBUTION STATEMENT (of this Report) Approved for public release; distribution unlimited.		
17. DISTRIBUTION STATEMENT (of the abstract entered in Block 20, if different from Report)		
18. SUPPLEMENTARY NOTES This work sponsored by the Defense Nuclear Agency under RDT&E RMSS Code B322078464 S99QAXHI00248 H2590D.		
19. KEY WORDS (Continue on reverse side if necessary and identify by block number) Aurora, NO ⁺ Vibrationally Excited in Aurora, CO ₂ 2.7 to 4.3 μm Fluorescence, 4.3 μm Aurora, 4.55 μm Aurora, N ₂ O, ¹⁴ N ¹⁵ N, CO, Nuclear Bomblight Fluores- cence, Auroral Simulation of Nuclear Effects, OH Airglow, OH Mechanism for CO ₂ 4.3 μm Airglow, Optical Systems, Infrared		
20. ABSTRACT (Continue on reverse side if necessary and identify by block number) The report documents coordinated <u>laboratory</u> and <u>data evaluation</u> research efforts which are relevant to the DNA program for developing capability to predict nuclear enhanced atmospheric infrared background radiance. The labo- ratory effort involves the use of a dye laser pumped LiNbO ₃ optical paramet- ric oscillator in order to produce a tunable source of intense 2.7 μm light for the purpose of laboratory simulation of the infrared effects of solar or nuclear illumination of the atmosphere. The source is used to excite the		

DD FORM 1473 1 JAN 73 EDITION OF 1 NOV 65 IS OBSOLETE

UNCLASSIFIED

SECURITY CLASSIFICATION OF THIS PAGE (When Data Entered)

UNCLASSIFIED

SECURITY CLASSIFICATION OF THIS PAGE(When Data Entered)

20. ABSTRACT (Continued)

specie $\text{CO}_2(101)$ which can re-radiate at $2.7 \mu\text{m}$ via $101 \rightarrow 000$ or at $4.3 \mu\text{m}$ via $101 \rightarrow 100$, the latter process is predicted to be a major nuclear effect at $4.3 \mu\text{m}$ under certain conditions since theoretically it is predicted to occur more often than the former by ratio 20:1. A primary purpose of our laboratory effort was to confirm this prediction, our initial results place a lower limit of 10:1 on the branching ratio. This low precision result can be enhanced by utilizing simple techniques that were not within the scope of the initial effort, namely by the use of (1) well documented techniques for improving laser frequency stability, (2) a cooled $2.7 \mu\text{m}$ filter mounted in the detector dewar, (3) a multiple pass fluorescence cell, and (4) faster electronics for recording the $2.7 \mu\text{m}$ signal. Implementation of these techniques should improve the precision of the measurement by more than 2 orders of magnitude. Additionally, the initial effort has demonstrated the applicability of the laser source and peripheral vacuum and electronics equipment for the high precision measurements of quenching & vibration transfer rate coefficients. In this effort a precision rate for the quenching of $\text{CO}_2(v_3)$ by Argon was determined as was a rate for rapid resonance vibration transfer between the naturally occurring isotopic species of CO_2 and N_2 .

The data evaluation project included two tasks. First, to improve our existing model for auroral zenith spectral radiance to include N_2O and CO in addition to CO_2 and to exercise the improved model against rocket borne CVF spectrometer data in the 4.5 to $4.6 \mu\text{m}$ region that were obtained in auroral conditions on 12 March 1975.

Highlights of the study were as follows, (i) prompt auroral N_2O and/or CO emissions might explain in part the data near $4.5 - 4.6 \mu\text{m}$ provided that severe constraints concerning the observability of the ambient radiance of these species can be satisfied, (ii) spectral radiance data near $4.42 \mu\text{m}$ cannot be explained via CO_2 , N_2O , or CO emission, (iii) potential mechanisms for prompt auroral N_2O and/or CO emission include (1) $\text{N}_2(\text{A}) + \text{O}_2 \rightarrow \text{N}_2\text{O}(\text{OO1}) + \text{O}$, and (2) $\text{NO}^+(v) + \left\{ \begin{array}{l} \text{N}_2\text{O} \\ \text{CO} \end{array} \right\} \rightarrow \text{NO}^+(v-1) + \left\{ \begin{array}{l} \text{N}_2\text{O}(\text{OO1}) \\ \text{CO}(v=1) \end{array} \right\}$; but these are not exclusive, (iv) the $4.3 \mu\text{m}$ data taken on 12 March 1975 are consistent with our model for CO_2 emission.

To achieve a better understanding of the 12 March 1975 CVF data in the 4.4 to $4.7 \mu\text{m}$ region it will be necessary to (1) examine the spectral data obtained 12 March 1975 in more detail, (2) examine data from related experiments, and (3) include NO^+ in the spectral model.

The second data evaluation task was to subject absorption data obtained in a prior laboratory fluorescence experiment which used a chopped blackbody $2.7 \mu\text{m}$ source to a detailed analysis in order to resolve apparent inconsistencies that a previous, simplified analysis of these data had suggested. The detailed analysis included the effects of detailed radiation transport, wall reflectivity, temperature difference between the fluorescence and absorption cell, spatial diffusion of excitation within the fluorescence cell, and finally, atmospheric absorption on exposed optical paths adjoining the system components.

UNCLASSIFIED

SECURITY CLASSIFICATION OF THIS PAGE(When Data Entered)

TABLE OF CONTENTS

SECTION	PAGE NO.
1. INTRODUCTION	3
1.1 The Fluorescence Experiment	3
1.2 The Data Evaluation Effort	6
2 THE FLOURESCENCE MEASUREMENTS	9
2.1 Laser System Description	9
2.2 Fluorescence at 4.3 μm	17
2.2.1 Background Characterization at 4.3 μm	17
2.2.2 Fluorescence Analysis, 1 Torr CO_2 , 300 Torr Argon	20
2.2.3 Side Looking Geometry	24
2.2.4 Analysis for 0.03 Torr CO_2 and 50 Torr A	28
2.2.5 Analysis for 0.3 Torr CO_2 and N_2 and 50 Torr Argon	31
2.3 Preliminary Measurement the 101-100 and 101-000 Branching Ratio	39
3 DATA EVALUATION	53
3.1 Field Data Evaluation	53
3.1.1 Motivating Data	53
3.1.2 Approach	58
3.1.3 Excitation Mechanisms	67
3.1.4 Results	71
3.1.5 Conclusions and Recommendations	82
3.2 Laboratory Data	87
3.2.1 Introduction	87

SECTION	PAGE
3.2.2 Detailed Radiation Transport Calculation	91
3.2.3 Other Effects	97
3.2.4 Conclusions	102
4 CONCLUSIONS AND RECOMMENDATIONS	103
4.1 The Laboratory Effort	103
4.2 The Data Evaluation Effort	105
5 REFERENCES	109

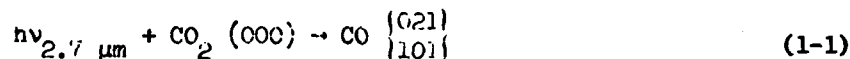
Accession For	
NTIS GRA&I	<input checked="" type="checkbox"/>
DDC TAB	<input type="checkbox"/>
Unannounced	<input type="checkbox"/>
Justification _____	
By _____	
Distribution/ _____	
Availability Codes	
Dist.	Avail and/or special
A	

1.0 INTRODUCTION

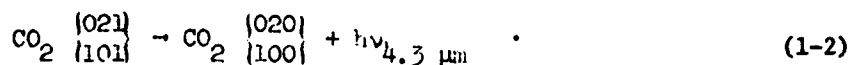
This report documents our coordinated laboratory and data evaluation research efforts which are relevant to the DNA program for developing capability to predict nuclear enhanced atmospheric infrared background radiance.

1.1 The Fluorescence Experiment

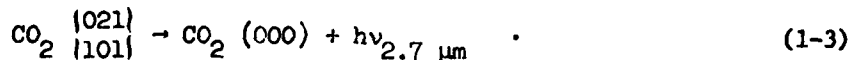
The laboratory effort is aimed at achieving confirmation of the CO₂ 2.7 to 4.3μm pumping mechanism. The mechanism has been predicted theoretically by James and Kumer (1973a). The mechanism involves excitation via CO₂ absorption of 2.7μm radiation



followed by fluorescence



The CO₂ can also decay and emit 2.7 μm radiation via

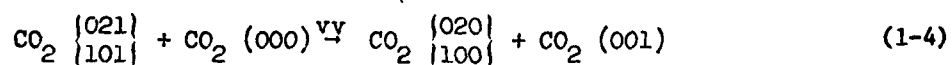


James and Kumer (1973a) theoretically predict that the radiative decay of CO₂ CO₂ $\begin{matrix} \{021\} \\ \{101\} \end{matrix}$ is approximately 95% likely to occur by fluorescent emission of 4.3μm radiation via process (2) and about 5% likely to occur by re-emission of 2.7μm radiation via process (3). The mechanism is theoretically predicted to dominate the formation of the 4.3μm earthlimb near the tangent altitude 80 km.

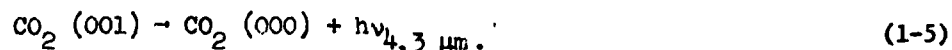
The mechanism is also predicted to contribute to major brightening of the 4.3μm earthlimb at points far removed from a nuclear detonation for long time periods

(=100 sec.) under certain conditions. These nuclear implications were first addressed by James and Kumer (1973b) and were reviewed at the Falmouth, Mass., DNA IR data review meeting by Kumer (1977). The James and Kumer theoretical prediction that the probability is ~95% that the CO₂ levels 101 and 021 should decay by emission of 4.3 rather than 2.7μm radiation is an essential element of the nuclear mechanism. There is a second potential nuclear effect in which the CO₂ branching ratio for emission to 4.3 rather than 2.7μm from the states CO₂ $\begin{Bmatrix} 021 \\ 101 \end{Bmatrix}$ plays a major role. Namely these CO₂ species have been mentioned as potential candidates for the upper state of a possible long lived 2.7μm auroral emission which has been noted in the ICECAP data by Mitchell (1977). If there is indeed a long lived component of 2.7μm auroral emission, then it would have profound implications for the nuclear case. Since the CO₂ 2.7 to 4.3μm pumping mechanism may impact on both 4.3μm and 2.7μm nuclear interference it is essential to obtain laboratory confirmation.

A major complication in achieving a laboratory confirmation of direct CO₂ 2.7 to 4.3μm fluorescence via processes (1-1) and (1-2) and in measuring the branching ratios for 4.3μm emission by process (1-2) compared to 2.7μm emission by process (1-3) is the existence of a competitive mechanism which indirectly produces 4.3μm fluorescence, namely



followed by



This mechanism is not important at high altitudes in the atmosphere where the low CO₂ number densities favor processes (1-2) and (1-3). However, the

mechanism does impose severe restrictions on performance of laboratory studies of processes (1-2) and (1-3). For example, the use of a chopped black body 2.7 μ m source to study processes (1-2) and (1-3) has been shown impractical since this source is not intense enough to produce a detectable signal for CO₂ partial pressures low enough so that the processes (1-2) and (1-3) are competitive with the process (1-4).

In this report we document our initial efforts to study the processes (1-2), (1-3) and (1-4) by the use of a Chromatix CMX-4 and Infrared Accessroy CMX-4/IR-V laser system which is tuneable in the 2.7 μ m region and which provides a 2.7 μ m source intense enough so that CO₂ partial pressures can be reduced to the point where the processes (1-2) and (1-3) are competitive with (1-4).

Our initial effort has shown the branching ratio for process (1-2) rather than (1-3) is greater than or equal to approximately 10:1. This low precision lower limiting result is not completely satisfactory, however the precision can be vastly improved by utilizing a number of simple techniques that were not in the scope of our initial effort, namely the use of (1) well documented techniques for improving laser frequency stability, (2) a cooled 2.3 μ m filter mounted in the detector dewar, (3) a multiple pass fluorescence cell, and (4) faster electronics for recording the 2.7 μ m signal.

Additionally, the initial effort has demonstrated the applicability of the laser source and peripheral vacuum and electronics equipment for the high precision measurements of quenching vibration transfer rate coefficients. In this effort a precision Argon quenching rate was determined as was a rate for rapid resonance vibration transfer between the naturally occurring isotopic species of CO₂ and N₂.

1.2 THE DATA EVALUATION EFFORT

The data evaluation effort included two tasks, (1) the evaluation of auroral zenith radiance data in the 4.5 to 4.6 μ m region (Stair, 1977) that were obtained by a rocket mounted CVF spectrometer on 3/12/75, and (2) a detailed evaluation of laboratory data obtained in a previous effort (Kumer and James, 1977) which utilized a chopped black body 2.7 μ m source and attempted to utilize a CO₂ absorption cell to discriminate the weakly self absorbed direct 4.3 μ m fluorescence formed by process (1-2) from the strongly self absorbed indirect 4.3 μ m fluorescence that is formed by processes (1-4) and (1-5).

FIELD DATA EVALUATION: The 4.5 to 4.6 μ m spectral region may become important for some potential systems applications and the apparent presence of an auroral signal in this spectral region indicates a requirement to identify a mechanism or mechanisms in order to facilitate extrapolation to the nuclear case. Our previous model (Kumer and James, 1977) for auroral zenith spectral radiance near 4.3 μ m included just CO₂ as the emitter and, therefore, predicts essentially no auroral signal in the 4.5 to 4.6 μ m region. In this effort we attempted to explain the 4.5 to 4.6 μ m data by the inclusion of N₂O and CO into our spectral model.

Highlights of the study were as follows:

- o Prompt N₂O and/or CO emissions might explain in part the data near 4.5 - 4.6 μ m provided that severe constraints concerning the observability of the ambient radiance of these species can be satisfied.

- o Spectral radiance data near $4.42\mu\text{m}$ cannot be explained via CO_2 , N_2O or CO emission
- o Potential mechanisms for prompt auroral N_2O and/or CO emission include (1) $\text{N}_2(\text{A}) + \text{O}_2 \rightarrow \text{N}_2\text{O}(\text{O}01) + \text{O}$ and (2) $\text{NO}^+(\text{v}) + \left\{ \begin{array}{l} \text{N}_2\text{O} \\ \text{CO} \end{array} \right\} \rightarrow \text{NO}^+(\text{v}-1) + \left\{ \begin{array}{l} \text{N}_2\text{O}(\text{O}01) \\ \text{CO}(\text{v}=1) \end{array} \right\}$; but these are not exclusive.
- o The $4.3\mu\text{m}$ data taken on 3-12-75 are consistent with our airglow and auroral models for CO_2 emission.

To achieve a better understanding of the 3/12/75 CVF data in the 4.4 to $4.7\mu\text{m}$ region it will be necessary to (1) examine the spectral data obtained 3/12/75 in more detail, (2) examine data from related experiments (HIRIS and SPIRE for example) and, (3) include NO^+ in the spectral model.

LABORATORY DATA EVALUATION: In a previous laboratory effort which used a chopped black body $2.7\mu\text{m}$ source (James and Kumer, 1977), a CO_2 absorption cell was employed in an attempt to distinguish weakly self absorbed direct $4.3\mu\text{m}$ fluorescence from the strongly self absorbed indirect $4.3\mu\text{m}$ fluorescence. The scope of the effort permitted just a preliminary evaluation of these data which assumed a single absorption and reemission for each photon and which assumed black walls for the fluorescence and absorption cells. The results of this analysis were not consistent with our independent analysis of the behaviour of these data as a function of source chopper frequency, and were also not consistent with pertinent data reported by other authors (Finzi and Moore, 1975).

Our purpose then was to subject these absorption data to more detailed scrutiny in an attempt to resolve the apparent inconsistencies. To this end we quantitatively examined the effects of detailed radiation transport, wall reflectivity,

temperature difference between the fluorescence and absorption cell, spatial diffusion of excitation within the fluorescence cell, and finally, atmospheric absorption on exposed optical paths adjoining the system components.

Taken individually each of these effects nudged the interpretation of the absorption data towards consistency, however, the sum of the effects is still not sufficient to resolve the inconsistency. Additionally, the absorption measurements are also inconsistent with our most recent laboratory data obtained with the 2.7 μ m laser source. We can only conclude that although we've quantitatively tested every effect that was obvious to us, there is still some key effect, perhaps geometric, that needs to be accounted for to resolve the apparent inconsistency of the absorption data.

2.0 THE FLUORESCENCE MEASUREMENTS

The laboratory effort proceeded in a logical order of increasingly sophisticated tasks. It began with the establishment and implementation of procedures for tuning the 2.7 μm laser system output on to absorbing CO_2 lines, this task is discussed in Section 2.1. The next step was to set up and use equipment to record the 4.3 μm fluorescence data, and to sensibly interpret these data, this effort is described in Section 2.2. The final and most sophisticated task involved setting up, testing out, calibrating, and utilizing equipment to simultaneously record the laser pumped CO_2 emission at both 2.7 and 4.3 μm , and to extract the branching ratio for emission at 4.3 μm relative to 2.7 μm from these data, this final effort is described in Section 2.3.

2.1 Laser System Description

The basic characteristics of our laser system are summarized in Figure 2-1a. The laser consists of a Chromatix CMX-4 Flash lamp pumped dye laser plus an optical parametric oscillator consisting of a LiNbO_3 crystal in a temperature regulated oven. The visible output of the dye laser is dependent on the particular dye selected. For a particular dye, the output is tuned over the allowable spectral interval for that dye by the rotation of a birefringent filter placed between two polarizers. The resulting output has a total bandwidth of about 3 cm^{-1} . This output can be further narrowed by means of etalons which are placed within the laser cavity, the particular etalon desired being placed in position by rotation of a filter wheel. With a low finesse etalon in place, the output can be narrowed to 0.25 to 0.35 cm^{-1} , and with a high finesse etalon in place the output can be narrowed to 0.1 to 0.15 cm^{-1} .

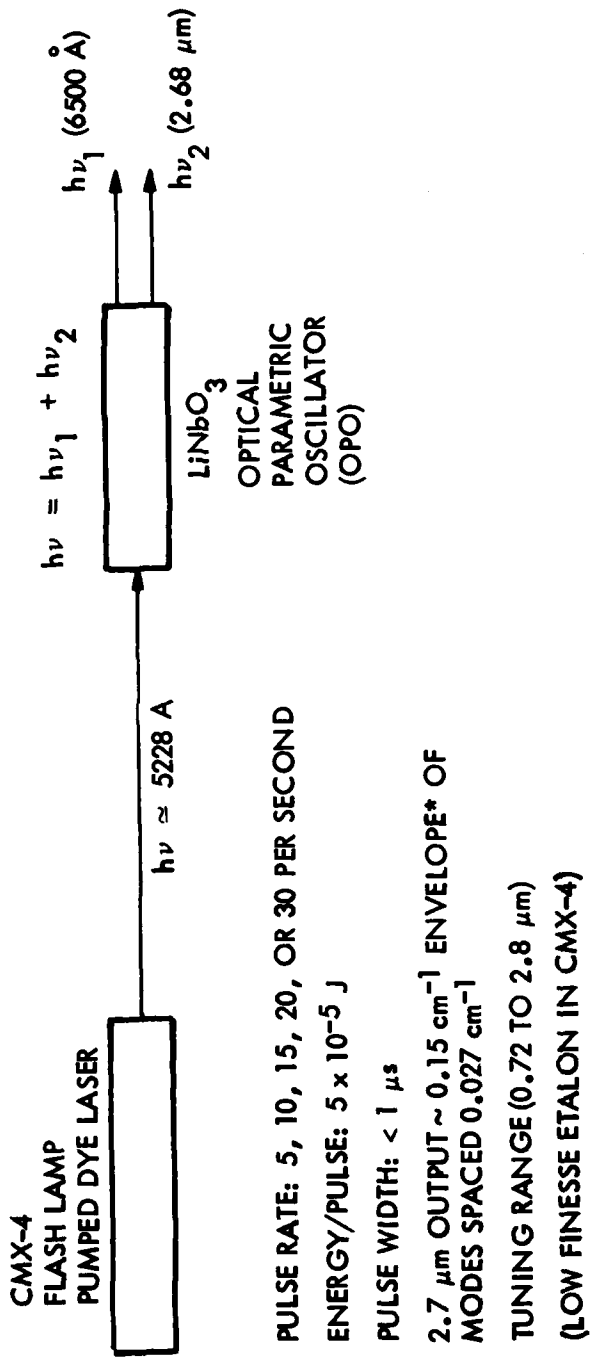


Fig. 2-1a Basic Laser System and Characteristics

The output from the CMX-4 laser is then passed through the Optical Parametric Oscillator (OPO) with the result that the visible beam is split into two infrared beams which satisfy the energy conservation equation $\omega_p = \omega_s + \omega_i$ where ω_p is the visible pump frequency and ω_s and ω_i are the signal and idler frequencies (which are the shorter and longer wavelength infrared beams respectively). Tuning is accomplished by varying the temperature of the oven containing the LiNbO_3 crystal. Figure 2-1b shows examples of the variation of the idler wavelength vs. the visible pump wavelength for two different temperatures. Our experiments were done by selecting a visible wavelength and oven temperature which produced infrared output near the R(18) line of the 101-000 band of CO_2 . The infrared output wavelength was determined by means of a small Jarrell-Ash monochromator.

Our experiments were most successful using the low finesse etalon in the CMX-4. Corresponding to the 0.3 cm^{-1} envelope of visible output, the output at 2.68 microns was calculated to be about 0.15 cm^{-1} by using the information contained in the tuning curves (Figures 2-1b). From the spacing of the cavity mirrors in the OPO and the refractive index of the LiNbO_3 crystal, it can be calculated that the infrared output at $2.7 \mu\text{m}$ consists of modes with a spacing of 0.027 cm^{-1} . Thus, under the conditions of our experiments, the infrared output consisted of something like 5 or 6 modes. In order to observe fluorescence, it is necessary to place these individual modes on a CO_2 absorption line. This can be done by slight changes in the OPO mirror spacing which will shift the mode pattern. Changing the mirror spacing by one-half of the wavelength results in a shift of the pattern by one mode spacing. The method we have used to tune the infrared output onto a CO_2 line will be discussed following a general

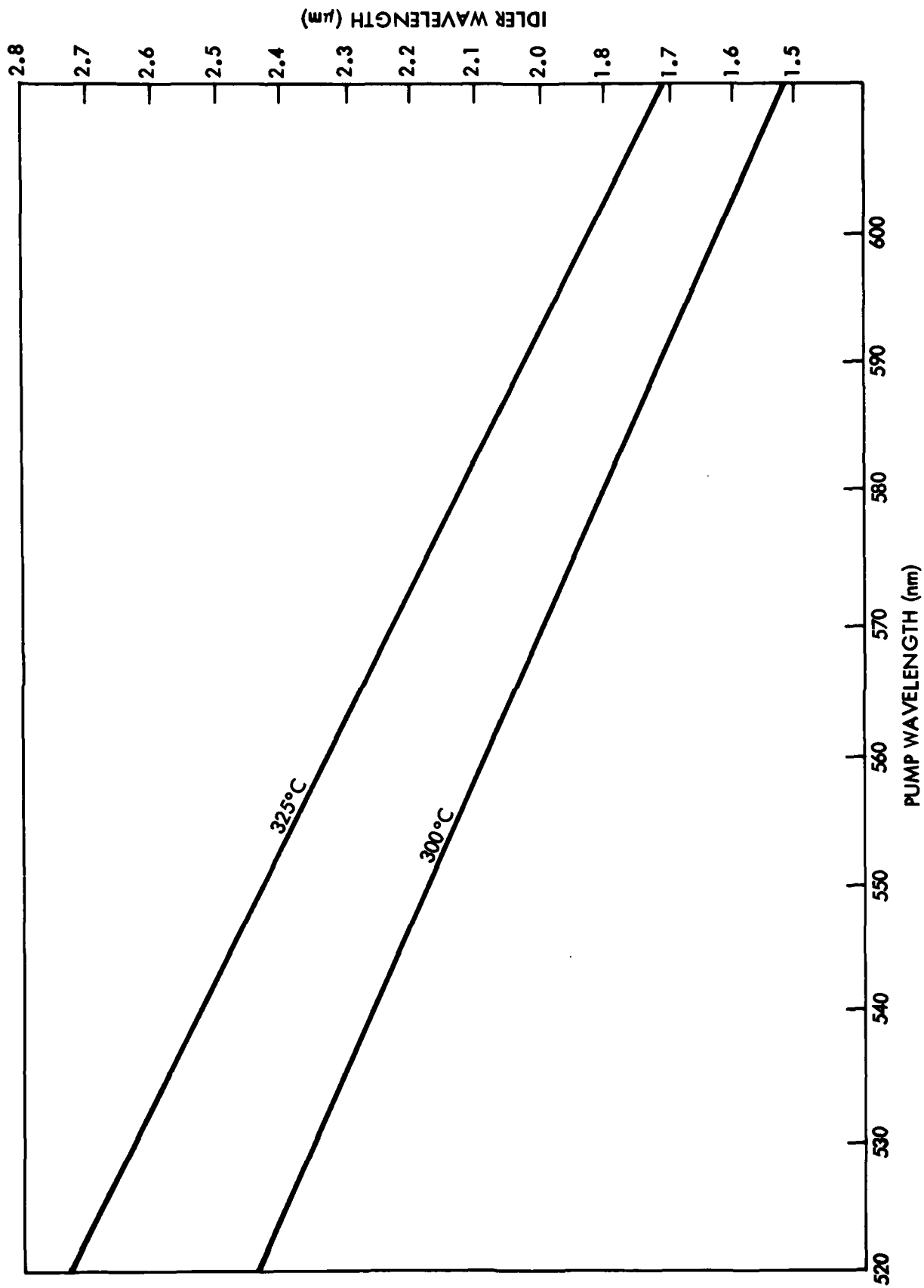


Fig. 2-lb Variation of Infrared Wavelength vs. Pump Wavelength for Different OP0 Temperatures

description of the experimental setup which we used to initially observe the fluorescence at $4.3 \mu\text{m}$.

In our initial attempts to observe the fluorescence at $4.3 \mu\text{m}$, we used the same geometrical arrangement which had been successful in our earlier studies using a blackbody source, namely the exciting beam directed along the axis of a cylindrical fluorescence cell and the detector for $4.3 \mu\text{m}$ radiation also viewing along this direction. This is shown in Figure 2-2. We also chose a CO_2 pressure of 1 torr as we had been successful in detecting $4.3 \mu\text{m}$ fluorescence at this pressure in our earlier studies. In order to be sure of obtaining a signal we used a considerably higher Argon pressure in the absorption cell. This was done so as to broaden the CO_2 absorption lines so that if the envelope of infrared frequencies was centered on an absorption line that we could be assured that an individual mode would fall within the absorption line profile. From the pressure broadening coefficient for $\text{CO}_2 + \text{Ar}$ the full width of the line at half maximum intensity is of the order of 0.04 cm^{-1} at 300 torr of Argon. Thus this pressure assured us that some of the individual modes would fall within the absorption profile.

The use of such a large Argon pressure results in fairly rapid quenching of the $4.3 \mu\text{m}$ fluorescent signal so that it was necessary to be able to measure the signal on a short time scale. At 300 torr of Argon the $4.3 \mu\text{m}$ fluorescent signal can be expected to have a lifetime of the order of 65 microseconds. The observed signal from an InSb detector was passed through a pre-amplifier and amplifier which had a time constant of the order of 10 μsec . This signal was then fed into a Hewlett-Packard Model 5421A signal averager which had the capability of sampling the input signal in 10 μsec intervals. Actual tuning

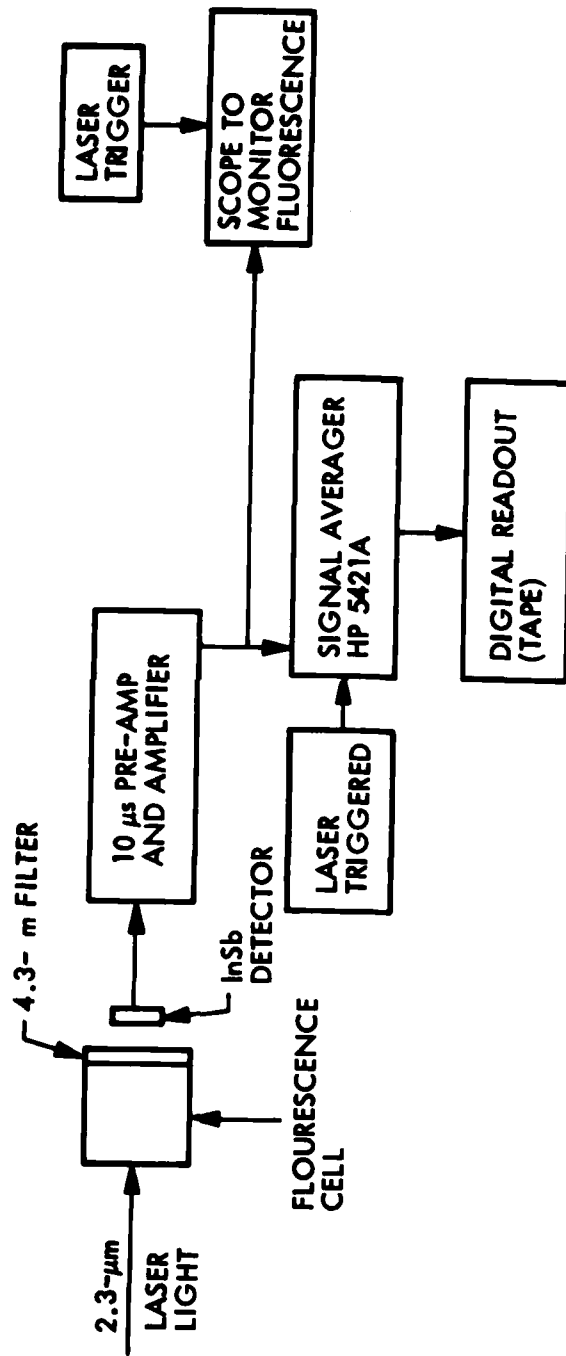


Fig. 2-2 Geometry & Electronics for Initial 4.3 μm Fluorescence Measurements

of the infrared output from the OPO onto a CO_2 absorption line was done by monitoring the output from the pre-amplifier and amplifier on an oscilloscope as the visible wavelength into the OPO was varied.

Although initially we had a number of difficulties in observing and maintaining a good fluorescence signal at $4.3 \mu\text{m}$, improvements in the Chromatix system which resulted from replacing certain faulty components plus experience gained in operation of the system resulted in acquiring data on the signal averager which had excellent signal to noise, even though the system was still erratic on a pulse to pulse basis. The analysis of this data obtained with axial viewing geometry as shown on Figure 2-2 is described in the following section along with the analysis of additional $4.3 \mu\text{m}$ data which were obtained via side viewing geometry.

In the process of working with the laser we became more adept at acquiring and maintaining a fluorescent signal. Our procedure is to take the 3 cm^{-1} broadband output of the CMX-4 visible laser without the etalons in place and adjust that wavelength so that for the operating temperature of the OPO, the infrared output of the OPO is centered near the line R(18) of the 101-000 band of CO_2 . Once this has been fixed, the low finesse etalon is put in place in the CMX-4. Since this narrows the output in the infrared to about 0.15 cm^{-1} , additional tuning is necessary to place this infrared output on a CO_2 line since the CO_2 lines are separated by about 1.6 cm^{-1} . This tuning is accomplished by tilting the etalon which results in a scan of the visible output across the broad 3 cm^{-1} envelope with a resultant change in the infrared wavelengths.

By observing the output from the InSb detector on an oscilloscope, we determine when the infrared output is coincident with a CO₂ absorption line by observing fluorescent pulses. Additional improvements in the signal could be made by slightly tilting the LiNbO₃ crystal which has been shown by Hordvik and Sackett to result in a smoothing out of the distribution of the output between the various modes. Slightly tilting one of the OPO cavity mirrors results in slight changes in the mirror spacings which produced shifts in the mode pattern. By this process of making minor adjustments we found that we could improve the magnitude and stability of the fluorescent pulses.

We have found that after several days of use, the stability of the system decreases considerably which is presumably due to the deterioration of the Dye over a period of time. Failure to adequately consider this was the cause of some of our initial difficulties with the operation of the system. We still have problems in that the fluorescence is not stable on a pulse to pulse basis. Some of this may be due to mechanical vibrations and the fact that individual modes are unstable in frequency and/or due to shifts in the output between various modes so that the amount of energy going into a particular mode which is coincident with a CO₂ line is varying from pulse to pulse. Steps which we might take to improve this stability are described later in this report.

2.2 Fluorescence at 4.3 μm

2.2.1 Background Characterization at 4.3 μm

There are sources of background signal that need to be characterized in order to extract the fluorescence signal from the data. These backgrounds are shown on Figure 2-3. The background labelled beam blocked is obtained by blocking the laser beam and then making a 1000 pulse run. The run is performed with the detector - preamp - amplifier - HP 5421A Signal Averager configuration functioning as shown on Fig. 2-1 and triggered by the laser electronics but there is no laser related light allowed to fall on the detector. In this case the electronics are seen to produce what might be thought of as a "DC offset" as shown by the background curve labelled "beam blocked" on Fig. 2-3. This background curve may be the result of random noise in the electronics, background photon fluctuations on the detector, or perhaps room lights. Its level is found to be slightly dependent on the amplifier gain setting. Our analysis was restricted to data obtained with the gain set to 100, the curve "beam blocked" on Fig. 2-3 was obtained at this setting.

Note that the number of signal averager units in the first bin, 0 to 10 μsec , is depressed with respect to that in subsequent bins. This seems a consistent feature which is independent of whether or not the beam is blocked and whether or not there is fluorescing CO_2 in the cell. To avoid complications we excluded data in the first bin from our analysis in all cases.

Also shown on Figure 2-3 are two curves labeled "preprocessed empty cell."

These are the results of runs for which the fluorescence cell is evacuated and for which the laser beam enters the cell unobstructed. The runs differ in that a larger fraction of the laser beam is subtended by the detector in one case than in the other, this is done by slightly tilting or offsetting the detector

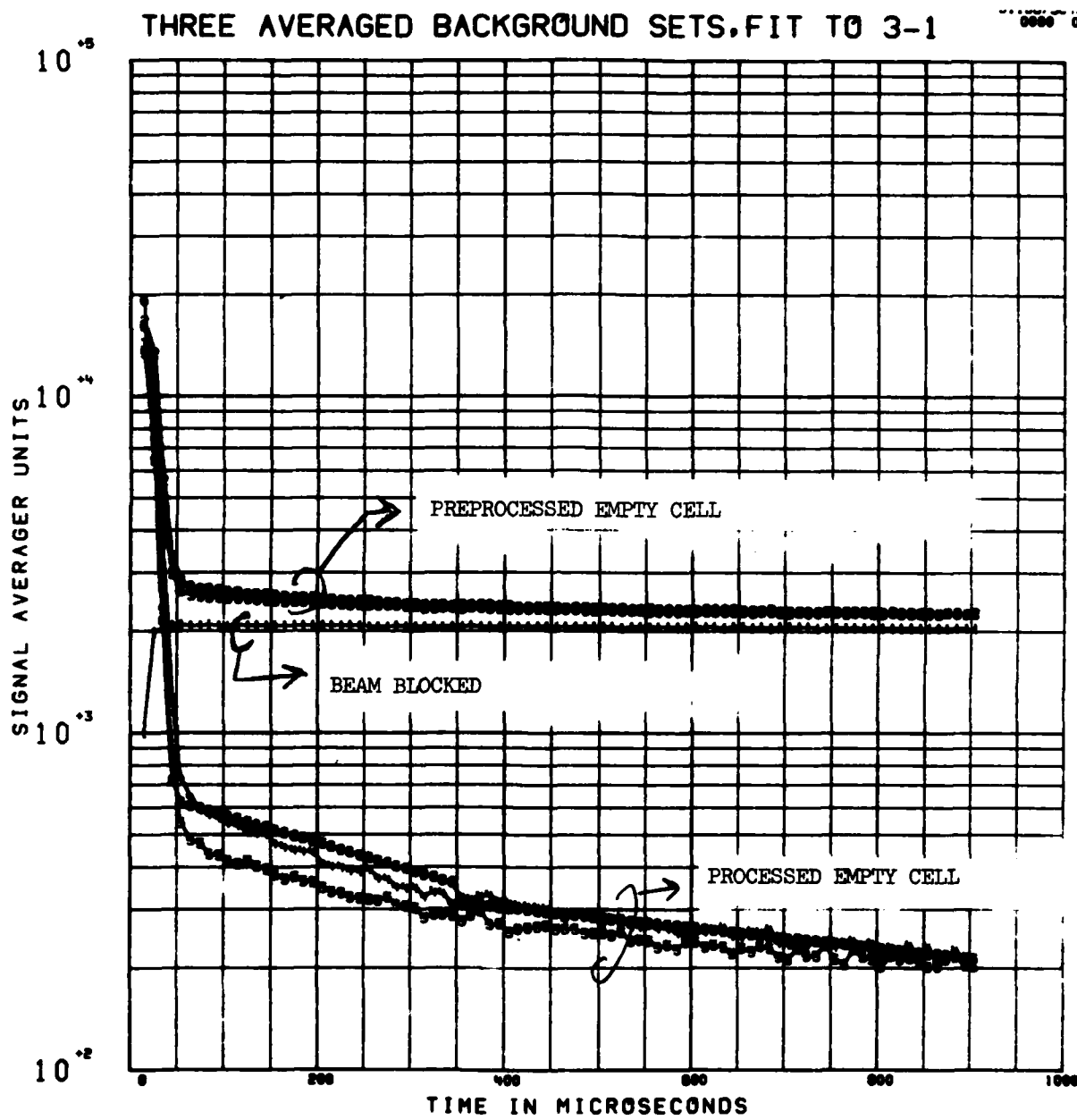


Fig. 2-3 Background Data Characterization

with respect to the beam. The large enhancement in the first few bins is the result of leakage of 2.7 μm laser light through the wings of the 4.3 μm filter. The laser light pulse duration is approximately 1 μsec , inspection of the curves labelled "preprocessed empty cell" on Figure 2-3 indicates the electronics are much slower than 1 μsec . Also, inspection of the curves "preprocessed empty cell" and "beam blocked" suggest the former might be the sum of the latter plus a component that is the response of the electronics to a very fast pulse input. Subtraction of the latter from the former results in the curves labelled "processed empty cell signal" which can be considered the electronics response to a very fast pulse input at the detector. This response looks like the sum of three simple exponential curves with time constants which are approximately $\tau_1 \cong 10 \mu\text{sec}$, $\tau_2 \cong 529 \mu\text{sec}$, and $\tau_3 \cong 1447 \mu\text{sec}$. The normalized electronics response R_e to a fast pulse at the detector is given by the sum

$$R_e = \sum_{i=1}^3 R_i \exp(-t \tau_i^{-1}) \text{ where } R_1 = .98922, R_2 = 6.83 \times 10^{-3} \text{ and}$$

$$R_3 = 3.96 \times 10^{-3}.$$

2.2.2 Fluorescence Analysis, 1 Torr CO₂, 300 Torr Argon

On Figure 2-4 are shown data (the curves labelled data cases) taken in several runs of 1000 pulses and with 1 Torr CO₂ and 300 Torr Argon in the fluorescence cell. The runs were taken under conditions of moderately consistent fluorescence as determined by methods described above. The runs were taken with the detector considerably more offset from the laser beam than was the case in generating the curves labelled "preprocessed empty cell" on Figure 2-3. These curves and the "beam blocked" curve are reproduced on Figure 2-4 for comparative purposes. Even though the beam is further offset from the detector than was the case in generating the "preprocessed empty cell" background characterization curves shown on Figures 2-3 and 2-4, the presence of the fluorescence produces an increase in signal over these cases by about 500 to 1000 signal averager units in the range $t \approx 50$ to 100 μ sec.

To analyze these data we subtract the "beam blocked" curve from the data and fit two components to the remainder which is the curve labelled "processed data" on Figure 2-5. One of the components should be due to laser light leakage and should have temporal dependence identical with the "processed empty cell" curve shown on Figure 2-3. The second component is due to fluorescence of CO₂ at 4.3 μ m. This latter component is considered to produce a detector signal which decays like e^{-qt} where q is the quenching rate of CO₂(ν_3) by argon, $q = k_A[A]$ where $k_A \approx 1.5 \times 10^{-15}$ cm³/sec (James and Kumer, 1977) and $[A] \approx 1.06 \times 10^{19}$ cm⁻³ since there is 300 Torr of argon in the cell, hence $q \approx 1.59 \times 10^{-2}$ / μ sec. The finite response time of the electronics modifies the fluorescence signal F so that it ultimately is given by

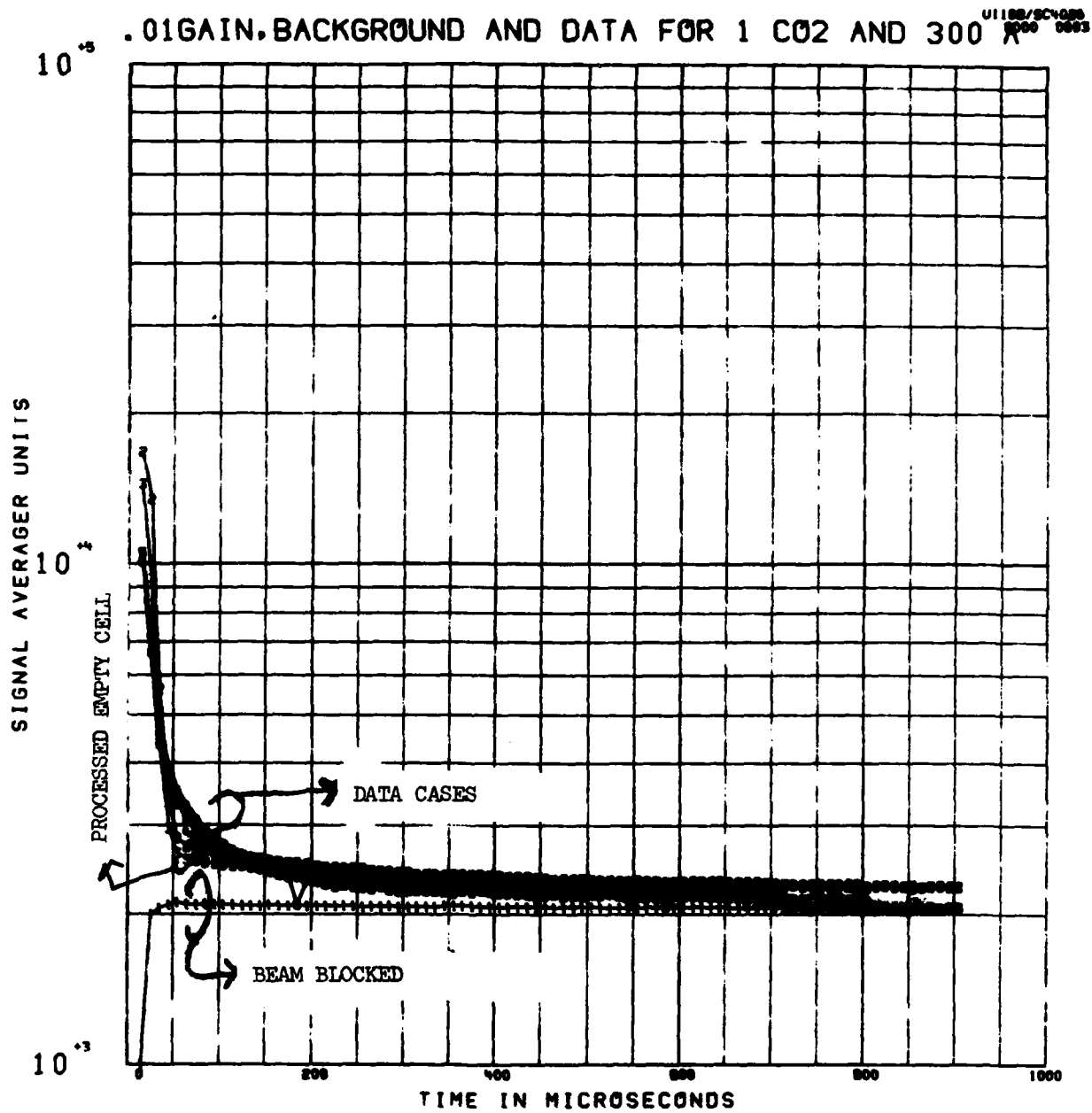
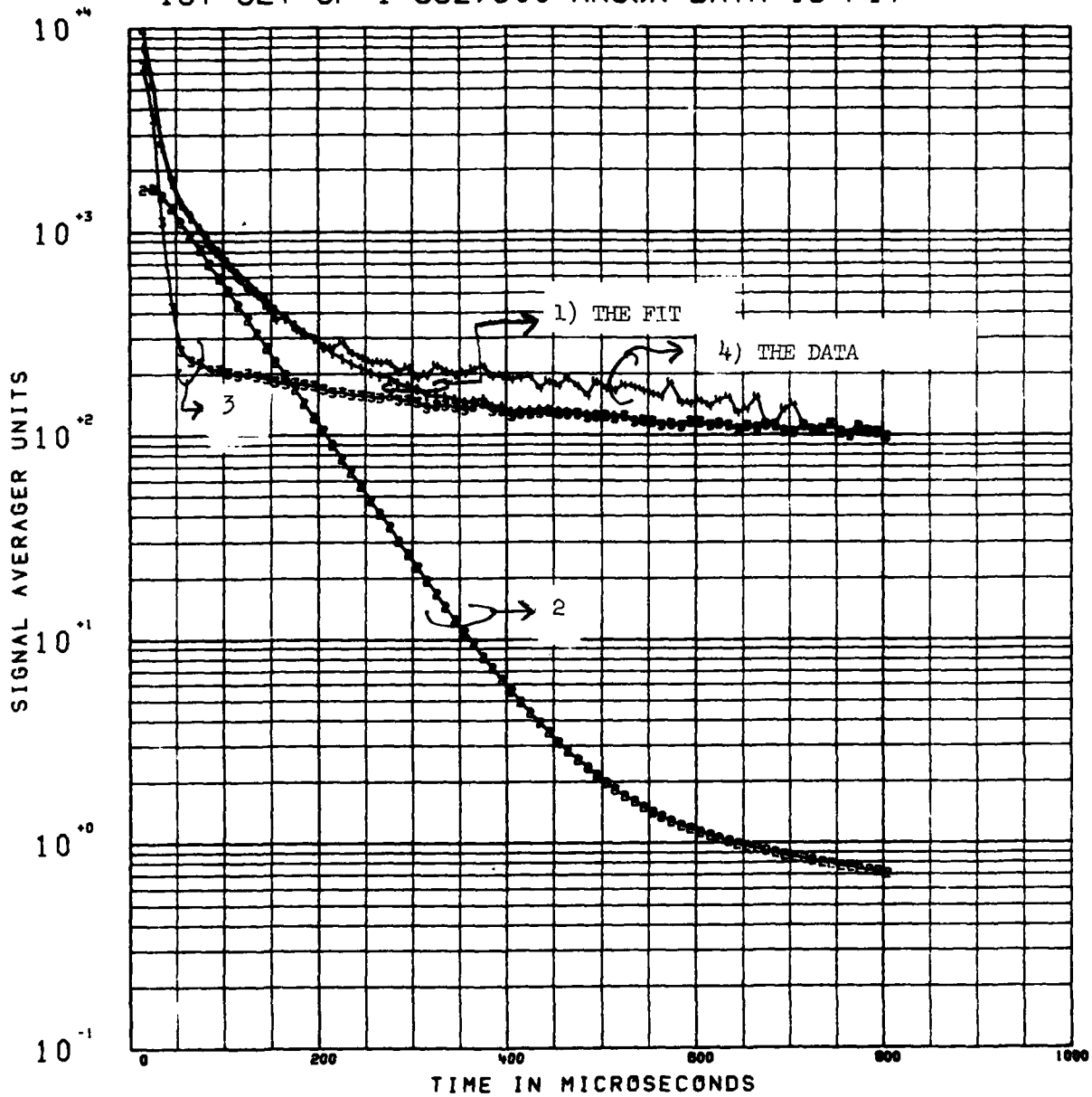


Fig. 2-4 Data Cases for 1 Torr CO₂ and 300 Torr Argon

CURVE 4 THE DATA
 CURVE 3 SCATTERED LIGHT LEAKAGE
 CURVE 2 FLUORESCENT COMPONENT
 CURVE 1 SUM OF 3+2

1ST SET OF 1 CO2,300 ARGON DATA IS FIT



$$a_{in} = 1.59E - 2/\mu\text{sec} \quad (\tau = 62 \mu\text{sec})$$

Fig. 2-5 Fit to First Data Set

$$F(t) = \sum_{i=1}^3 R_i \tau_i^{-1} / (q - \tau_i^{-1})(\exp(-t \tau_i^{-1}) - \exp(-qt))$$

The temporal dependence of the "processed empty cell" component is given by $R_e(t)$ and of the fluorescence component by $F(t)$, the "processed data" $D_p(t)$ may be fit by a sum $D_p(t) \approx A_R R_e(t) + A_F F(t)$ where the coefficients A_R and A_F are determined by a least squares fit technique. The least squares technique used to obtain A_R and A_F proceeds as follows, define

$$Q \equiv \sum_n (D_p(t_n) - A_R R_e(t_n) - A_F F(t_n))^2$$

then set

$$\frac{dQ}{dA_R} = 0 = \frac{dQ}{dA_F}, \quad (2-1)$$

and solve for A_R and A_F . To obtain A_F and A_R as illustrated by Figure 2-5, just the first 40 signal averager bins ($t_n \leq 400 \mu\text{sec}$) were utilized. The fit is not particularly good in the region $t \geq 300 \mu\text{sec}$ but this is to be expected since the form of equation (2-1) preferentially weights the points associated with the largest value of $D_p(t)$.

It is possible to use the data $D_p(t)$ to determine k_A as follows, set

$$D_p = A_R R_e + \delta A_F F + \delta q A_F \frac{dF}{dq} \quad (2-2)$$

and solve for A_R , δA_F and δq by a least squares fit technique in order to determine new values for A_F and q , namely $A_F \rightarrow A_F + \delta A_F$ and $q \rightarrow q + \delta q$, iterate until convergence is achieved. The results of application of this technique to the processed data set $D_p(t)$ are shown on

Figure 2-6, the value $q = 1.65 \times 10^{-2} / \mu\text{sec}$ achieves the best fit to the data. Results of applying the technique to "processed data" obtained in two additional 1000 pulse runs at 1 Torr CO_2 and 300 Torr Argon are shown on Figures 2-7 and 2-8. The values of q that best fit these data runs are $q = 1.55 \times 10^{-2}$ and $1.66 \times 10^{-2} / \mu\text{sec}$ respectively. From analysis of these three runs we find

$$q = (1.62 \pm .05) \times 10^{-2} / \mu\text{sec} ,$$

this high precision determination of q is consistent with the literature value for k_A .

In summary, our first recorded fluorescence measurements were performed in the geometry shown in Figure 2-2 since we were initially most successful in observing fluorescence on the oscilloscope when this geometry was employed. The high argon pressure 300 Torr was used in order to broaden the CO_2 lines to facilitate tuning the laser light onto the absorption lines. The absorption line full width half max is $\approx 0.04 \text{ cm}^{-1}$ and the spacing between the lines about 1.6 cm^{-1} .

A fluorescence signal with large signal/noise was clearly evident in the three runs that were selected for analysis. The background was found to be both consistent and simple to characterize. It was possible to extract the quenching rate q of $\text{CO}_2(\nu_3)$ by argon to better than 4% precision from the data that was analyzed.

2.2.3 Side Looking Geometry

In preparation for the ultimate branching ratio measurement a second intermediate step involving side viewing of $4.3 \mu\text{m}$ fluorescence needed to be taken. The main purpose was to demonstrate that good signal to noise could be achieved at $4.3 \mu\text{m}$

RESULT OF NON LINEAR LEAST SQUARE FIT

$$q_{in} = 159 \text{ E-2}/\mu\text{sec}$$

$$q_{out} = 1.65 \text{ E-2}/\mu\text{sec}$$

FIT BY REGRESSION

0000 0005

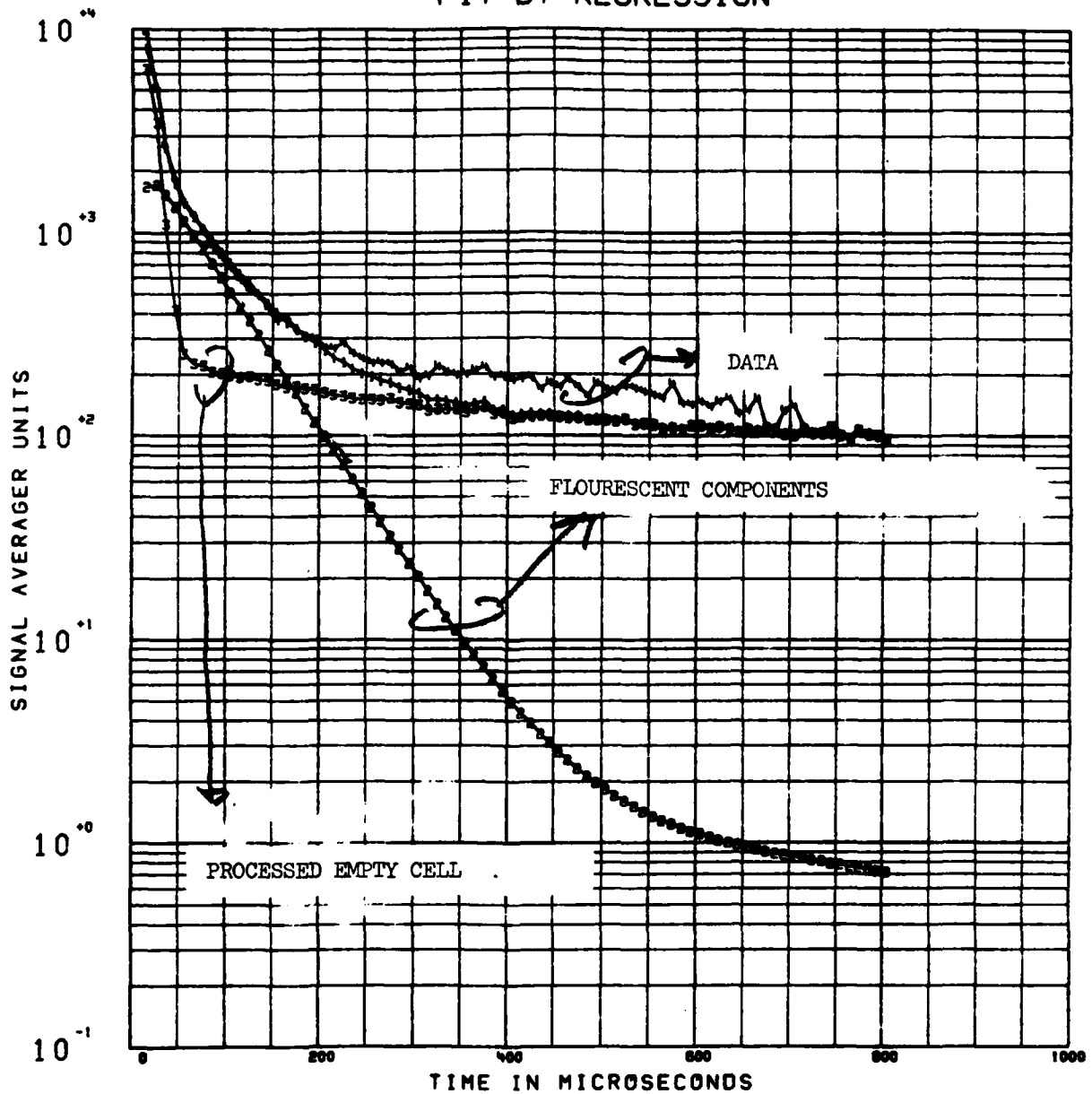


Fig. 2-6 First Data Set is Fit by Nonlinear Least Squares Technique

$$q_{in} = 1.59E-2/\mu\text{sec}$$
$$q_{out} = 1.55E-2/\mu\text{sec}$$

FIT BY REGRESSION

U1106/SC-020
0000 0007

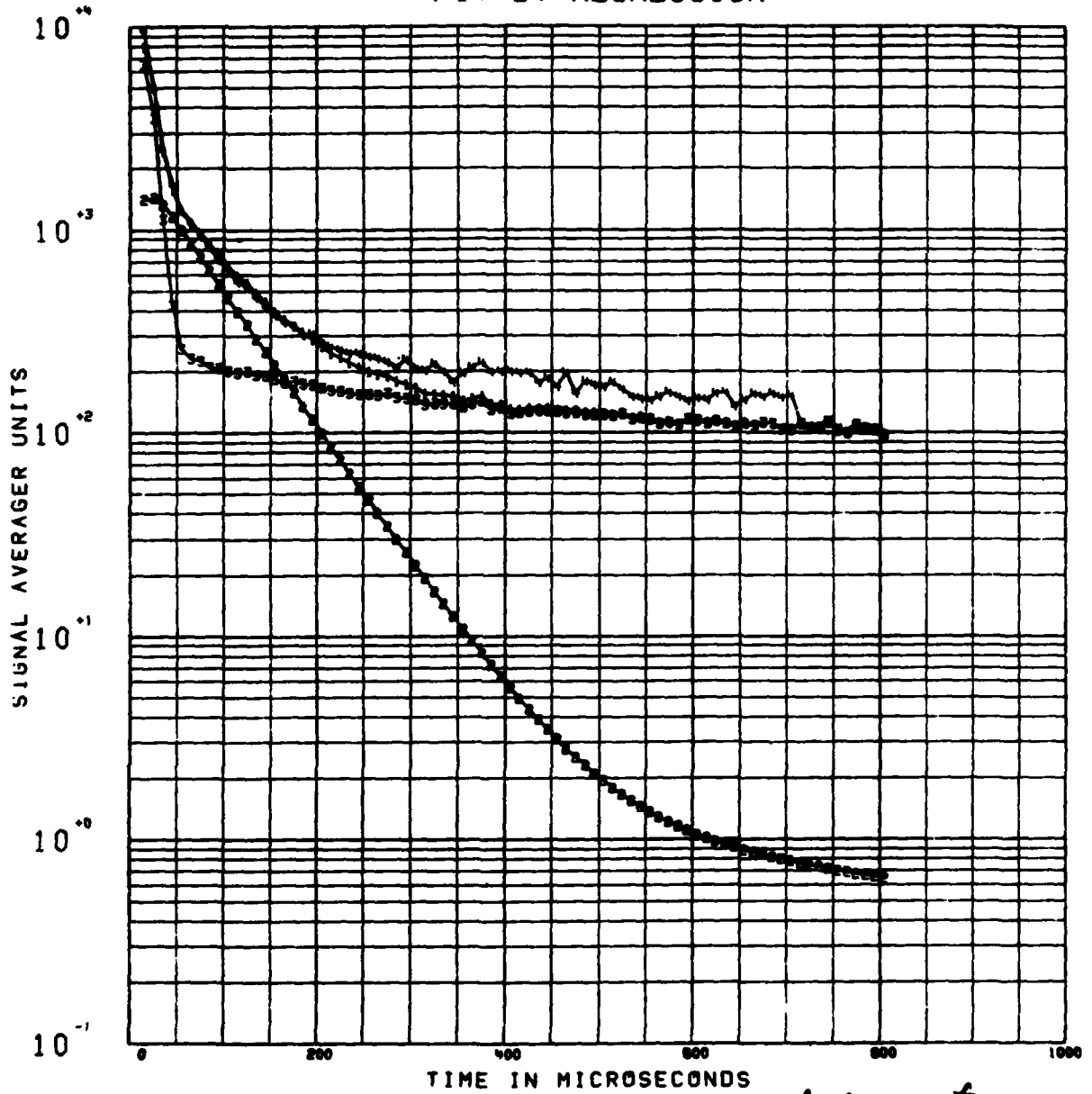


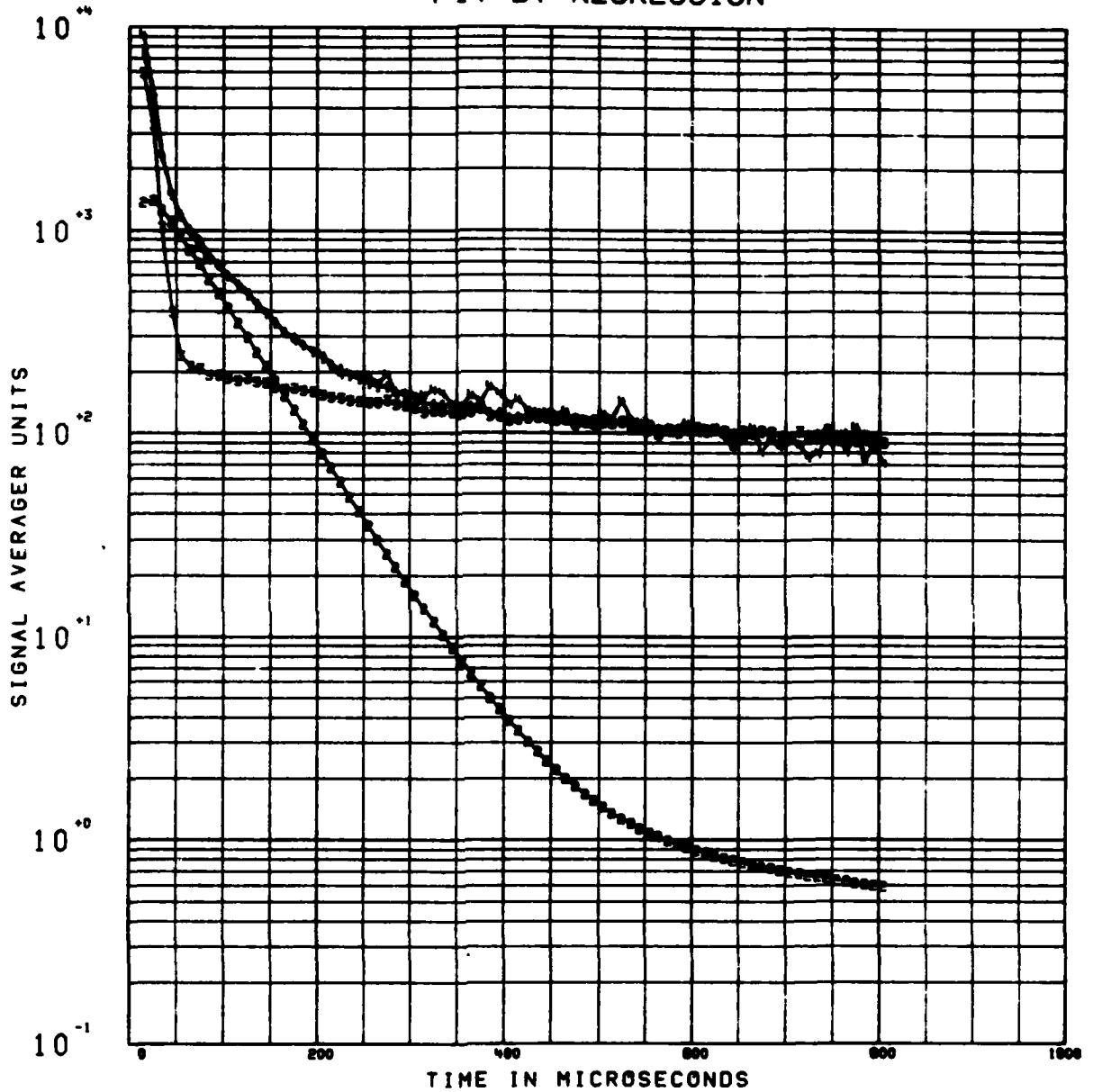
Fig. 2-7 Nonlinear Least Squares Analysis of 2 cd Data Set

$$q_{in} = 1.59 \text{ E-2}/\mu\text{sec}$$

$$q_{out} = 1.66 \text{ E-2}/\mu\text{sec}$$

FIT BY REGRESSION

U1108/SC-0001
0000 0000



REGRESSIVE RESULTS (3 cases)

$$q = 1.62 \pm .05 \times 10^{-2}/\mu\text{sec}$$

Fig. 2-8 Analysis of 3rd Data Set and Overall Results of Nonlinear Analyses

with side viewing geometry for CO_2 partial pressures P_{CO_2} low enough so that the time constant $\tau_{2.7}$ for decay of the CO_2 laser pumped excited states 101 and 021 by the process $\begin{Bmatrix} 101 \\ 021 \end{Bmatrix} + 000 \rightarrow \begin{Bmatrix} 100 \\ 020 \end{Bmatrix} + 001$ should be long compared to the duration ($\approx 1 \mu\text{sec}$) of the laser pulse. The time constant is reported (Finzi and Moore, 1975) to be $\tau_{2.7} = 0.25 \mu\text{sec}/P_{\text{CO}_2}$ where P_{CO_2} is measured in Torr. Hence it was necessary to show that good $4.3 \mu\text{m}$ signal to noise could be achieved for partial pressures P_{CO_2} of the order .025 Torr or less such that $\tau_{2.7} \gg 1 \mu\text{sec}$. To this end we describe the analysis of some $4.3 \mu\text{m}$ fluorescence data obtained with the side viewing geometry and the electronics that are shown on Figure 2-9, and with $P_{\text{CO}_2} \approx 30$ Torr. The electronics employed in the side viewing configuration shown on Figure 2-9 were identical to those described above in Section 2.1.2. The cell was designed so the laser light could be passed as shown on Figure 2-9 through diametrically aligned sapphire windows of radius ≈ 9 mm. In this way it could also be possible to simultaneously view the fluorescing region from both sides of the cell.

2.2.4 Analysis for 0.03 Torr CO_2 and 50 Torr A

Two side viewing preprocessed data cases, with 0.03 Torr CO_2 and 50 Torr A in the cell, are shown on Figure 2-10 in comparison with the "beam blocked" and "preprocessed empty cell" data that were shown previously on Figure 2-3 above. For $\tau \geq 70 \mu\text{sec}$ these preprocessed data show the presence of fluorescence over and above the large "preprocessed empty cell" signal that was obtained for the direct laser beam/detector incidence geometry that is illustrated by Figure 2-2 above.

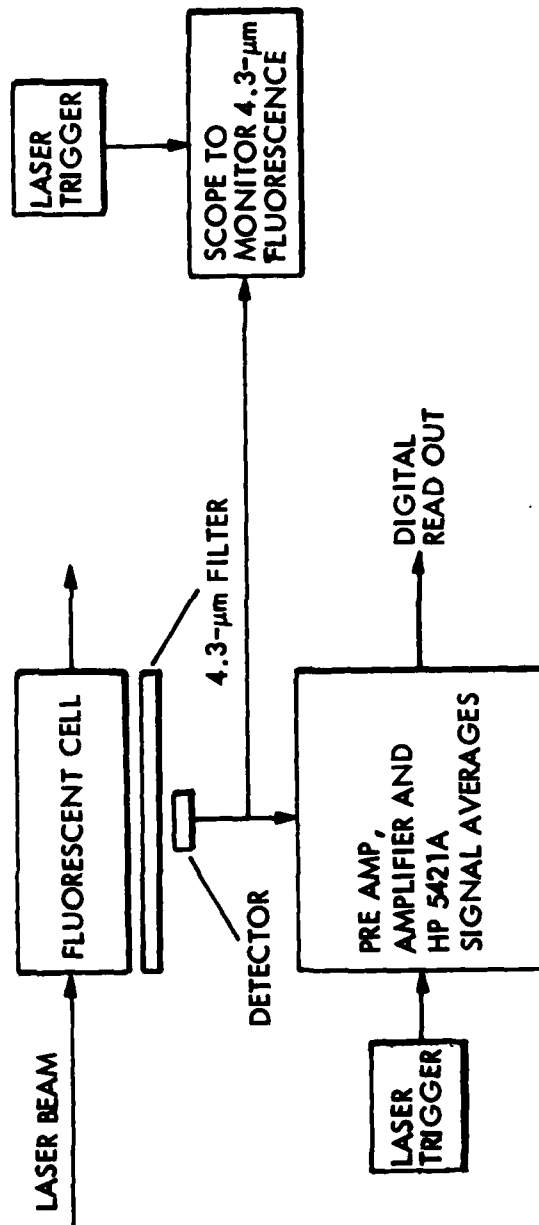


Fig. 2-9 Side Looking Geometry and Electronics

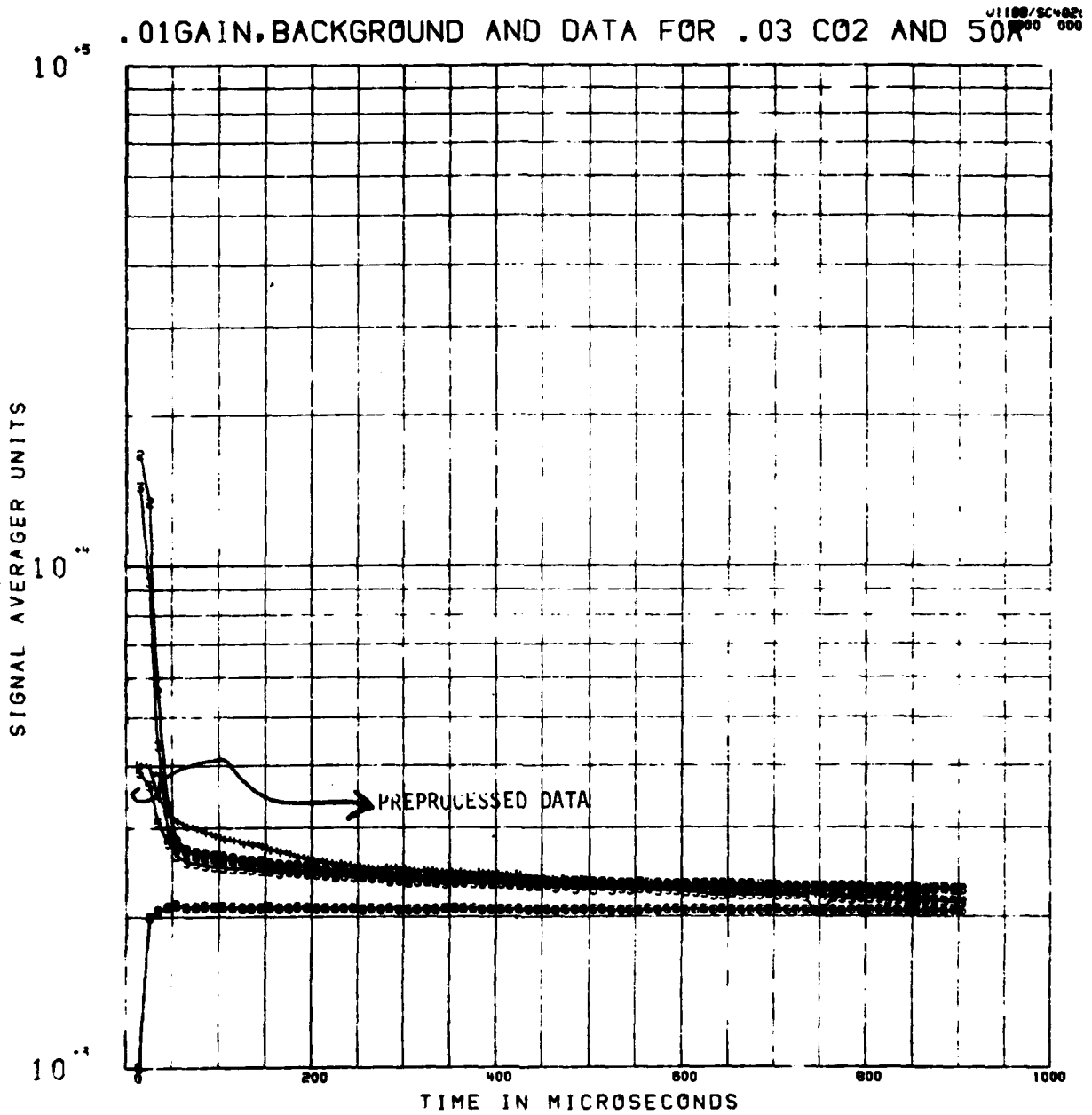


Fig. 2-10 Two Preprocessed Side Viewing Data Sets for 0.03 Torr CO₂ and 50 Torr Argon

On Figure 2-11 one set of the processed data are shown fit by the sum $A_R R_e(t) + A_F F(t)$ where the quenching due to argon is given by $q = (50/760) \times 2.69 \times 10^{19} \times 1.5 \times 10^{-15} / 10^6 = 2.65 \times 10^{-2} \mu\text{sec}^{-1}$. We see that (i) the fit is excellent, an indication that side viewing geometry reduces the amplitude of the "processed empty cell" signal but does not change its temporal dependence, and that (ii) the $4.3 \mu\text{m}$ fluorescence component dominates the processed data. The fit to a second set of the processed data is shown on Figure 2-12 and reinforces the conclusions (i) and (ii) above. The first set is seen to have a somewhat larger fluorescence component, the fluorescence amplitude $A \cong 900$ and 630 signal averager units (SAU) respectively for the two runs. The "processed empty cell" amplitudes are similar in both cases and are reduced from that observed for the geometry of Figure 2-2 by a factor 10 to 4 dependent on the laser beam/detector offset.

The quenching that best fits the two data sets was determined to be $3.1 \times 10^{-2} \mu\text{sec}^{-1}$ and $2.61 \times 10^{-2} \mu\text{sec}^{-1}$ respectively, these compare well with the quenching $q = 2.65 \times 10^{-2} \mu\text{sec}^{-1}$ that is computed above from the literature value $k_A = 1.5 \times 10^{-15} \text{ cm}^3/\text{sec}$ for the rate coefficient for the quenching of $\text{CO}_2(\nu_3)$ by argon.

2.2.5 Analysis for 0.3 Torr CO_2 and N_2 , and 50 Torr Argon

Several runs at 0.3 Torr CO_2 and N_2 and 50 Torr argon were performed. These runs were performed to demonstrate the utility of our equipment for obtaining accurate measurements of very fast rate constants such as the vibration transfer rate constant k_{VV} for the reaction

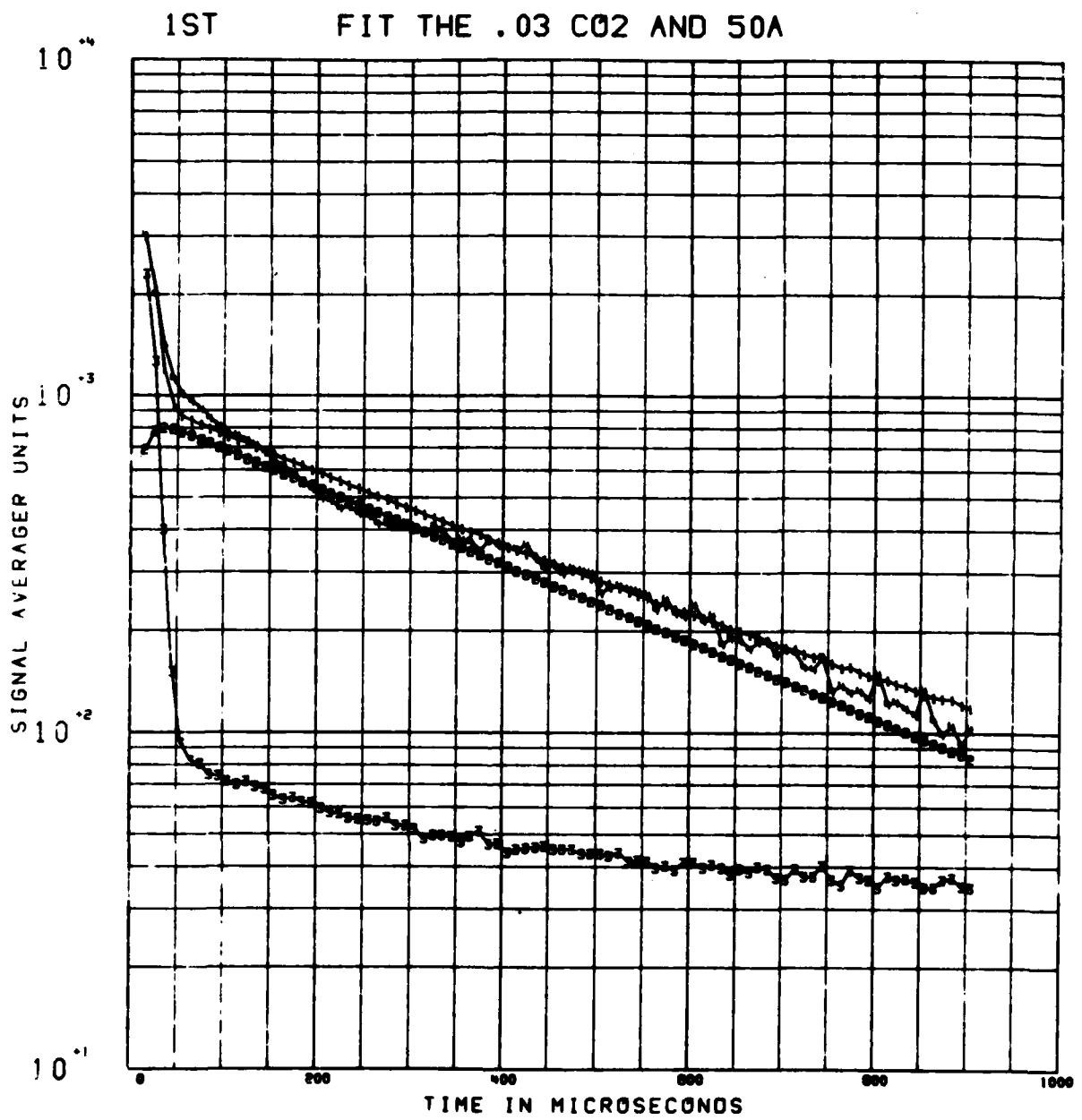


Fig. 2-11 Analysis of First Data Set

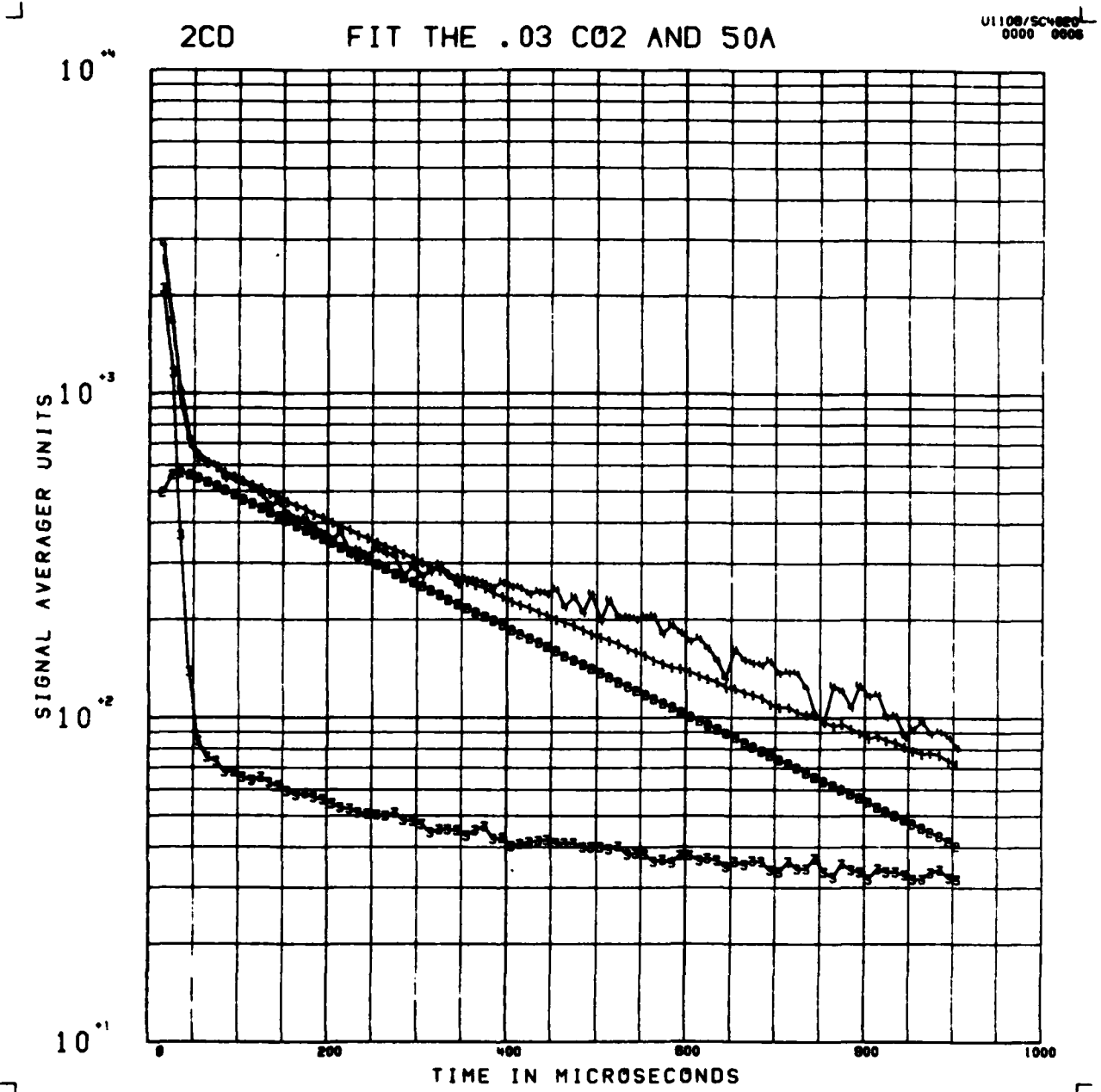
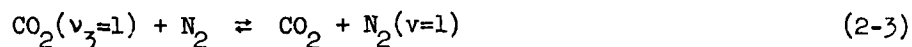


Fig. 2-12 Analysis of 2cd Data Set



To demonstrate this utility we will go through a simple minded analysis of a sample of this data. The scope of our effort does not permit a detailed analysis of all these data. The processed data from one of the runs is shown on Figure 2-13. The least squares fit analysis Eqn. (2-2) is used to determine an effective quenching q that yields a best fit to the data. The analysis was applied to the data bins 2 through 14 which are located approximately on the time interval $15 \leq t \leq 135$ μsec . During early times the effective quenching should be given approximately by

$q \cong k_A[A] + k_{VV}b[\text{N}_2]$ where $b = \exp(-(\text{hc}/k) \Delta E/T)$ and where $\Delta E \approx 18 \text{ cm}^{-1}$ is the energy defect between the $^{12}\text{C}^{16}\text{O}_2(001)$ state and the $^{14}\text{N}_2(v=1)$ state. At late times however, when the vibrational temperature of nitrogen approaches that of CO_2 , the effective quenching should be approximated by $q \cong k_A[A] ([\text{CO}_2]/([\text{CO}_2] + [\text{N}_2]))$.

The interval $t \leq 135$ μsec was selected for application of the least squares analysis given by Eqn. 2-3 since this time $\approx (k_{VV}[\text{N}_2]b)^{-1} = 157$ μsec is approximately the time that is required for the vibrational temperature of the nitrogen to approach that of the CO_2 . An effective quenching $q \approx 6.46 \times 10^{-3} \text{ } \mu\text{sec}^{-1}$ is found to best fit the data in the time regime $t \leq 140$ μsec . It is possible to determine the rate constant k_{VV} from these data as follows. Let X_1 and X_2 represent the populations of vibrationally excited CO_2 and N_2 respectively. The time dependence of these species then obey the equations

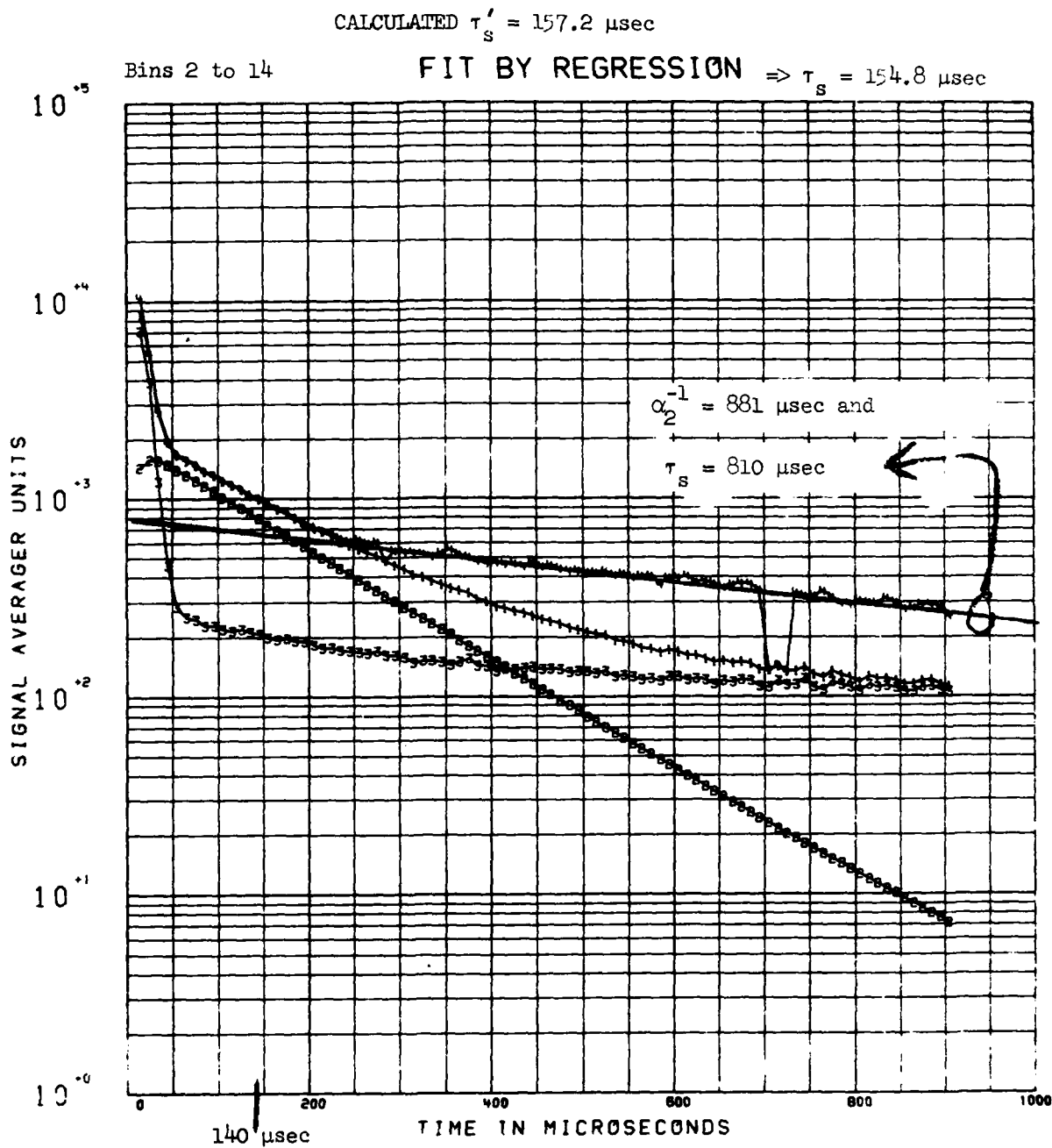


Fig. 2-13 Analysis of Data Obtained with Side Viewing Geometry,
0.3 Torr CO_2 and N_2 , and 50 Torr Argon

$$\frac{d}{dt} X_1 = -k_A[A] X_1 - k_{VV}[N_2] X_1 + k_{VV}b[CO_2] X_2$$

$$\frac{d}{dt} X_2 = k_{VV}[N_2] X_1 - k_{VV}b[CO_2] X_2 \quad (2-4)$$

The notation is streamlined by defining $q_A = k_A[A]$ and $v = k_{VV}[N_2]$. The two eigenvalues α_i of the linear first order Eqn. (2-4) are given in terms of the quantities defined by

$$\alpha_A \equiv (q_A + v(1 + b)) / 2$$

and

$$\alpha_B \equiv \frac{1}{2} \sqrt{q_A^2 + (v + vb)^2 + 2 q_A v(1-b)}$$

as

$$\alpha_1 = \alpha_A + \alpha_B$$

and

$$\alpha_2 = \alpha_A - \alpha_B \quad (2-5)$$

The unnormalized solution for X_1 is given by

$$X_1 = e^{-\alpha_1 t} + y e^{-\alpha_2 t} \quad (2-6)$$

where $y = (\alpha_1 - q_A - v) / (q_A + v - \alpha_2)$.

Now we can compute

$$q' = t_0^{-1} \ln (X_1(t_0) / X_1(t_0, 0))$$

from Eqn. (2-6) where $t_0 = 140 \mu\text{sec}$.

The result is $q' = 6.36 \times 10^{-3} \mu\text{sec}^{-1}$ if we assume the literature value $k_{VV} = 6 \times 10^{-13} \text{ cm}^3 \text{ sec}^{-1}$. This compares within 1.5% with the value $q = 6.46 \times 10^{-3} \mu\text{sec}^{-1}$ that is determined from the data as described above.

In order to determine k_{VV} from the data we set

$$q = q' + [N_2] \delta k_{VV} \frac{dq'}{dv}$$

and solve for δk_{VV} and then set $k_{VV} = 6 \times 10^{-13} \text{ cm}^3 / \text{sec} + \delta k_{VV}$. The result is $k_{VV} = 6.4 \times 10^{-13} \text{ cm}^3 \text{ sec}^{-1}$. The literature value $k_{VV} \approx 6 \times 10^{-13} \text{ cm}^3 \text{ sec}^{-1}$.

To further demonstrate the potential accuracy of the technique for determining rate constants consider the late time ($t \geq 300 \mu\text{sec}$) data, these should decay like $e^{-\alpha_2 t}$. To check this one can use a ruler to draw a straight line through the late time processed data as is shown on Figure 2-13. The slope of this line gives a time constant $\tau_L \approx 810 \mu\text{sec}$ for the late time data decay time which is in good agreement with the value $\alpha_2^{-1} \approx 881 \mu\text{sec}$ that one may calculate by the use of Eqn. (2-5) and the value $k_{VV} \approx 6.4 \times 10^{-13} \text{ cm}^3 \text{ sec}^{-1}$ as derived from the early time data.

This sample analysis suggests that the accuracy which may be achieved by this technique in the determination of k_{VV} is remarkable, particularly on consideration that (i) the fluorescent cell and/or vac system may have been leaky, thereby admitting atmospheric N_2 at some undetermined rate, and (ii) the "beam blocked" and the "processed empty cell" functions that were used in the data analysis had been determined from data taken several days prior to the day on which the 0.3 Torr CO_2 and N_2 and 50 Torr A data that are discussed here were taken. If measurement of k_{VV} had been a primary goal of the experiment it would have easily been possible to make the effort that is required to

neutralize these deleterious effects. Even so, the work we report here has served to demonstrate that our equipment is suitable for making highly accurate measurements of fast vibration transfer rates. In particular, the equipment could be used to measure k_{vv} for reaction (2-3) for the minor CO_2 isotopes 636 ($^{13}\text{C}^{16}\text{O}_2$), 628, and 627. This would provide input that is necessary to more accurately calculate the altitude dependence of the atmospheric response time near 80 km to nuclear events for CO_2 4.3 μm emission due to processes similar to those discussed in the report DNA 4260F (HAES Report No. 57, or see J. Geophys. Res. 82, 2203). The use of a refrigerated fluorescence cell would permit measurements of k_{vv} at temperatures including realistic mesopause temperatures for all isotopic species of CO_2 . Similar vibration transfer measurements between N_2 and NO , N_2O , CO could also be performed with this equipment. It is not inconceivable that some adaptation of the equipment could be used to study quenching and vibration transfer for short lived species such as OH and NO^+ .

2.3 Preliminary Measurement the 101-100 and 101-000 Branching Ratio

In this section we describe initial efforts to measure the 4.3 μm /2.7 μm branching ratio by simultaneously measuring the signal at 2.7 μm and 4.3 μm following absorption of the laser pulse at 2.7 μm .

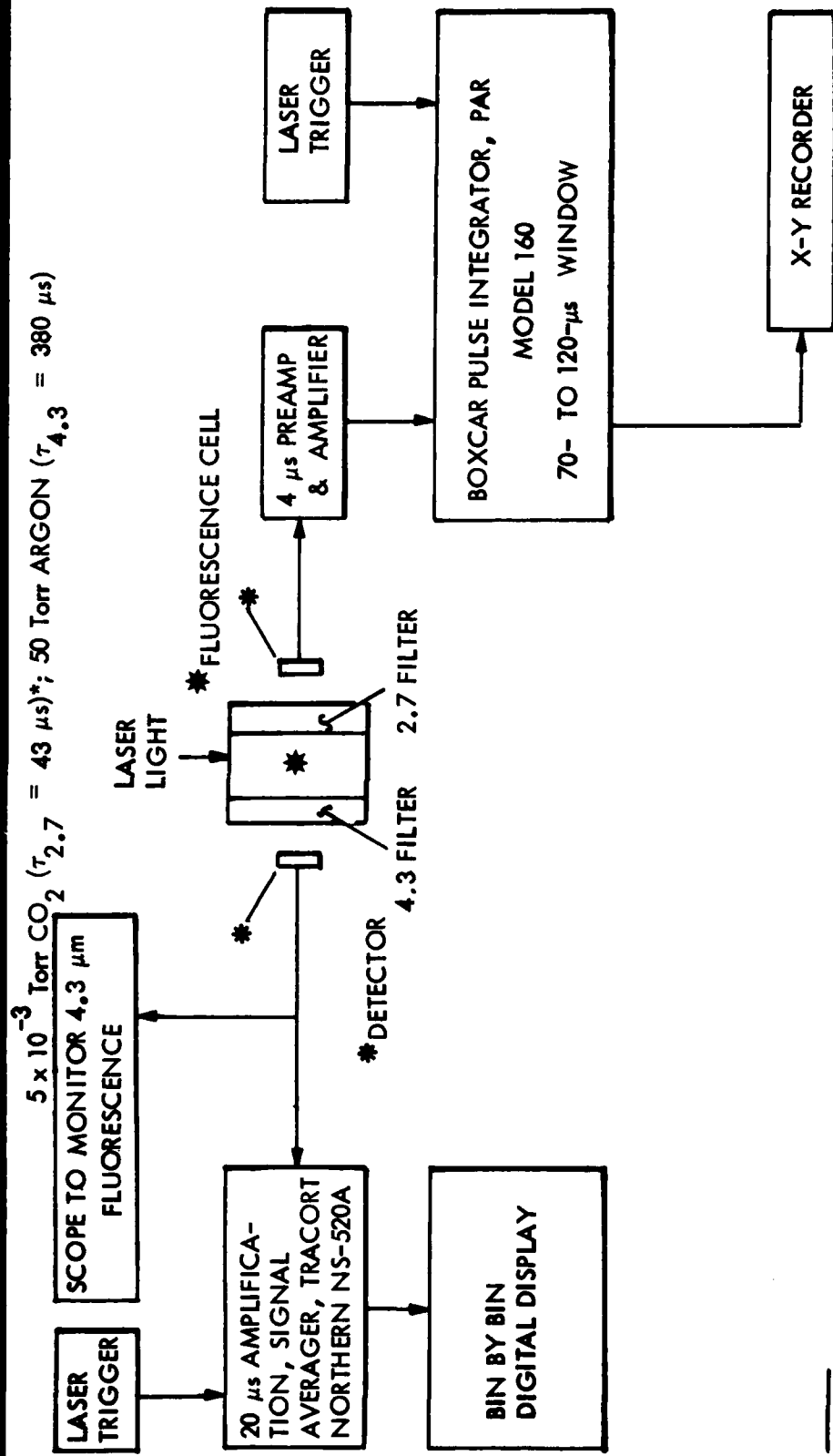
A signal originating from the radiation from the 101 level via 2.7 μm emission decays extremely rapidly due to rapid exchange of ν_3 excitation on collision with ground state CO_2 . The quenching rate of this level at a pressure of 1 Torr is $4.5 \cdot 10^6 \text{ sec}^{-1}$ which corresponds to 0.217 μsec lifetime. This rapid decay requires that we have fast response detectors and pre-amplifiers. In order to be able to separate the fluorescence from scattered background at 2.7 μm which originates from the initial pulse, it is necessary to work at pressures well below 1 Torr. Working at lower pressures increases the lifetime of the 101 level which in addition to permitting the 2.7 μm fluorescence to be time resolved from the scattered input radiation also relaxes somewhat the requirement for fast electronics.

While lowering the partial pressure has the advantage of increasing the lifetime of the 101 level, the loss in signal associated with working at lower number densities eventually places a lower limit on the usable pressure. Our experience with measuring the 4.3 μm fluorescence at 0.03 Torr (30 μm) showed that we had a strong signal at 4.3 μm with excellent signal to noise. Therefore we decided to try even lower pressures of 0.02 and 0.01 and .05 Torr to see if we could still observe the 4.3 μm fluorescence on an oscilloscope so that we could manually tune onto a CO_2 line. In all of these cases we were able to observe 4.3 μm fluorescence on an oscilloscope after amplification.

Since we were able to obtain a good 4.3 μm fluorescence signal at 5 μm , we decided to use this pressure for our branching ratio measurements. We had made some earlier attempts at 10 μm of CO_2 , but those results were unreliable due to large noise signals in the Boxcar integrator (to be described later) and will not be discussed.

The procedure used in our effort to measure the branching ratio was to manually tune the laser output onto a CO_2 line as evidenced by observable 4.3 μm fluorescence on an oscilloscope. Once the fluorescence was observable, we then simultaneously measured the signals at 4.3 μm and 2.7 μm using two detectors and the same fluorescence cell. Figure 2-14 shows a diagram of the experimental arrangement. We simultaneously monitor the signals at 4.3 μm and 2.7 μm . The 4.3 μm signal was measured with an InSb detector and a preamplifier. The preamplifier is shown on Figure 2-15. This same circuit was used except the 510 pf capacitor in parallel with the load resistor was replaced by a 15 pf capacitor and the load resistor was 680 K Ω . This should give the preamplifier about a 10 μsec response time. The output of this preamplifier was then amplified using the AC amplifier in a Keithly model 840 lock in amplifier. The bandwidth of this amplifier was only a few hundred kHz so that the input pulse from the preamplifier was broadened to approximately 15 μsec .

In our experiments to simultaneously look at the 2.7 μm fluorescence and the 4.3 μm fluorescence, the Hewlett-Packard signal averager which we had used in the 4.3 μm runs was not available as it was out for repair. In its place we used a Tracor Northern Model NS-570A signal averager which has a time resolution of 20 μsec per channel. The experiments were done with



* $\tau_{2.7} \approx 0.25 \mu\text{s}/\text{P CO}_2$ (IN Torr)

Fig. 2-14 Experimental Arrangement for Branching Ratio Measurement

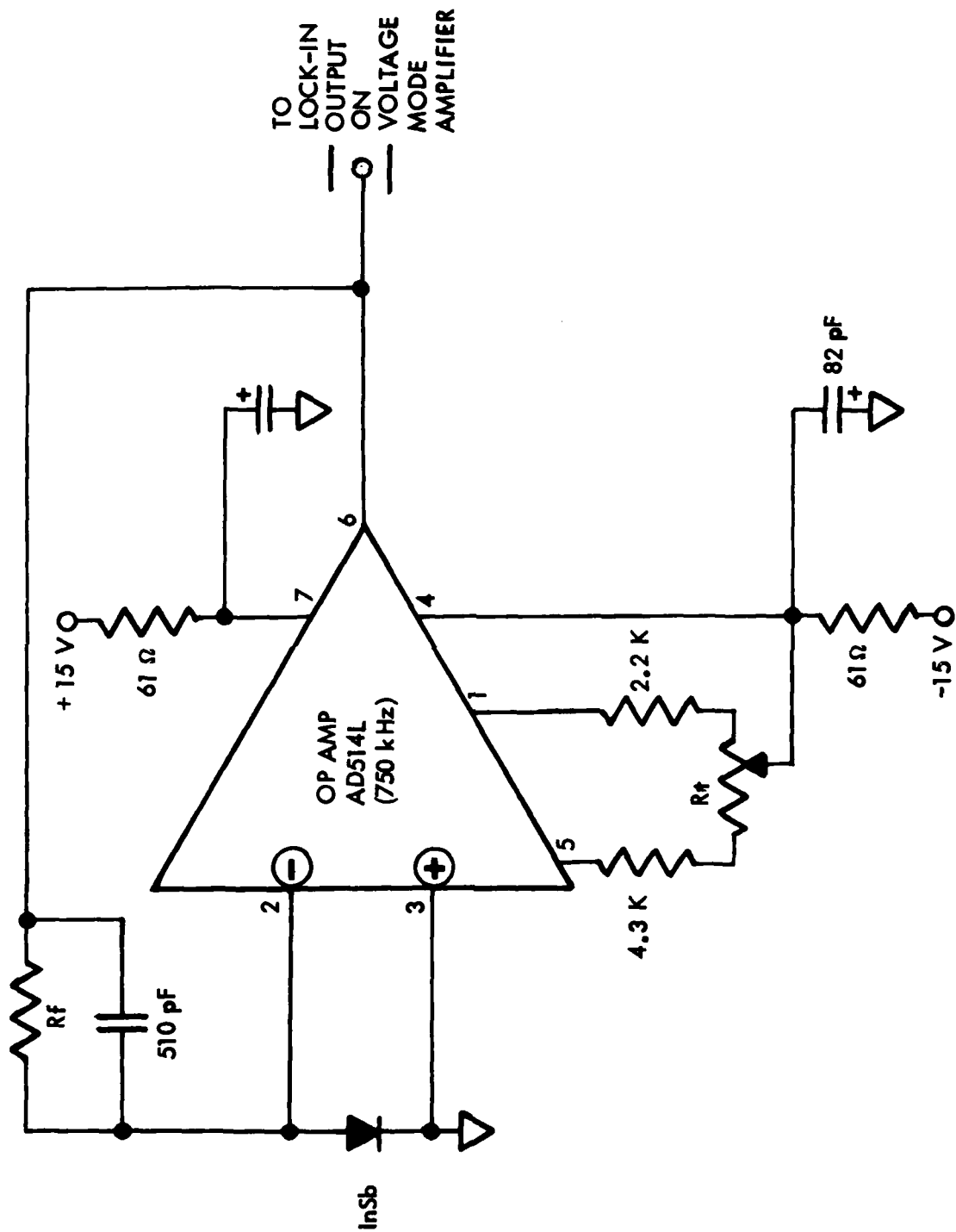


Fig. 2-15 Transimpedance Preamplifier

50 Torr of Argon in the fluorescence cell with a corresponding decay rate of 376 μsec for the 4.3 μm signal. The Tracor-Northern signal averager therefore had time resolution which was more than adequate for measuring the 4.3 μm fluorescence under these conditions.

At a partial pressure of 5 μm of CO_2 the lifetime of the 101 level is approximately 43 μsec , so that a faster response amplifier was desirable. In order to increase the response of the preamplifier we used the same circuit as described above except that we reduced the load resistor to 240 K. However we found that a larger capacitor was required to prevent ringing. The capacitor used was 56 pf which gave the preamplifier a response of the order of 13 μsec .

The signal from the 2.7 μm detector-preamplifier was amplified by a factor of 5 using the vertical output of a Hewlett-Packard Model 1715A oscilloscope. This signal was then further averaged using a Tektronix Model 1121 Amplifier with a 17 MHz bandwidth and a gain of 100. The signal was then fed into a PAR Model 160 boxcar integrator.

The 2.7 μm signal had a large scattered component from the initial laser pulse. We found that in order to obtain a stable boxcar output we had to look at a portion of the 2.7 μm fluorescence pulse which was quite a way away from the initial laser pulse. We found that by using a window from 70 to 120 μsec away from the main laser pulse, we could obtain fairly stable boxcar results.

The scattered pulse from the laser was reduced significantly by using a filter in front of the 2.7 μm detector which had less than 1% transmission at the laser wavelength and transmitted the P Branch of the 101-000 band. This filter is shown in Figure 2-16.

In the case of the 4.3 μm signal, it was possible to eliminate all of the scattered radiation by using a 4.3 μm filter and carefully masking around the detector. The fraction of the 2.7 μm band transmitted by the 2.7 μm filter was about 1/3 of the fraction of the 4.3 band transmitted by the 4.3 μm filter.

Figure 2-17 shows the results of the 4.3 μm fluorescence obtained on the TRACOR signal averager. The results were plotted from the digital readout which is displayed on the signal averager cathode ray tube. This figure also shows the results for the 2.7 μm boxcar signals obtained for each 4.3 μm fluorescence curve plotted.

The boxcar integrator was set with a 50 μsec window, as mentioned previously, and a time constant of 30 msec. Since the pulse rate was 5 pps and only 50 μsec are sampled in each pulse it took several minutes for the 2.7 μm signal to build up to its final value. This is illustrated in Figure 2-18 in which a signal received by the boxcar is changed as a result of placing a card in front of the laser output. This shows that it takes on the order of 3 minutes for the boxcar to reach its final value. This figure also indicates that the boxcar output was noisy with fluctuations of the order of 1 mv on a time scale less than 1 minute. This source of noise is not completely understood by us, and it did limit the precision of our results.

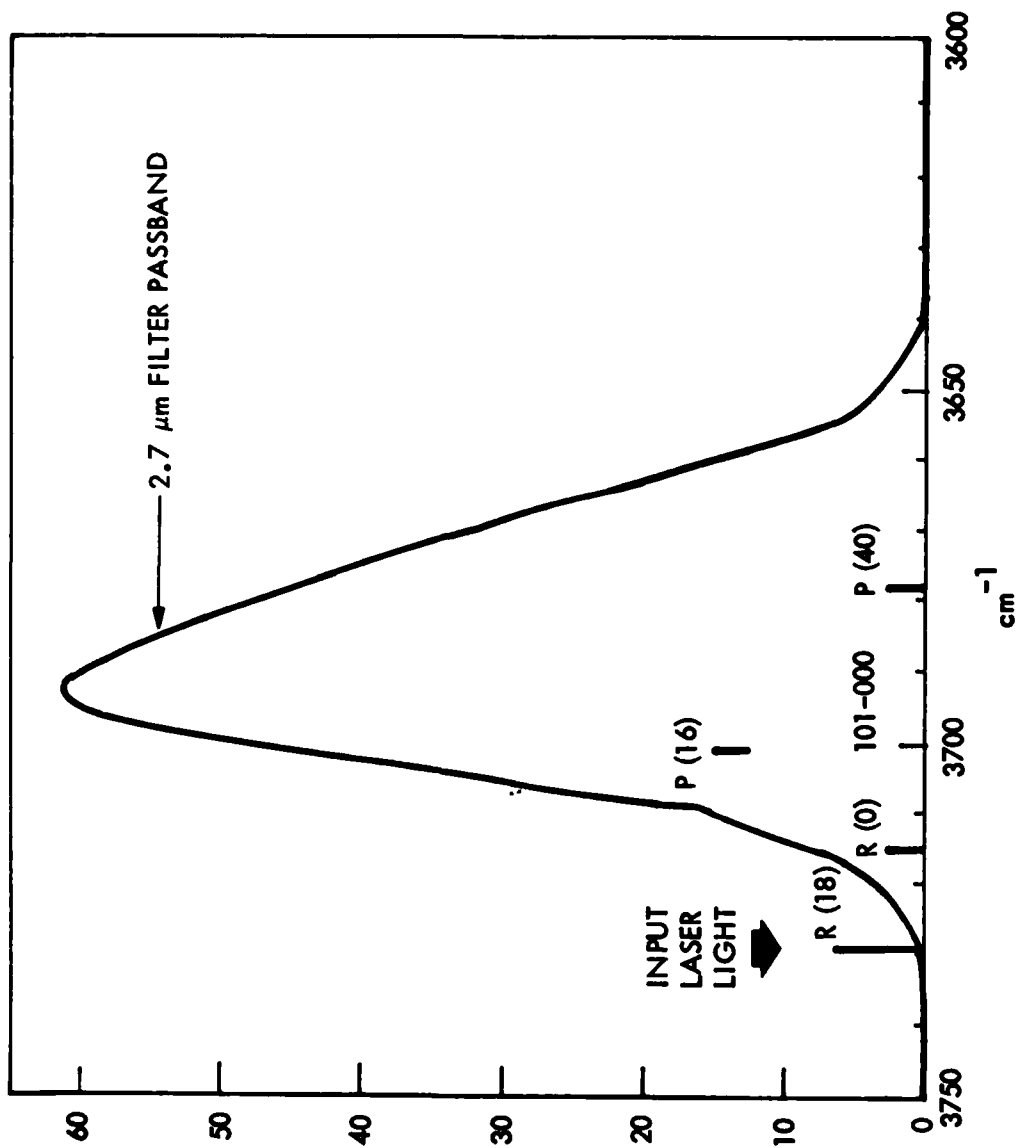


Fig. 2-16 101-000 P Branch Filter

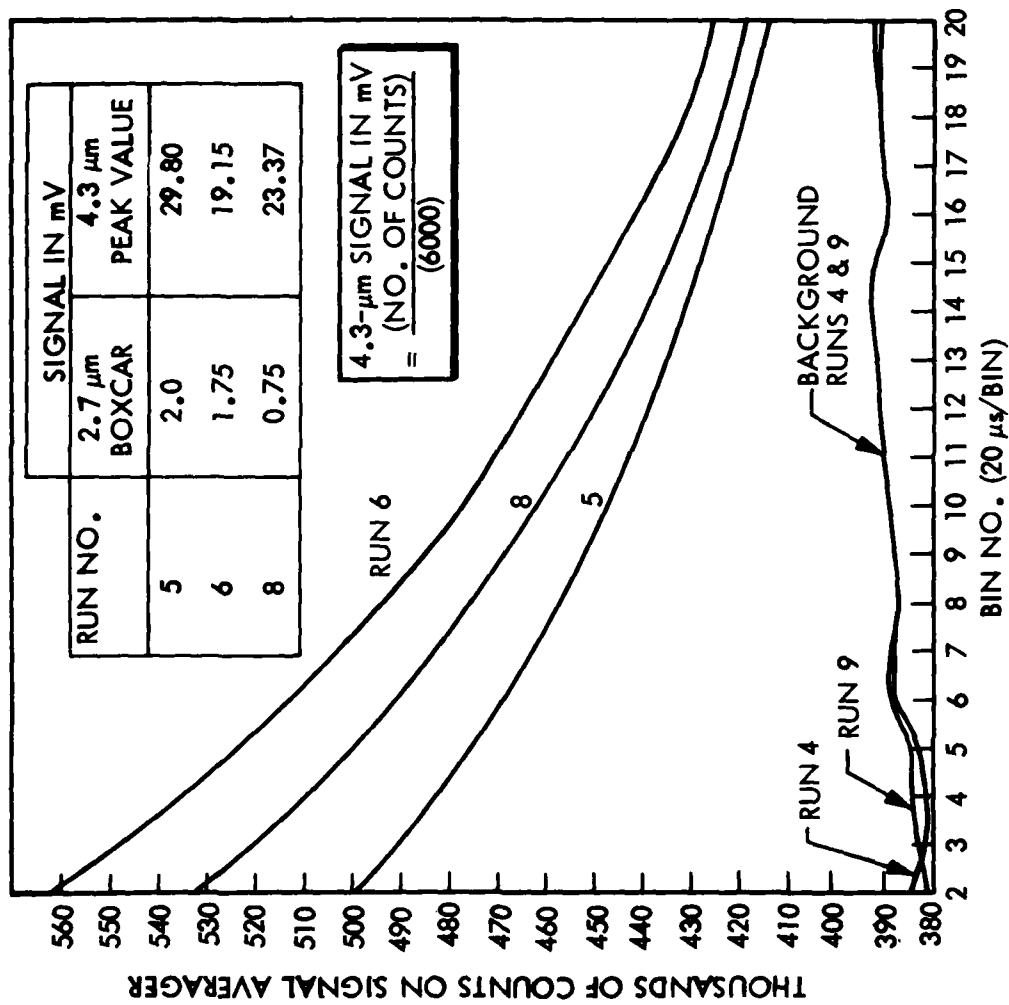


Fig. 2-17 Branching Ratio Data

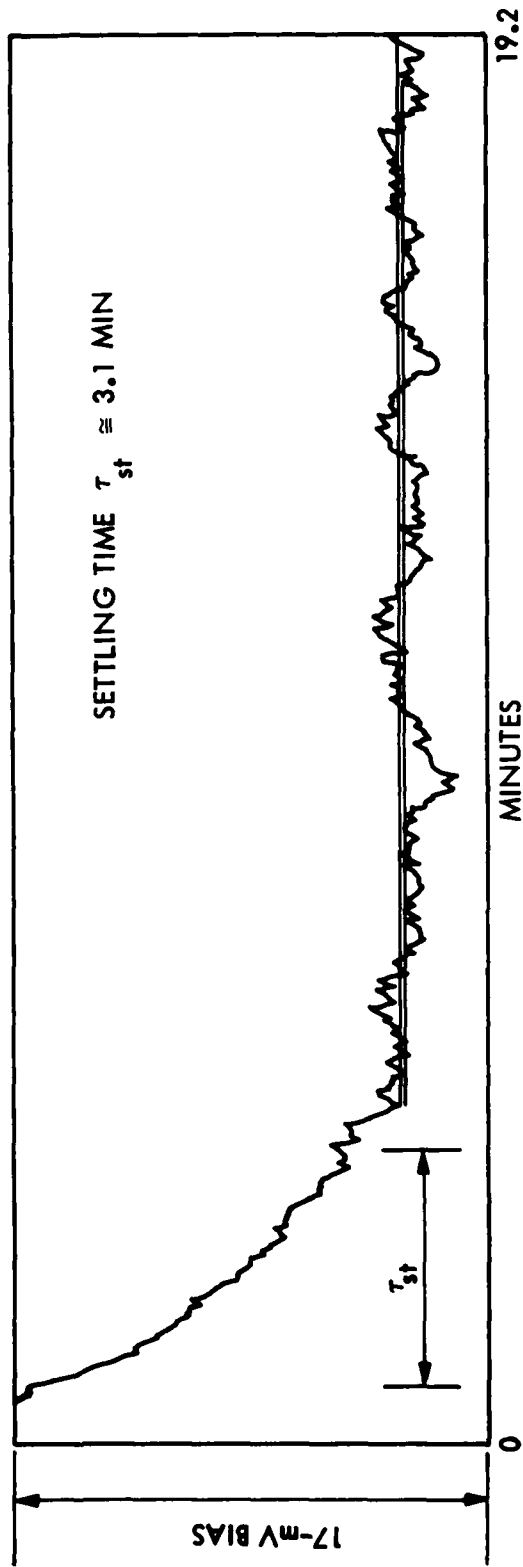


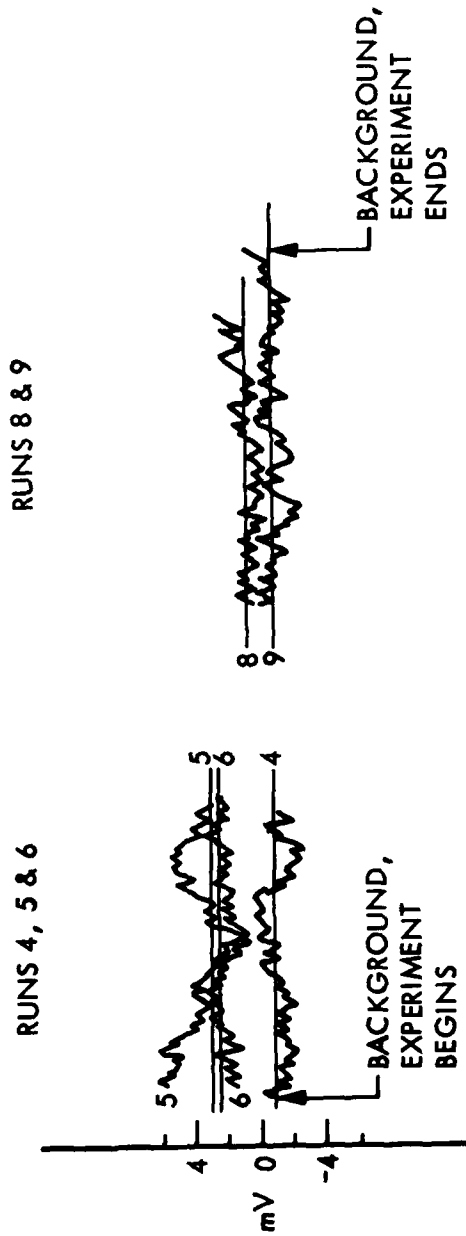
Fig. 2-18 Illustration of Boxcar Settling Time and Stability

Figure 2-19 shows the boxcar outputs obtained after 2048 pulses from the laser. The values for the 2.7 μm signal are taken from the average value in the last three minutes of each run. While the signal to noise in these runs is rather poor, there is no doubt that the boxcar signals corresponding to 2.7 μm fluorescence are real as can be seen by comparing runs in which fluorescence was observed with runs in which there was no fluorescence.

The factors which are required to calculate the branching ratio are summarized in Figure 2-20. The relative response of the 2.7 and 4.3 μm detectors was determined using an infrared industries blackbody source to compare the two detectors at both wavelengths. The relative response also takes into account the different load resistors used for each preamplifier and the response ratio refers to the voltage responsivity to a given number of photons. The gain used for measuring the 2.7 preamplifier signal was a factor of 5 greater than that at 4.3 μm .

The factor of $1/3$ in the relative transmission of the 2.7 and 4.3 μm bands has been mentioned previously. Finally the resulting boxcar signal at 2.7 μm is reduced from the peak 2.7 μm signal by an amount which depends on the distance (in time) away from the laser pulse and the width of the window. This is the last factor shown in the second line of Figure 2-20.

Figure 2-21 shows the branching ratios calculated for the three data sets shown previously. The uncertainties indicated are due to the noise obtained in the boxcar signals. The average value of the branching ratio obtained is ~ 17.7 . Due to the scatter in the data and the limited amount of data, this is not a very precise number. It is clear, however, that a large fraction of the radiative decay of the 101 level is via the emission of



BOXCAR X-Y OUTPUT ON 3.5 MINUTE INTERVALS

Fig. 2-19 2.7 μ m Signal for Runs 5, 6, & 8, and Background Runs 4 & 9

$$(\text{SIGNAL AT } 2.7 \mu\text{m}) = C \times (\text{SIGNAL AT } 4.3 \mu\text{m}) \times \frac{1}{\text{BR}}$$

$$C = \left(\frac{R_{2.7}}{R_{4.3}} \right) \left(\frac{G_{2.7}}{G_{4.3}} \right) \left(\frac{T_{2.7}}{T_{4.3}} \right) \left(\frac{e^{-t_1/\tau} + e^{-t_2/\tau}}{2} \right)$$

BR = BRANCHING RATIO

$$\text{RELATIVE RESPONSIVITIES} \frac{R_{2.7}}{R_{4.3}} = 4.09$$

$$\text{GAIN} \frac{G_{2.7}}{G_{4.3}} = (500/100)$$

$$\text{FILTER TRANSMISSION} \frac{T_{2.7}}{T_{4.3}} = (1/3)$$

$$\text{BOXCAR WINDOW } t_1 = 70 \text{ \& } t_2 = 120 \mu\text{s}$$

$$\tau = 43 \mu\text{s AT } P_{\text{CO}_2} = 0.005 \text{ TORR}$$

● RESULT _____ C = 0.88

Fig. 2-20 Summary of Data Reduction

$$2.7\text{-}\mu\text{m SIGNAL} = (4.3\text{-}\mu\text{m SIGNAL}) \frac{(0.88)}{\text{BR}}$$

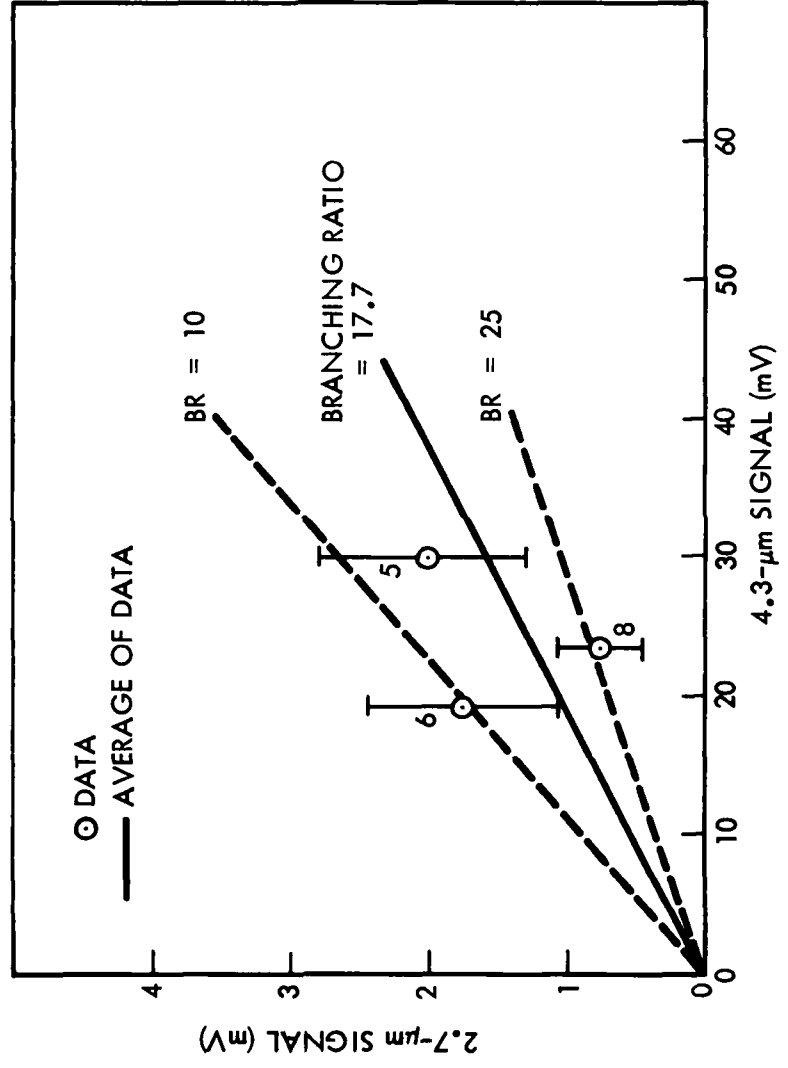


Fig. 2-21 2.7-μm Signal Versus 4.3-μm Signal

4.3 μm radiation rather than 2.7 μm radiation. From this figure it appears that the branching ratio favoring 4.3 μm emission over 2.7 μm emission can safely be said to be greater than 10.

3.0 DATA EVALUATION

3.1 FIELD DATA EVALUATION

3.1.1 Motivating Data

The zenith spectral radiance data measured in the interval 4.5 to 4.6 μm on 12 March 1975 by a rocket borne SWIR CVF spectrometer which was launched into an aurora are shown on Figure 3-1 (Stair, 1977). A sample CVF spectrum (Stair, 1977) obtained at 100.6 km on the upleg on 12 March 1975 is shown on Figure 3-2. A comparison of this data with a synthetic spectrum that is calculated on the basis of a mechanism in which the only radiating specie is CO_2 is shown on Figure 3-3. The CO_2 synthetic spectrum shown on Figure 3-3 is calculated by methods developed by Kumer (1977), Kumer and James (1977) and Kumer et al. (1978). A CVF resolution element (units μm) $\Delta\lambda = 0.01506 \lambda + 0.0545$ (Tom Condron, private communication 1977) was used in the computation of the synthetic spectrum. The spectral comparison indicates that CO_2 is not the emitting specie that is responsible for the data in the 4.5 to 4.6 μm region.

The 4.5 to 4.6 μm data on Figure 3-1 clearly show a maximum at altitude $z = 100$ km. The corresponding 3914 \AA data which are shown on Figure 3-4 (Stair, 1977) do not even show a hint of such a maximum occurring near 100 km altitude. We would expect that prompt auroral emission would resemble the 3914 \AA radiance profile if the emitting specie is optically thin, however comparison of the data in Figures 3-1 and 3-4 shows that this is not so. This dissimilarity is evidence that prompt emission by an optically thin species, such as NO^+ , is probably not responsible for the emission in the 4.5 to 4.6 μm region.

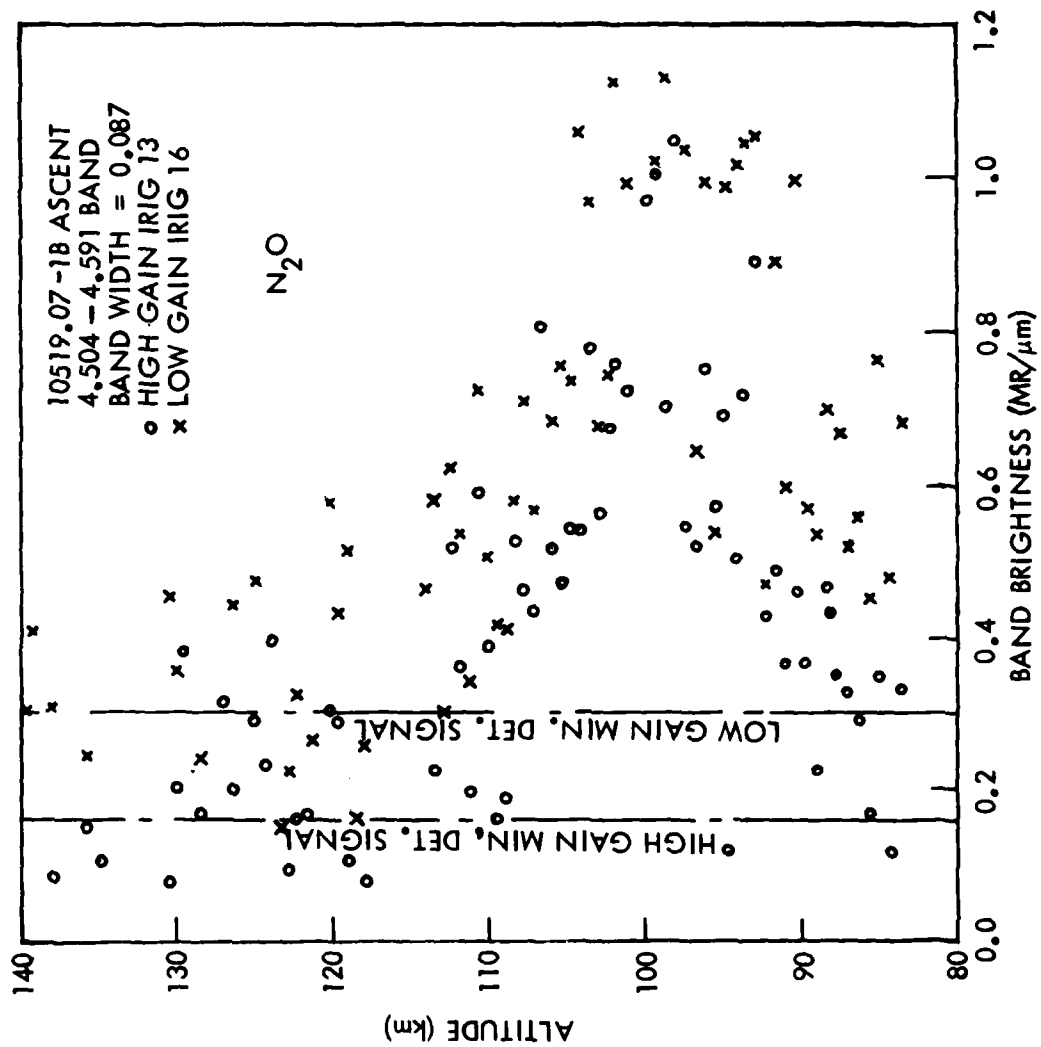


Fig. 3-1 Apparent Auroral (3-12-75) Data near 4.55 μm (A. T. Stair, 1977)

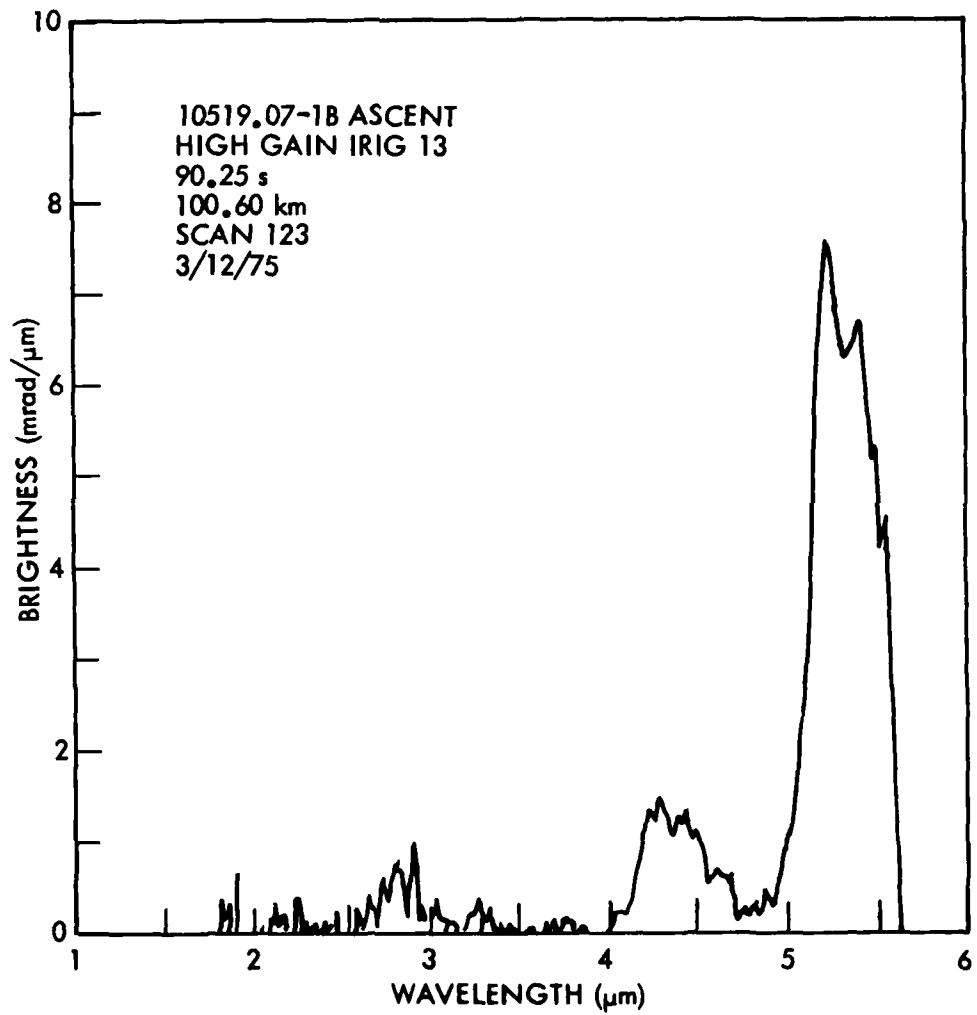


Fig. 3-2 Sample (3/12/75) Auroral Spectrum (A. T. Stair, 1977)

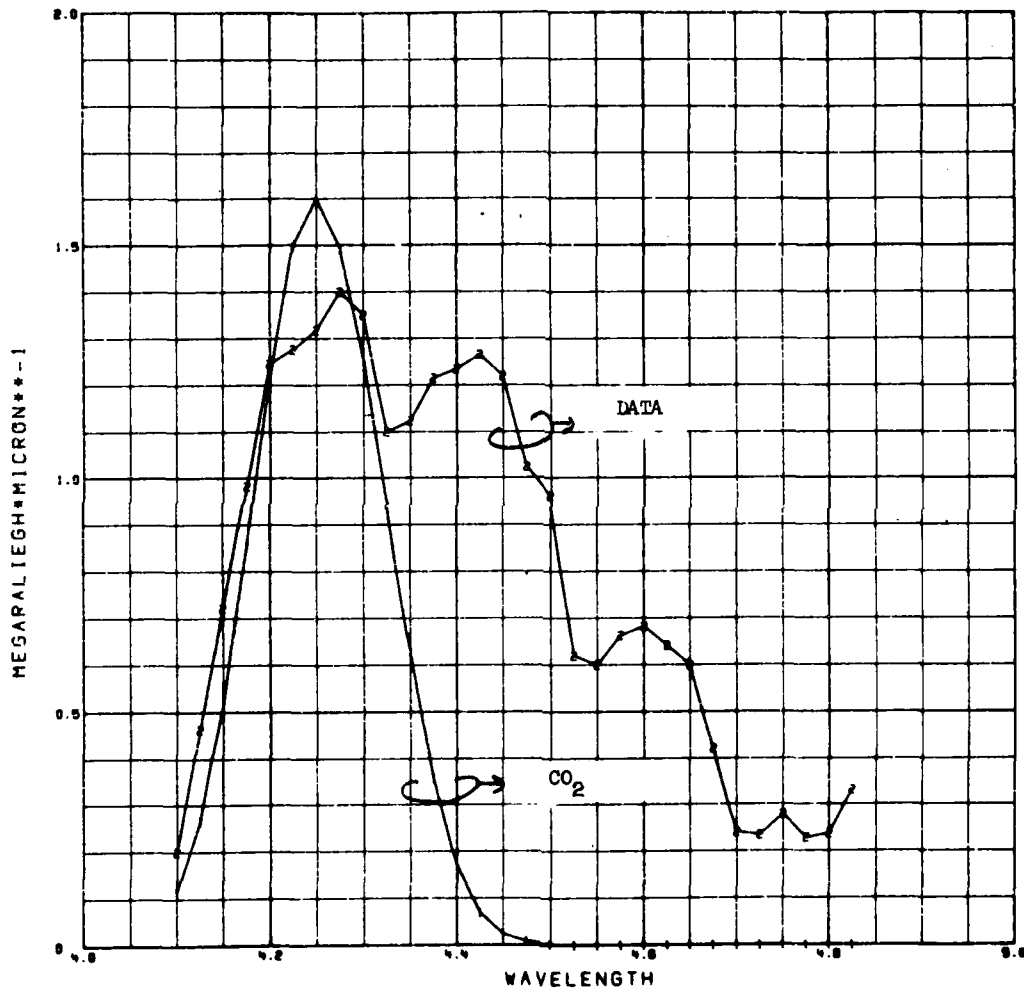


Fig. 3-3 Compare Data and CO₂ Emission at 100 KM

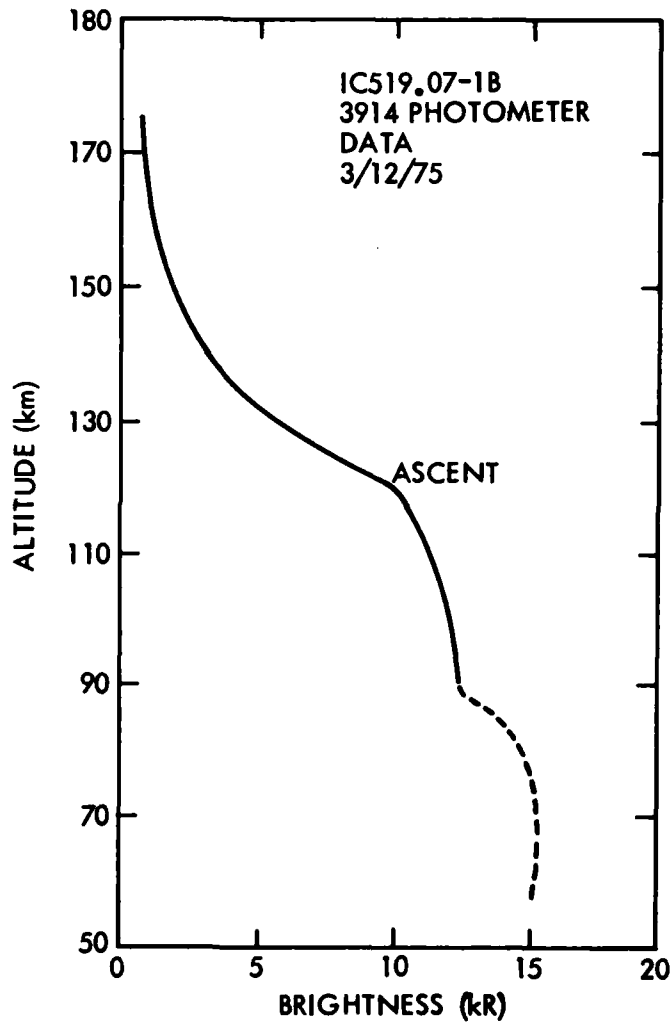
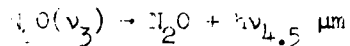


Fig. 3-4 Altitude Dependence of 3914A Zenith Radiance obtained 3-12-75 (A. T. Stair , 1977)

One might also postulate that a mechanism such as



followed by



might account for the data in the 4.5 to 4.6 μm region. The radiance profile near 4.3 μm that was also obtained on 12 March 1975 by the CVF is shown on Figure 3-5. It is fairly well established that this data is dominated by CO_2 emission and that the excitation is provided by vibrational transfer from vibrationally hot N_2 , via



which is analogous to process (3-1) above. The conclusion is that if the data on Figure 3-1 are the result of process (3-1), and if the atmospheric N_2O is optically thick below 100 km as is required by the data on Figure 3-1, then the altitude dependence of 4.3 μm data should resemble that of the 4.55 μm data which are shown on Figure 3-1. This is not the case, strongly suggesting that the process (3-1) is not responsible for the 4.55 μm data that are shown on Figure 3-1.

3.1.2 Approach

Initial consideration of the MWIR CVF spectral data and of the 3914 \AA photometer that were obtained 12 March 1975 suggest that a puzzling auroral feature near to 4.55 μm , which appears to be real although it had not been readily observed in previous CVF data of somewhat lower resolution, is probably not the result of emission by CO_2 , by NO^+ , by N_2O which is excited by process (3-1),

IC519.07-18

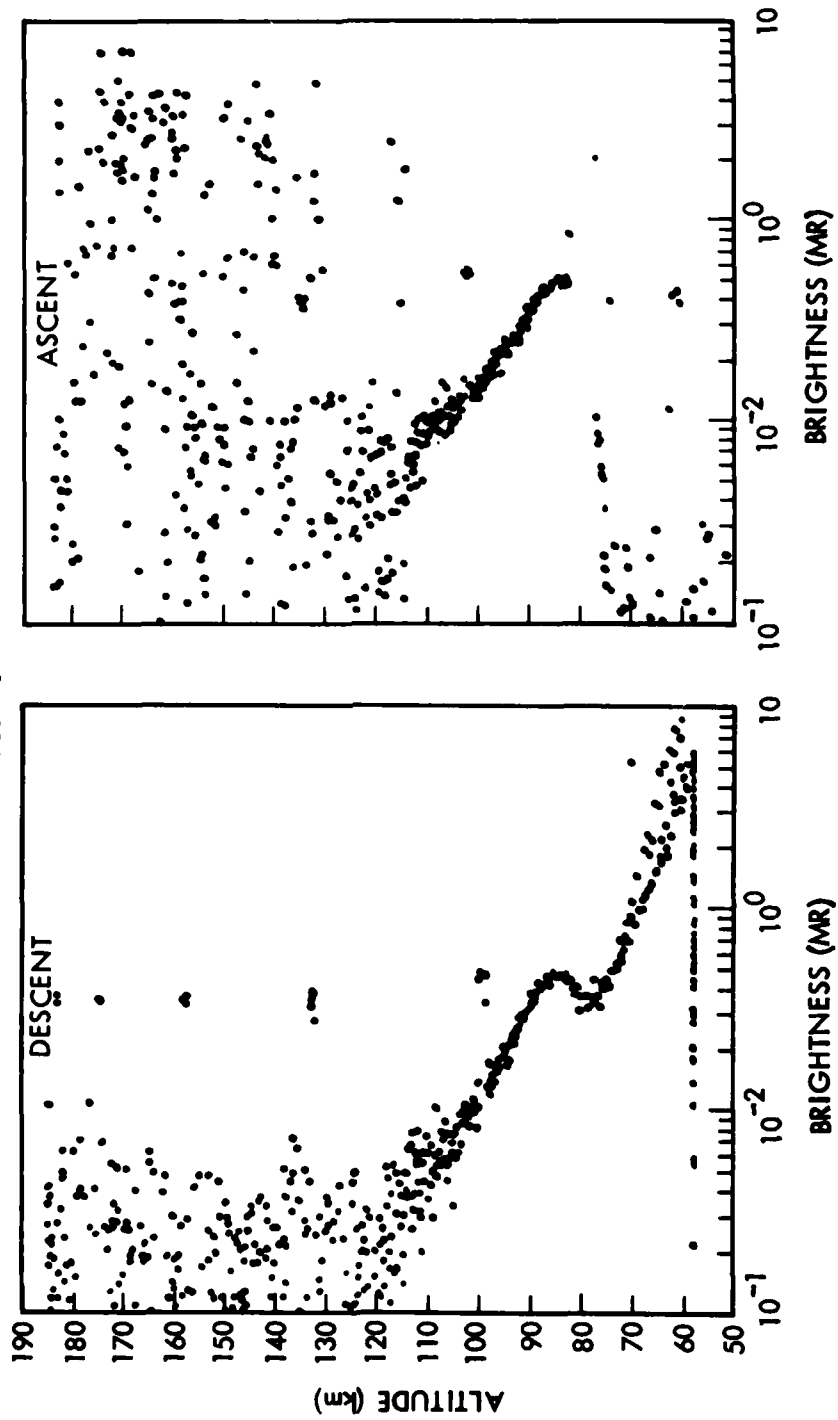


Fig. 3-5 4.3 μ m Data Obtained 3-12-75 (A. T. Stair, Private Communication)

or by CO or any other specie excited primarily by a process similar to (3-1), namely vibration transfer from vibrationally hot N_2 . However, consideration of the 4.5 to 4.6 μm radiance altitude profile shown on Figure 3-1 and of the 3914 Å radiance altitude profile shown on Figure 3-4 suggests that a prompt auroral excitation of a species that emits near 4.55 μm , and for which the atmosphere is optically thick below ≈ 95 km, might explain the data obtained near 4.55 μm on 12 March 1975. The optically thick requirement is driven by the existence of the maximum near 100 km in the 4.55 μm zenith radiance data, such a maximum would occur in the zenith radiance profile of a prompt emission if there is appreciable absorption below 100 km. In this task our goal is to thoroughly explore this postulate, to test consistency and to establish the constraints such a postulate imposes on the 12 March 1975 CVF data in particular, and on other infrared data obtained, or scheduled to be obtained, under the AFGL/DNA auroral measurement program in general. The approach was to include the two candidate emitters N_2O and CO into our model for computing ambient and auroral MWIR synthetic spectra (Kumer and James, DNA 4409F, HAES Report No. 70). Previously just CO_2 had been included as the radiating specie in the model.

We also considered the species NO^+ and $^{14,15}N^+N$ which might also emit close to 4.55 μm , but our initial decision was to exclude them from the model for the time being. The specie NO^+ is rejected since the high altitude ($Z \geq 80$ km) atmosphere is optically thin for NO^+ 4.3 μm radiation. The point is that if the emission mechanism near 4.55 μm is prompt (as is thought to be the case for NO^+) then it must require that the 4.55 μm emission originate from a specie for which the atmosphere is optically thick in the altitude region $80 \leq Z \leq 100$ km in order to produce the maximum that is observed in the

4.55 μm data on Figure 3-1 but that is not observed in the optically thin 3914 \AA data on Figure 3-4. The specie $^{14}\text{N}^{15}\text{N}$ is rejected on the basis of Bunker's (1973) calculation for the HD vibrational oscillator strength f_{12} and the fact that the $^{14}\text{N}^{15}\text{N}$ oscillator strength $f_{(14)(15)}$ should scale like $f_{(14)(15)} \approx (1/14)^4 f_{12}$ implies a radiative lifetime of ≈ 30 years for vibrationally excited $^{14}\text{N}^{15}\text{N}$. The Russian authors Gordiets, et al. (1976) use ≈ 50 sec for the radiative lifetime of vibrationally excited $^{14}\text{N}^{15}\text{N}$ in their calculations of upper atmospheric infrared radiance. We believe the 30 year figure derived from Bunker's paper and data for the HD oscillator strength is by far the more realistic of the two numbers, however it would be useful to reinforce this theoretically based belief with some firm laboratory data. For now we will proceed on the basis that the 30 year radiative lifetime for $^{14}\text{N}^{15}\text{N}$ vibrational decay is closest to reality in which case $^{14}\text{N}^{15}\text{N}$ cannot be an important MWIR emitting specie in the upper atmosphere.

The basic ingredients of our spectral model prior to inclusion of N_2O and CO are illustrated by the block diagram on Figure 3-6. The inputs N_j and f_j refer to the altitude dependent optical depths and to the fractional upper state excitation populations for the set of CO_2 bands which are listed on page 8 of the report (Kumer, DNA 4260 F, HAES Report No. 57). The calculation of the N_j and f_j is also discussed in the report DNA 4260F. In order to include N_2O and CO into the model it is necessary to calculate the appropriate $N_{j'}$ and $f_{j'}$ for each specie ($j' = N_2O$ or CO).

Calculation of $N_{j'}$ is trivial, it requires knowledge of the spectral parameters and reasonable models for the atmospheric number density distributions of the species N_2O and CO . The N_2O and CO mixing ratio models that we used in the study are shown on Figure 3-7. The model for CO was deduced by J. W. Waters et al from their microwave data (Science 191, 1174, 1976). The model for N_2O is selected (1) to provide the absorption between 100 km and 85 km that is required by the $4.55 \mu m$ data shown on Figure 3-1 and, (2) to join smoothly at lower altitudes to the N_2O mixing ratio that was recommended by the NASA UARS scientific working group (Banks et al., 1978). Adequate spectral information on N_2O and CO line positions and strengths can be obtained from the McClatchey tape described by McClatchey et al. (AFCRL-TR-73-0096, 1973).

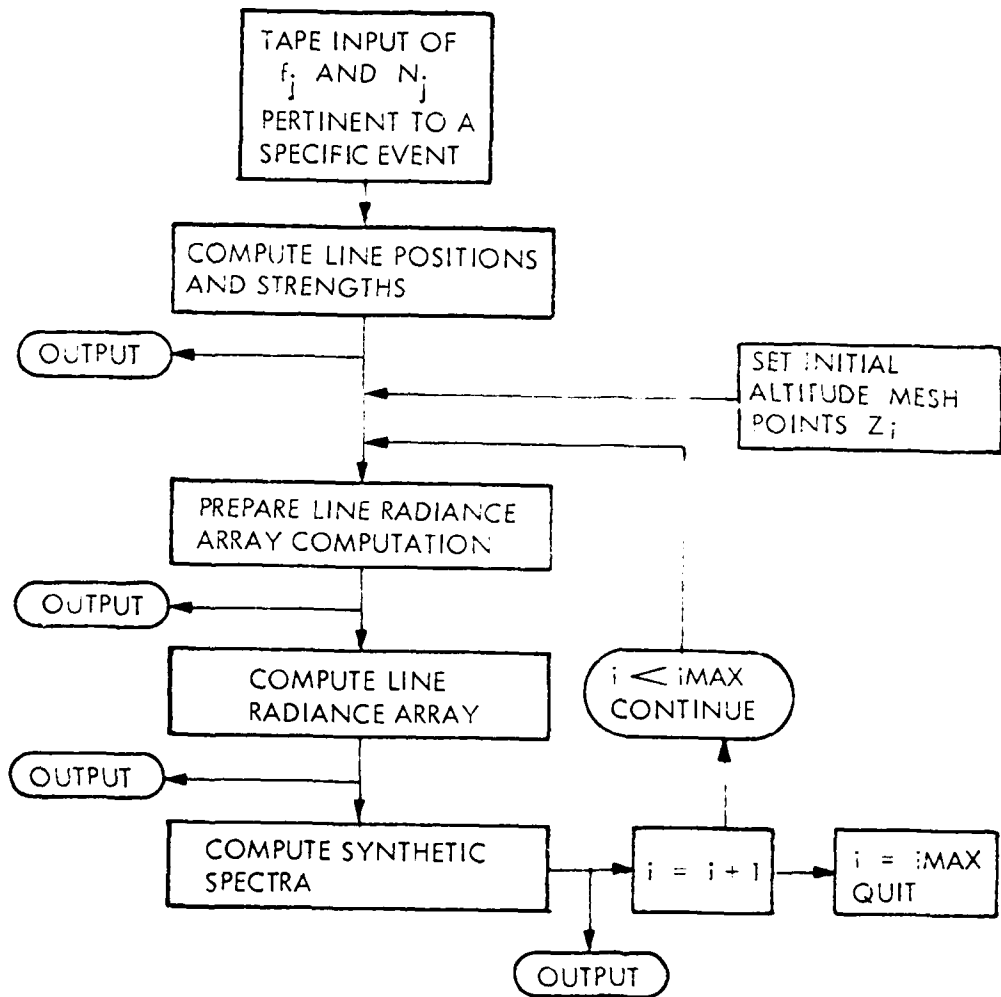


Fig. 3-6 A schematic of our model for predicting CO_2 $4.3 \mu\text{m}$ spectral zenith radiance.

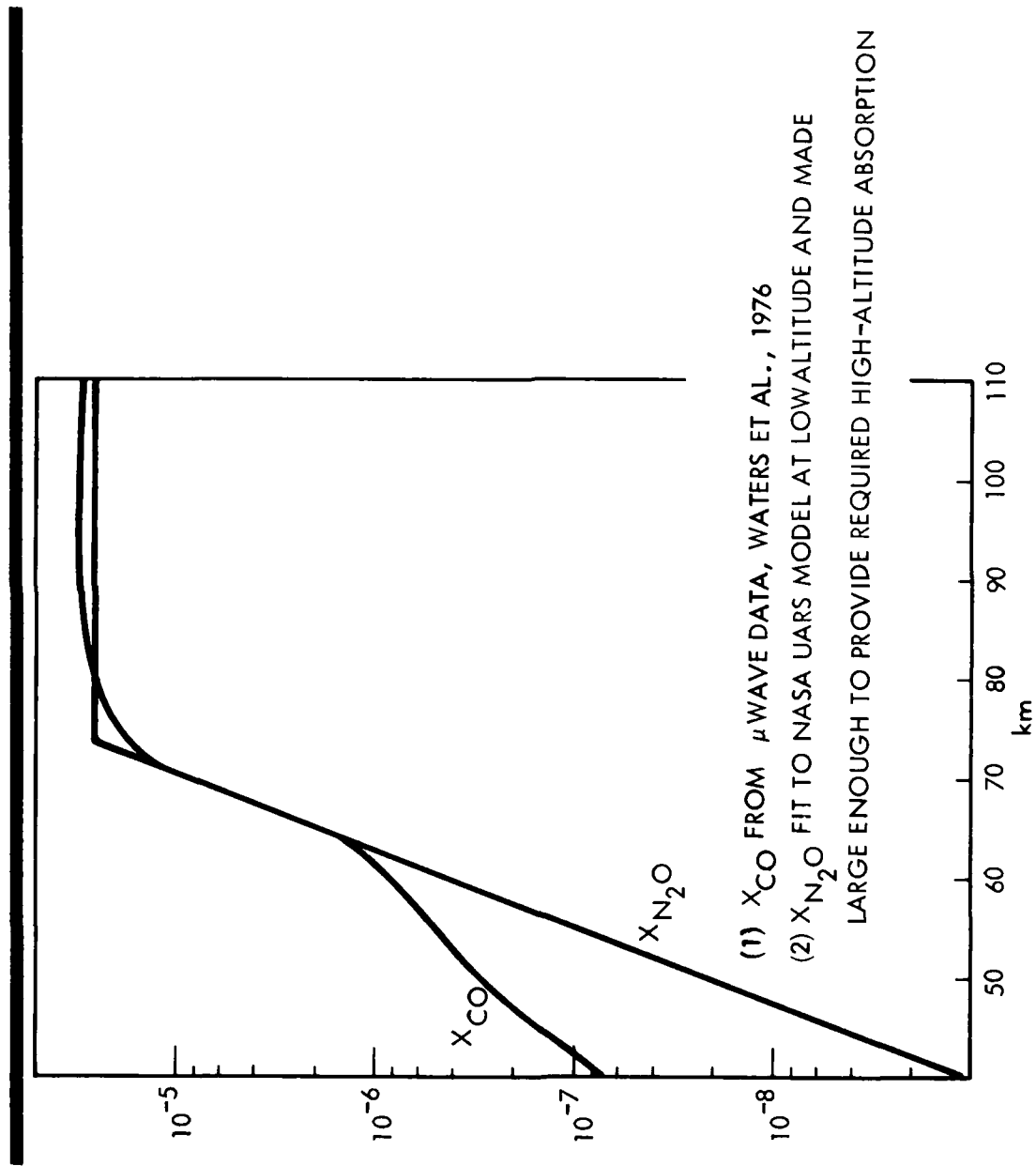


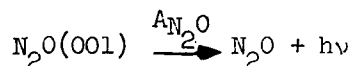
Fig. 3-7 Model CO and N₂O Mixing Ratios

The calculation of the fractional excitation $f_{j'}$ of $N_2O(v_3)$ and $CO(v=1)$ is accomplished by mathematically treating emission in the bands of N_2O and CO similar to that in the weak $CO_2 v_3$ bands. This treatment is given by Kumer (1977) and is also shown on page 9 of the report DNA 4260F. An obvious modification of the Qw approximation, which is also discussed in these references, is also utilized.

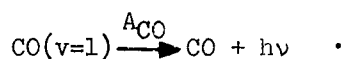
The specific modification to Qw is obtained by adding the terms

$$\sum k'_{2j'} [j'] (A_{j'} E_{j'} + k_{1j'} [M]) / (A_{j'} E_{j'} + k_{1j'} [M] + k_{2j'} [N_2])$$

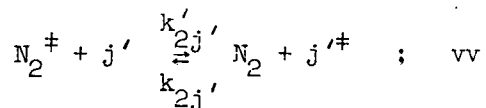
to the right hand side of Eqn. (5) in the paper by Kumer (1977). The sum is over $[j'] = [N_2O]$ and $[CO]$. The quantities $A_{j'}$ are the Einstein coefficients for spontaneous emission



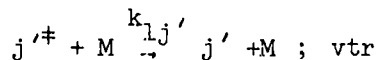
and



The $E_{j'}$ are the escape functions for these photons (see Kumer, 1977; and Kumer and James, 1974). The rates $k'_{2j'}$, $k_{2j'}$, and $k_{1j'}$ are defined by



and by



where M is O_2 or N_2 or O or H_2O , etc. These rate constants may be found in the review by R. M. Taylor (1974), except for some of the k_{1N_2O} , for these we use the corresponding rate constants for CO_2 .

The solution f_j' is given (directly analogous to Eqn. (8) in the paper by Kumer, 1977) by

$$f_j' = (k_{2j}, [N_2] f_N + \eta_j) / (k_{2j}, [N_2] + k_{1j}, [M] + A_j, E_j) \quad (3-3)$$

where the inhomogeneous term η_j is the direct excitation of $N_2O(001)$ or $CO(v=1)$. Some detailed discussion of potential candidate direct excitation mechanisms is given below.

Finally, the modification to the inhomogeneous term η_{NQW} for excitations of N_2^+ in the QW approximation is obtained by adding the terms

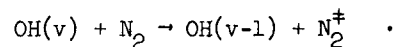
$$\Sigma [j'] F_{Nj'} \eta_j'$$

to the right hand side of Eqn. (7) in the 1977 paper by Kumer, where the $F_{Nj'}$ is given by

$$F_{Nj'} = \left(\frac{k_{2j}, [N_2]}{k_{2j}, [N_2] + k_{1j}, [M] + A_j, E_j} \right) \frac{[j']}{[N_2]}$$

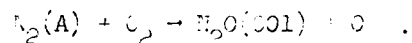
3.1.3 Excitation Mechanisms

Three mechanisms were considered. First, an ambient mechanism which includes thermal collisions, absorption of earthshine and excitation by vibrational transfer from N_2^+ that is vibrationally excited by the OH airglow (Kumer et al., 1978; Kumer, 1976) via the vibration transfer process



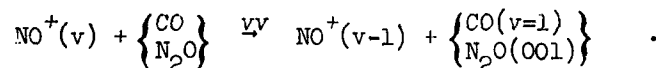
Second, a slow auroral mechanism, namely transfer of vibrational excitation from N_2^+ that is vibrationally excited by auroral precipitation. The slow auroral excitation of N_2^+ is modeled on the basis of R. D. Sears' (1976) ground based scanning photometric measurements of the spatial and temporal variation in the auroral blue (4278 Å) and red (6300 Å) emissions. These measurements were obtained continuously through the experiment on 12 March 1975 and were begun many minutes prior to launch time. Details of the photometric data and the method (Blue Red Input Model, BRIM) for using these data in order to predict the altitude distribution of N_2^+ are given in a previous report by Kumer (DNA 4260F, HAES No. 57, 1976). Third, a prompt auroral mechanism, selected with magnitude sufficient to produce an altitude profile of radiance near 4.55 μm that is generally similar to that shown on Figure 3-1. The altitude distribution of the prompt volume emission is set approximately proportional to that of the 3914 Å emission as determined from the data on Figure 3-4. Absorption below 100 km that is necessary to form a maximum near 100 km, similar to what is observed in the 4.55 μm zenith radiance data near 100 km, is the natural result of the model atmospheric mixing ratios X_{N_2O} and X_{CO} that are shown on Figure 3-7.

Comment on the possible physical basis of the hypothetical prompt auroral mechanisms is in order. By comparing the data shown on Figures 3-1 and 3-4 and remembering that the auroral fluorescence efficiency for producing 3914 Å radiation is approximately 5.7×10^{-5} , one can estimate that a production of approximately 0.4 $N_2O(001)$ per ionization event would be sufficient to explain the magnitude of the radiance in the 4.5 to 4.6 μm region as the result of prompt excitation of $N_2O(001)$ followed by $N_2O(v=0) \rightarrow N_2O + hv$. From the presentation by Caledonia (1977) one might hypothesize that the mechanism for prompt auroral $N_2O(001)$ production could be the reaction



The $N_2O(001)$ must be thermalized kinetically and rotationally if the atmosphere for $Z \leq 100$ km is to be optically thick for N_2O emission as is suggested by the data on Figure 3-1 if N_2O is indeed the emitter responsible for these data. Such a mechanism might also account for a formation rate of N_2O in the continuously dark polar winter atmosphere that is fast enough to maintain $X_{N_2O} \approx 2 \times 10^{-5}$ at $Z \approx 85$ km. In a static situation formation of N_2O must balance N_2O loss which is due to mechanisms such as solar photo-dissociation and reaction with $O(^1D)$. Both of these loss mechanisms are suppressed by the lack of sunlight.

Another potential prompt mechanism that might apply to some extent to both CO and N_2O was suggested by R. D. Sharma (1979) in a recent conversation (1 March 1979), namely



The vibration transfer rate constant would need to be extremely large, of the order 10^4 larger than for the reaction $\text{NO}^+(v) + \text{N}_2 \rightarrow \text{NO}^+(v-1) + \text{N}_2^{\ddagger}$ for example, in order that this be a serious possibility. We feel this is unlikely, however laboratory and/or theoretical studies to obtain at least an order of magnitude estimate for these rate constants are probably warranted, especially since the mechanism also might be pertinent to the apparent lack of unequivocal evidence of any major NO^+ contribution to emission near $4.3 \mu\text{m}$ in auroral data that have been analyzed to date.

The $4.3 \mu\text{m}$ data shown on Figure 3-5 may be used to verify that the ambient and slow auroral modeling is realistic. If $4.3 \mu\text{m}$ data can be modeled adequately then we are assured that we have a realistic model for the altitude dependence of the f_{N} that results from the two mechanisms; N_2^{\ddagger} excitation by vibration transfer from principal infrared airglow emitting specie $\text{OH}(v)$, and N_2^{\ddagger} excitation by auroral precipitation. We have seen in Eqn. (3-3) above that it is necessary to know f_{N} in order to calculate emission by N_2O or CO . The results that are obtained by modeling the $4.3 \mu\text{m}$ data are shown on Figure 3-8. Three CO_2 $4.3 \mu\text{m}$ mechanisms are considered, (A) collisions and absorption of earthshine, (B) excitation of N_2^{\ddagger} due to vibration transfer from $\text{OH}(v)$ and, (C) excitation of N_2^{\ddagger} due to auroral precipitation. The modeling of the $4.3 \mu\text{m}$ data as shown on Fig. 3-8 requires a total column vibrational transfer of approximately $0.09 \text{ ergs/sec cm}^2$ from $\text{OH}(v)$ to N_2^{\ddagger} that is peaked at $\approx 85 \text{ km}$, modeling the slow auroral component requires that approximately 16 N_2 vibrational quanta are produced per ionization event.

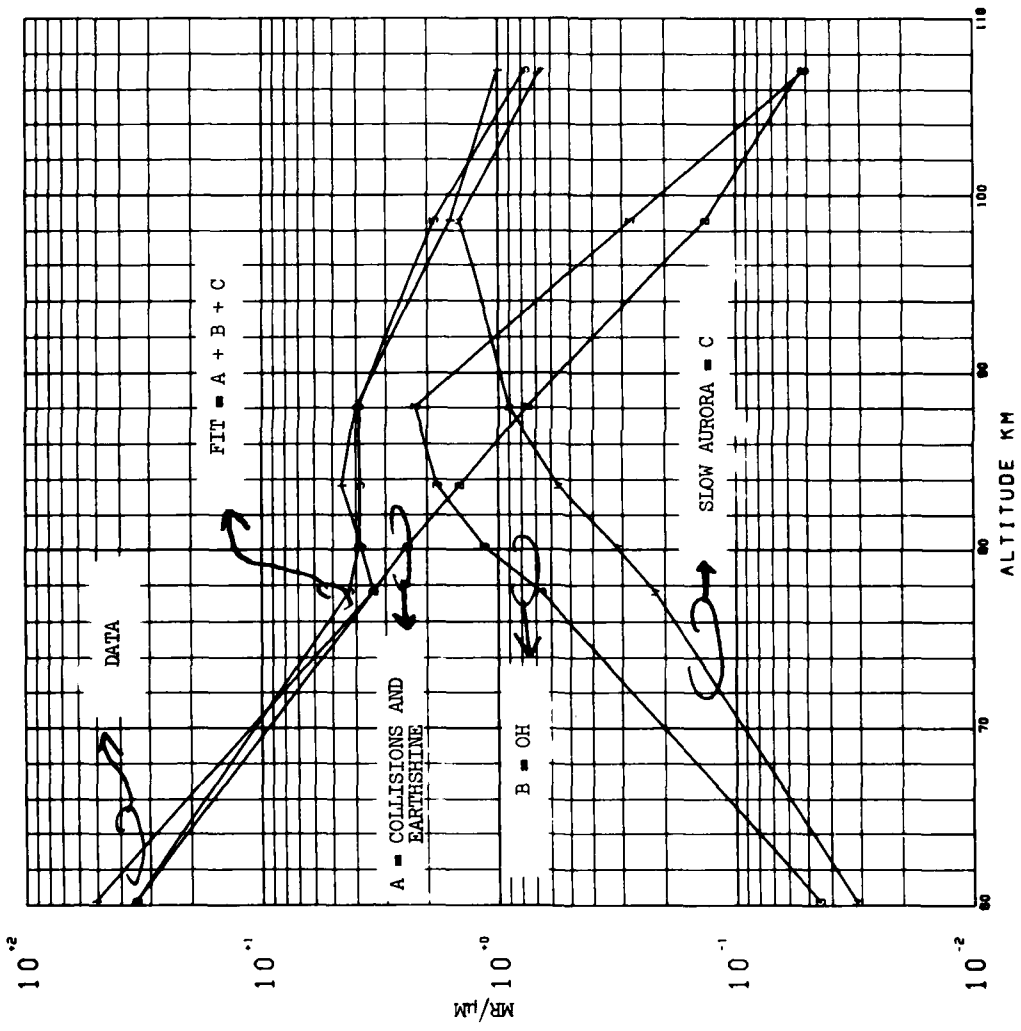


Fig. 3-8 Modeling the CO₂ 4.3 Data

To compute f_j , the fractional excitation of CO($v=1$) or N₂O(001) from Eqn. (3-3) for ambient conditions f_N which pertains for the sum A-B is used and $\eta_j = 0$, for the slow auroral mechanism the computation of f_j utilizes the f_N which applies for curve C and $\eta_j = 0$. for the prompt auroral mechanism $f_N = 0$, and the η_j are selected to achieve a fit to the data that are shown on Figure 3-1.

3.1.- Results

The 4.5 to 4.6 μ m data that were shown previously on Figure 3-1 are reproduced on Figure 3-9 in comparison with calculations of the altitude profile of the peak zenith spectral radiance of N₂O (solid curves) and CO (dashed curves) that are produced by the prompt auroral and by the ambient mechanisms. In either case (N₂O or CO) the prompt auroral component fits the data within reason, however, the presence of N₂O or CO in sufficient quantity to produce the absorption in the 30 to 100 km that the 4.55 μ m zenith radiance data seem to require is necessarily accompanied by an ambient component of zenith radiance which increases rapidly as a function of decreasing altitude as is shown on Figure 3-9. The ambient N₂O and CO zenith radiances that are predicted for the downleg region ($Z \geq 60$ km) on which data were taken are shown on Figure 3-10 in order to further emphasize this point.

On Figures 3-11 through 3-13 we show some comparisons of the spectral zenith radiance data at 100.6 km that were shown previously on Figure 3-2 versus synthetic spectra of CO₂, N₂O and CO. The three different synthetic spectra are calculated for extreme and intermediate assumptions regarding the relative contribution of N₂O and CO. This particular CVF spectral scan

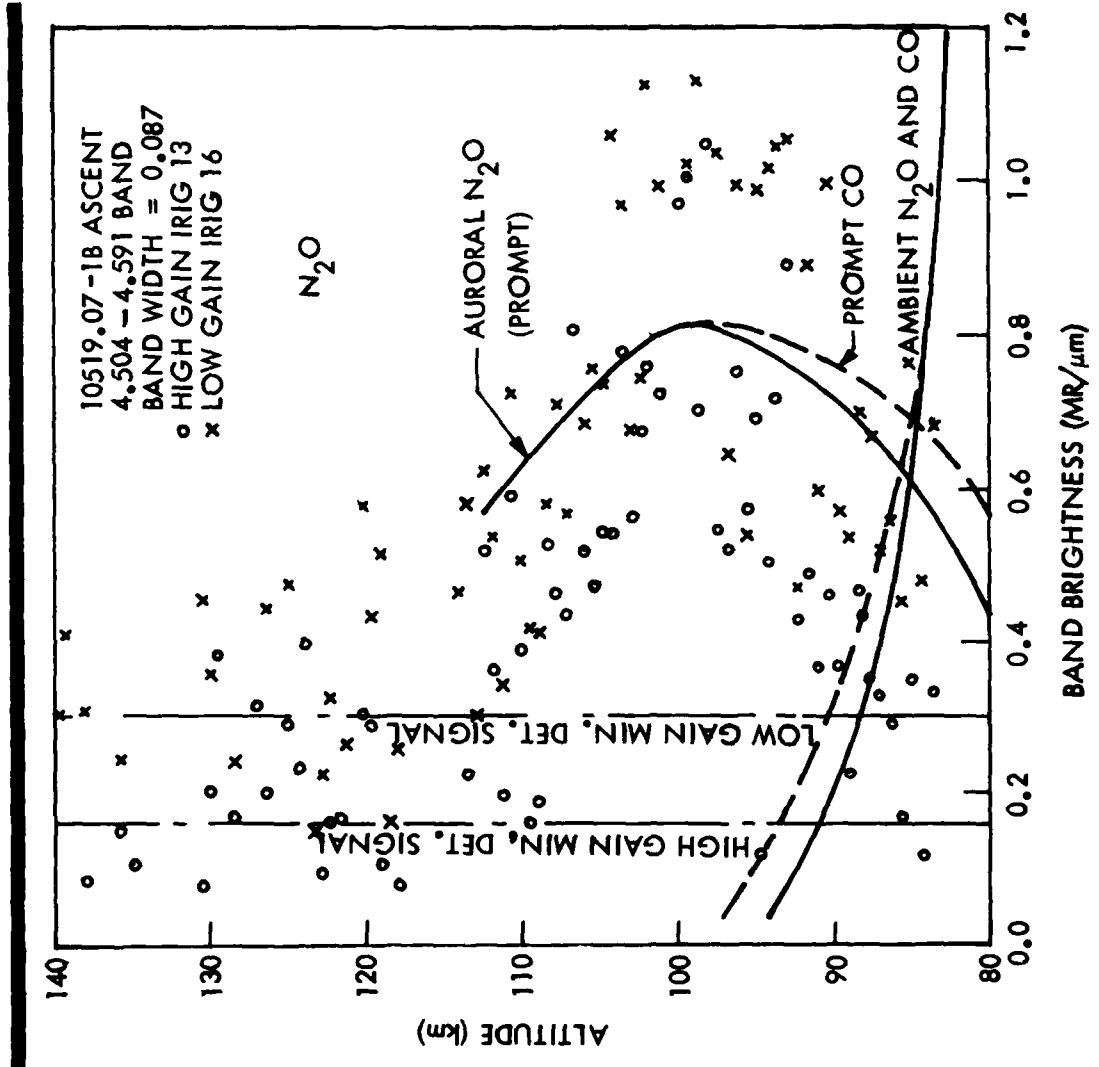


Fig. 3-9 Comparison Against N₂O and CO Models

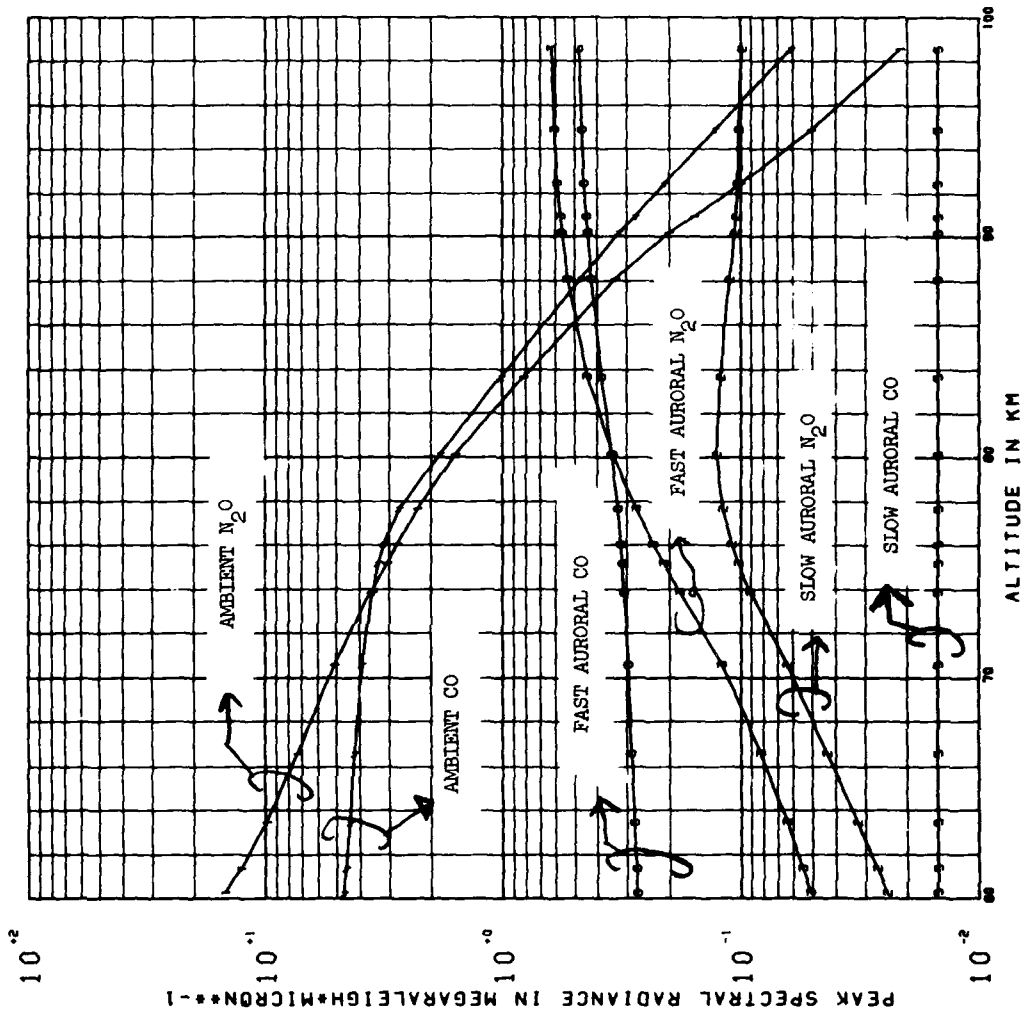
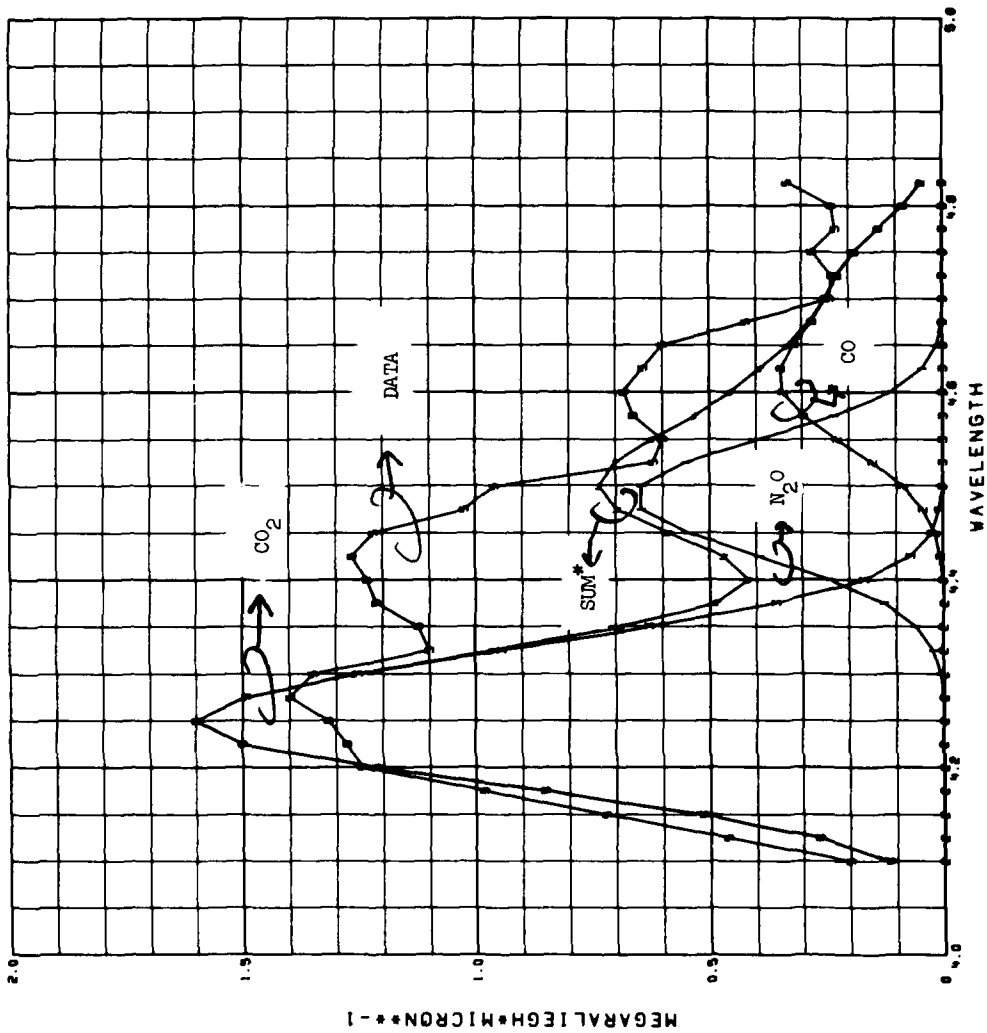


Fig. 3-10 N_2O and CO Peak Spectral Radiance Profiles



*SUM = CO₂ + N₂O + CO

Fig. 3-11 Aurora Blend Mechanism for CO-N₂O-CO₂ Data Fit at 100 km

Z = 100 km ;

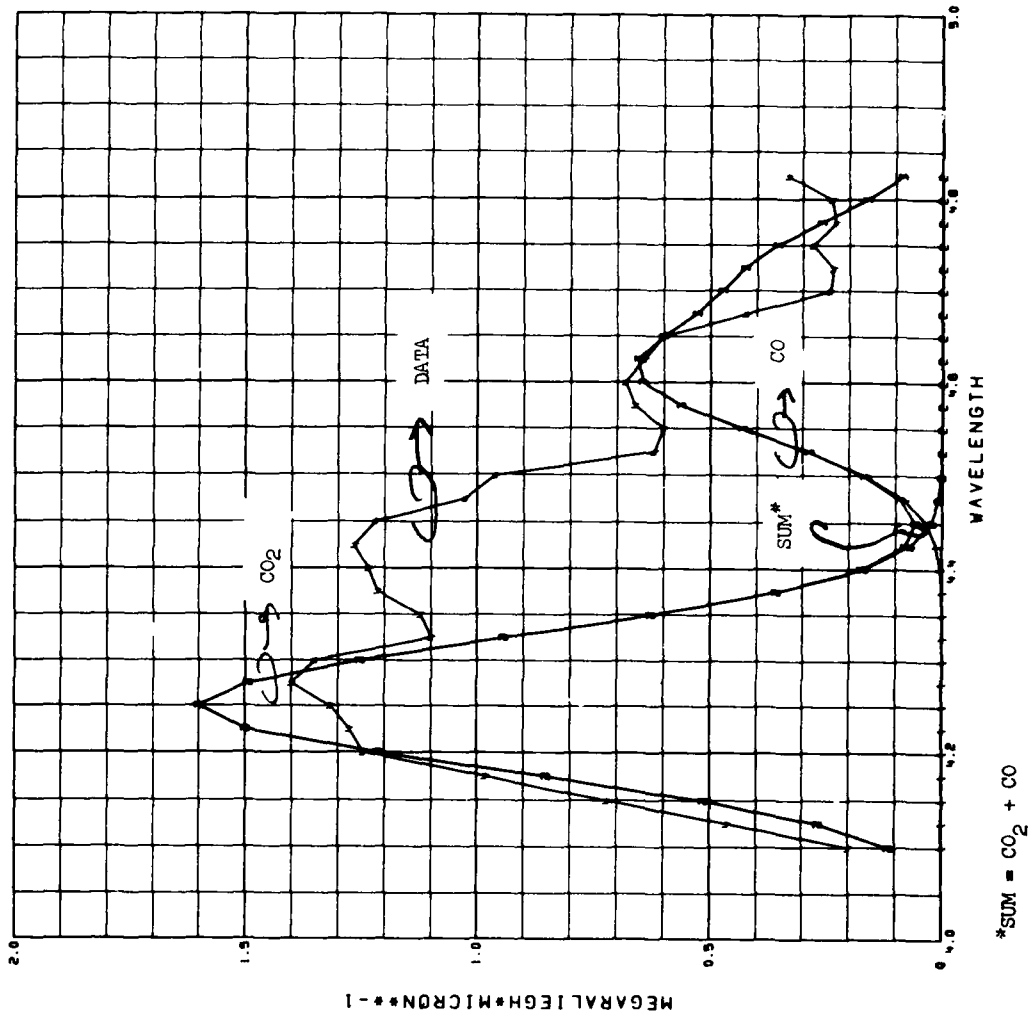


Fig. 3-12 CO₂ and CO

01108554020
0000 0017

Z = 100 km;

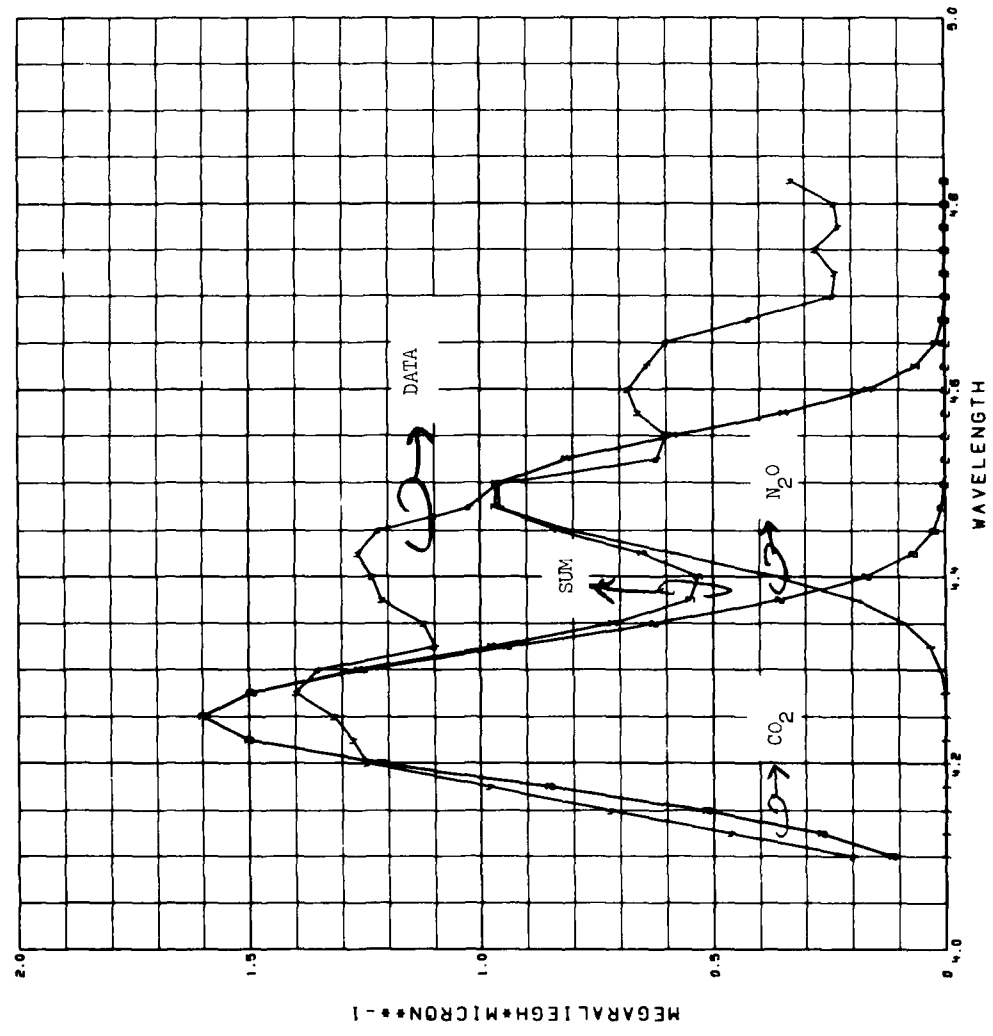


Fig. 3-13 CO₂ and N₂O

might appear to contain 3 distinct features which peak at ≈ 4.27 , 4.42 , and $4.6 \mu\text{m}$. The intermediate calculation shown on Figure 3-11 employs a blend of prompt auroral N_2O and CO components in an attempt to fit the apparent feature near $4.6 \mu\text{m}$, the calculation on Figure 3-12 is an attempt to fit the apparent feature near $4.4 \mu\text{m}$ with emissions by CO_2 and N_2O exclusively, and the calculations that are shown on Figure 3-13 is an attempt to fit the data via the emissions of CO_2 and N_2O exclusively. The feature near $4.42 \mu\text{m}$ cannot be explained in any of the 3 cases under consideration, thus suggesting the presence of an emitter that is not included in the model. The radiance in the 4.5 to $4.6 \mu\text{m}$ range could possibly be a blend of N_2O and CO emission, not necessarily proportioned as shown by Figure 3-11.

On Figures 3-14 and 3-15 are shown the synthetic spectra calculated for 93.66 and 60.6 km altitude. The N_2O and CO components are calculated via the ambient mechanism and would be present in the absence of an aurora if the actual mixing ratios $X_{\text{N}_2\text{O}}$ and X_{CO} are at all similar to those shown on Figure 3-7. It will be necessary to compare these synthetic spectra with the CVF spectral data obtained at altitudes $60 \leq Z \leq 100$ km on 12 March 1975 in order to make a judgement as to how realistic are the models of $X_{\text{N}_2\text{O}}$ and X_{CO} that are shown on Figure 3-7. It should indeed be possible to use these data in order to establish consistent models for $X_{\text{N}_2\text{O}}$ and X_{CO} . Comparison with undisturbed night time SWIR CVF spectral zenith radiance data obtained 11 April 1974 (Wheeler et al., AFGL-TR-76-0262) were not inconsistent with our model for X_{CO} for 12 March 1975 which is shown on Figure 3-7. Sample spectra obtained 12 April 1974 are reproduced

Z = 83.6 km

U1108/SC-0201-
510 0023

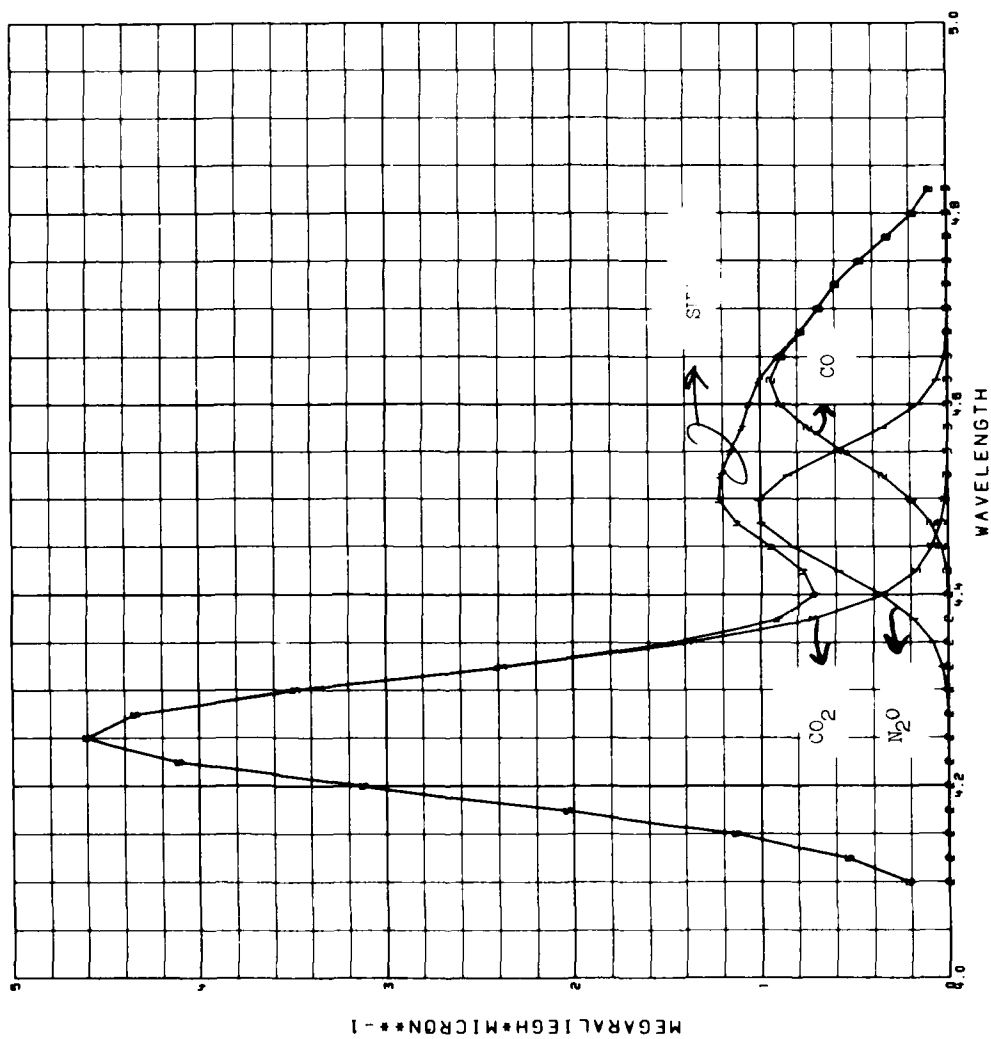


Fig. 3-14a Ambient Mechanism for CO, N₂O, CO₂

Z ≈ 83.6 km

11108/5C402
30 00

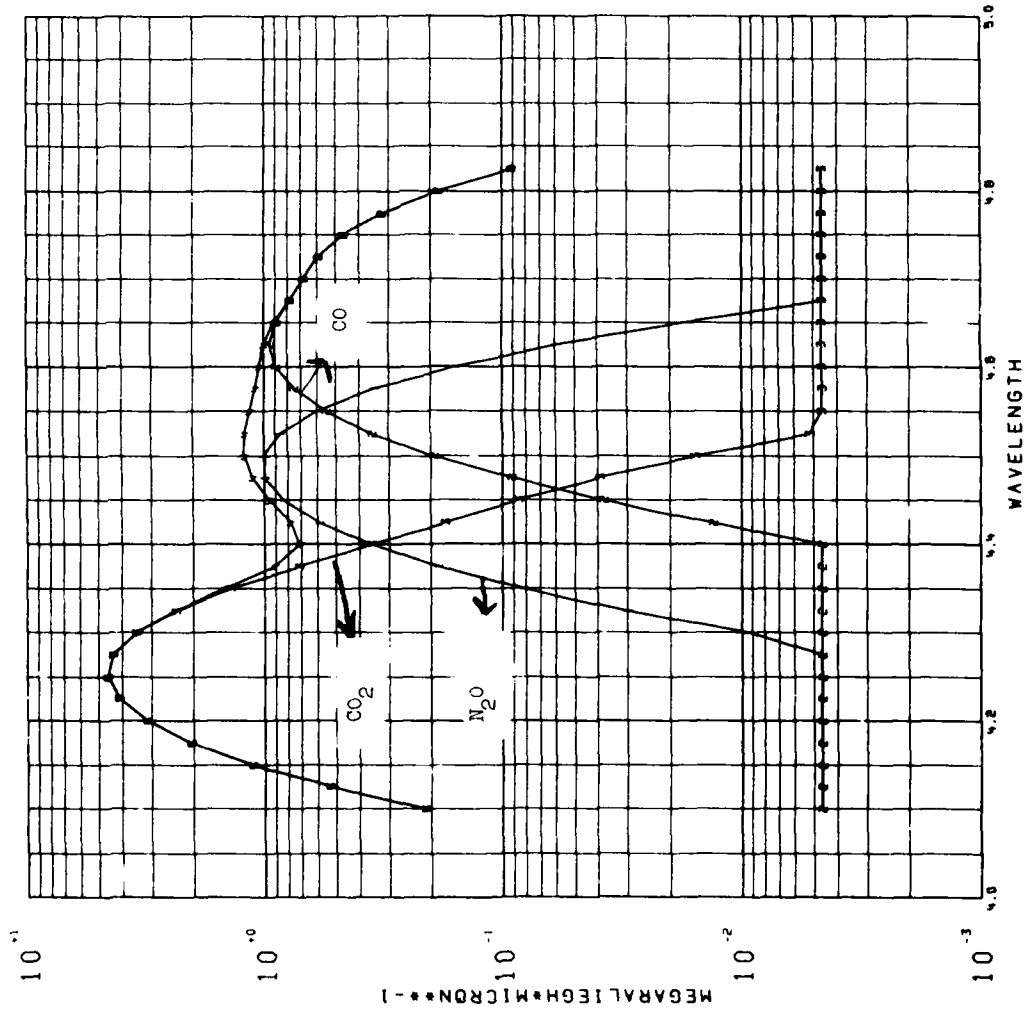


Fig. 3-14b Ambient Mechanism for CO, N₂O, CO₂

Z ≈ 60 km

11 08/50-020-
100 0039

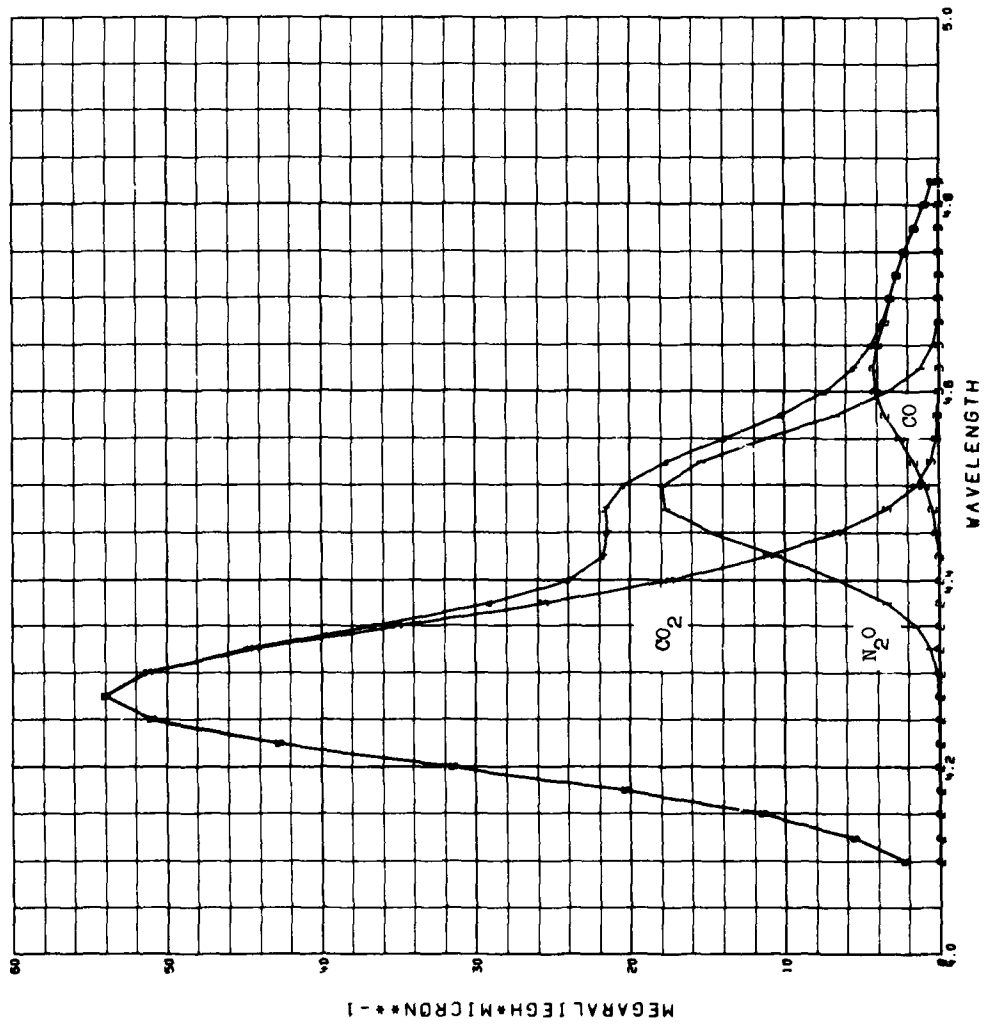


Fig. 3-15a Ambient Mechanism for CO, N₂O, CO₂

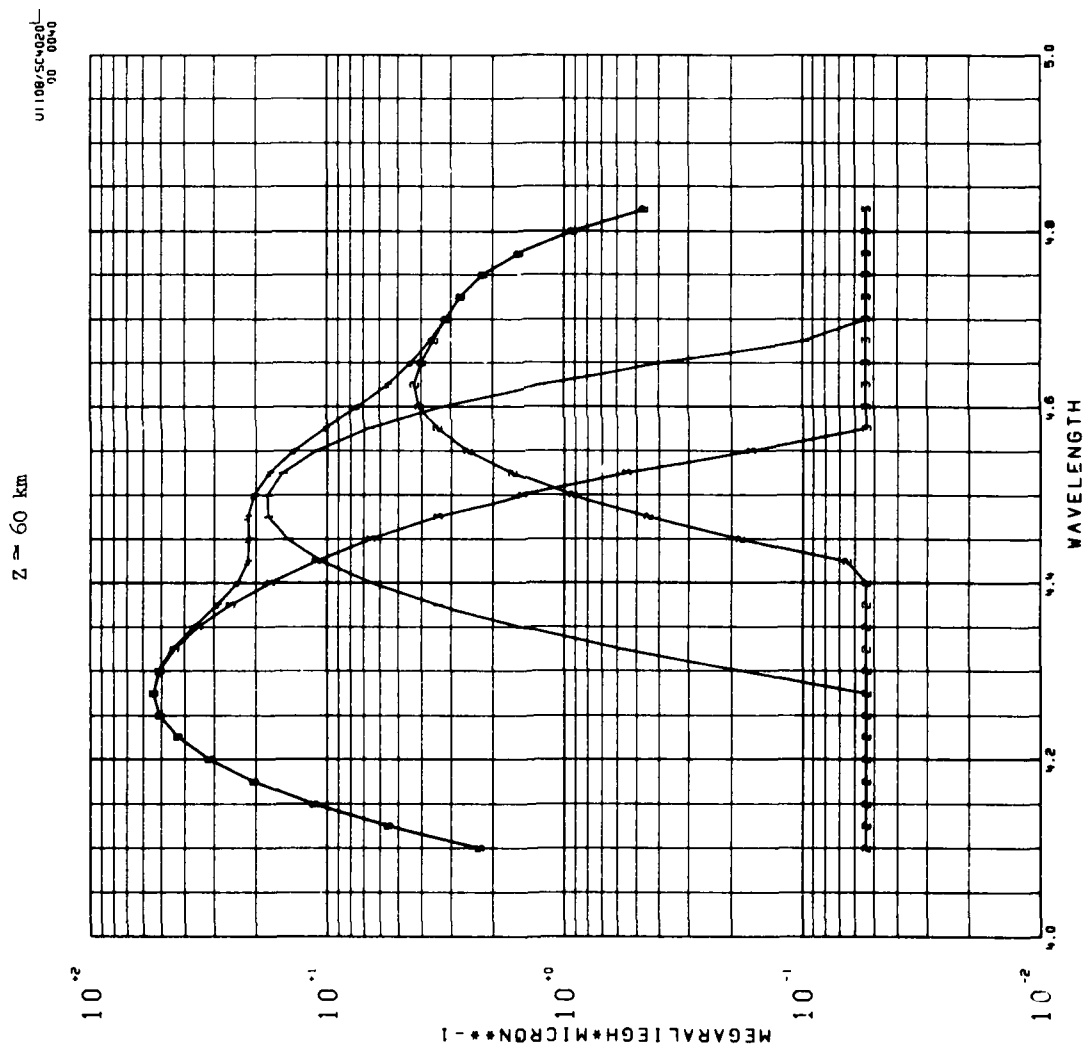


Fig. 3-15b Ambient Mechanism for CO, N₂O, CO₂

on Figure 3-16 for the convenience of the readers. Comparison of the calculations shown on Figures 3-14 and 3-15 with these data would indicate however that X_{N_2O} on 11 April 1974 was much less than in our model for 12 March 1975 which is shown on Figure 3-7. Even this is not inconsistent since the atmosphere above PKR is sunlit for much longer time periods in early April than in early March and, as noted above, this would tend to reduce X_{N_2O} in April with respect to X_{N_2O} in March.

3.1.5 Conclusions and Recommendations

A prompt auroral emission by either CO or N_2O can produce the altitude dependence of auroral zenith radiance data in the 4.5 to 4.6 μm band that were recorded by a rocket borne CVM spectrometer on 12 March 1975 provided that these species are abundant enough in the atmosphere to be optically thick below about 100 km for their vibrational resonance radiations near 4.6 and 4.5 μm respectively. Analysis of a spectral scan obtained at 100.6 km altitude weakly suggests that CO is the more likely candidate. Also, there appeared to be a feature in these data near 4.42 μm that was clearly not due to CO_2 , N_2O , or CO.

The requirement on optical thickness below 100 km is met by CO on the basis of independent ground based microwave data analyzed and reported by Waters and Shimabukuro (1976), on the other hand the large mixing ratio that is required to achieve appreciable optical depth below 100 km needs to be assumed to exist for N_2O . The required large mixing ratios above 85 km for N_2O and CO are found, necessarily, to be accompanied by large ambient lower altitude components of N_2O and CO radiance as the result of

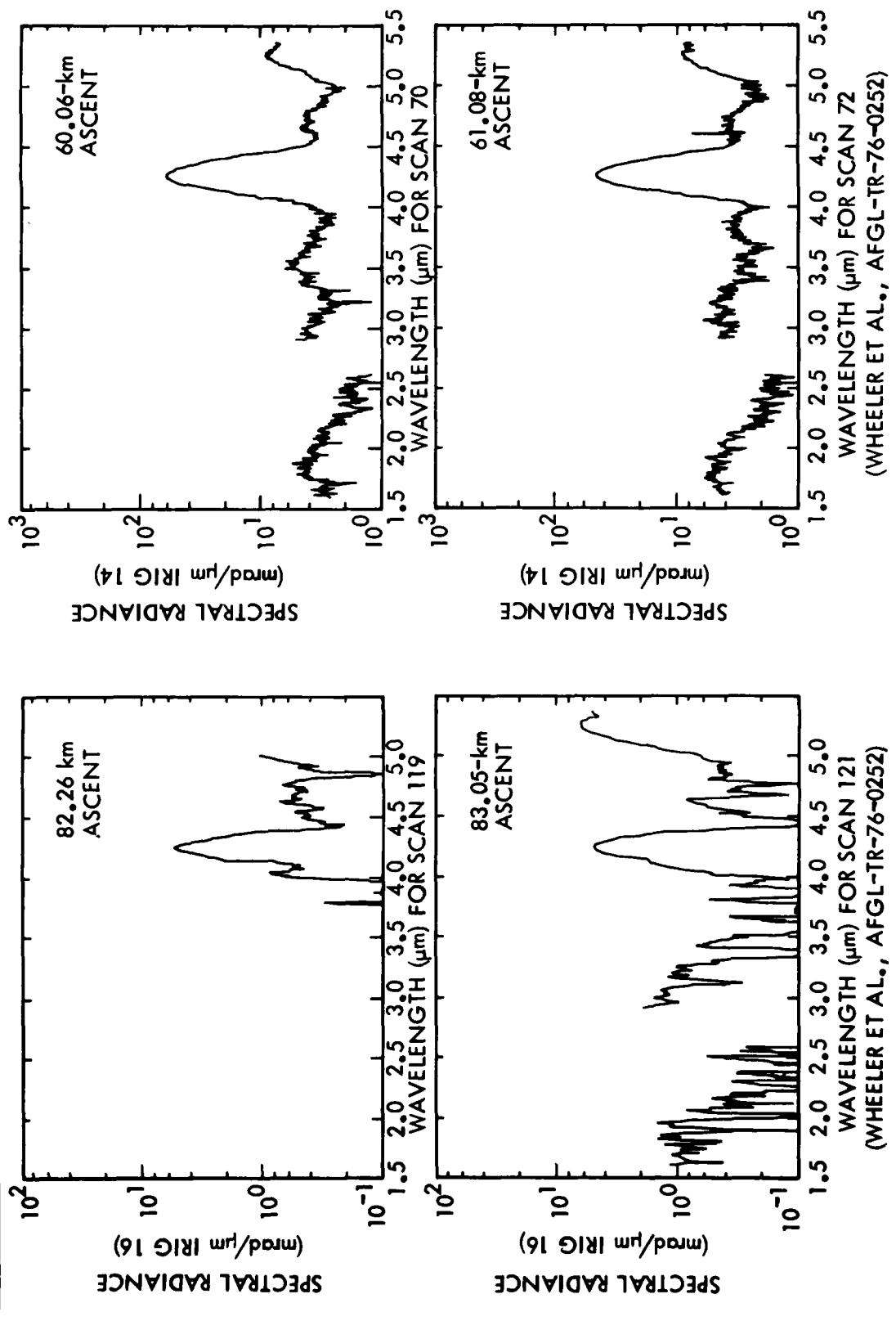
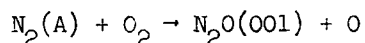


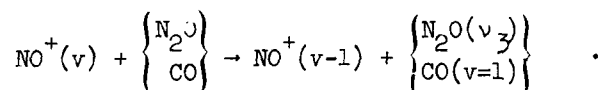
Fig. 3-16 4-11-74 NO Aurora (Wheeler et Al., 1976)

excitation by collisions, absorption of earthshine and vibration transfer from N_2^+ that has become excited by tapping the OH airglow via $OH(v) + N_2 \rightarrow OH(v-1) + N_2^+$. The large predicted ambient N_2O and CO radiances impose severe restraints on the number densities of N_2O and CO that could have actually existed on 12 March 1975. Analysis of a comprehensive amount of the 12 March 1975 CVF data is needed to quantify these restraints, however at this point we can say that major modifications in our assumed model for X_{N_2O} are called for. For CO the case, at this point, is not so clear cut.

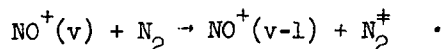
Also, it is somewhat of a puzzle as to what may be a prompt auroral mechanism for producing N_2O or CO emission, candidates are



and



The second mechanism is really very shaky since it must compete with



The vibration transfer process should be more rapid for the molecules N_2O and CO than for N_2 since N_2O and CO have permanent dipole moments while N_2 does not. The question is, can the transfer to N_2O and/or CO be 10^4 times faster than to N_2 so that N_2O and CO can receive a significant fraction of the total NO^+ vibration that is available?

Finally, a question that cannot help but come to mind with regard to the series of features of 4.42, 4.6 μm , and some weaker ones which may also be present at longer wavelengths (but shortward of the NO feature); could these features be a temporary instrumental ringing phenomena that degraded the data on just a very short part of the flight, namely when the rocket was between 80 and 110 km altitude on the upleg?

An analysis of the 4.3 μm data was also performed in addition to the analysis of the 4.5 to 4.6 μm data. This analysis was necessary in order to determine the population of vibrationally excited N_2 so that the contribution to N_2O and CO radiance which results from vibration transfer from N_2 could be calculated. The 4.3 μm data proved consistent with our established model for this wavelength region. In particular a column vibration transfer rate of $0.09 \text{ ergs/cm}^2 \text{ sec}$ from $\text{OH}(v)$ to N_2^+ and an efficiency of 16 N_2 vibrations produced per auroral ionization event was required to model the 4.3 μm data. These numbers are consistent with our understanding of other 4.3 μm data as described in our previous reports.

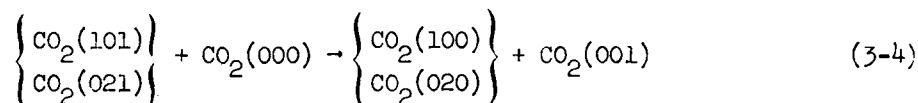
To better understand the 12 March 1975 data in the 4.4 to 4.7 μm region it will be necessary to (1) examine all the 12 March 1975 spectral scans to search for the existence, and if found, to determine the altitude dependence of ambient components of the CO and N_2O radiances in order to quantify the constraints these data place on the N_2O and CO mixing ratios, (2) examine data obtained in other experiments, such as HIRIS and SPIRE for example, in order to determine if the emissions of N_2O and/or CO are present in these data, and if so, to use these data to determine the abundance of N_2O and/or CO in the atmosphere, (3) examine the 12 March 1975

data in more detail in order to see if there is indeed a real feature present in these data near to $4.42 \mu\text{m}$, and finally, (4) include emission by NO^+ into the spectral modeling of data in the 4 to $4.8 \mu\text{m}$ region.

3.2 LABORATORY DATA

3.2.1 Introduction

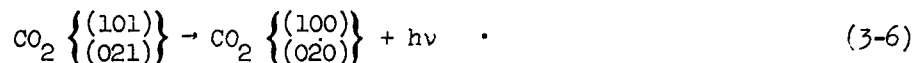
The apparatus, preliminary results, and data evaluation for an initial laboratory verification of the CO₂ 2.7 to 4.3 μm pumping mechanism have been described by James (DNA 4238F, HAES Report No. 60) and by Kumer and James (DNA 4409F, HAES Report No. 70). A sketch of the apparatus used in that experiment is shown on Figure 3-17. The major difference in our initial laboratory fluorescence measurement effort as compared with our current effort is the use of a chopped blackbody 2.7 μm light source in the former as compared with the laser system as described above which is employed in our current effort. The use of the laser allowed us to go to fluorescence cell CO₂ partial pressures about two orders of magnitude less than were employed in the initial effort. In the initial effort



followed by



dominated the direct fluorescence process



Results were published in the report by Kumer and James (DNA 4409F, HAES Report No. 70) and are reproduced here in Table 3-1 for the convenience of the reader. The column labelled R_M is the measured ratio of the 4.3 μm signal S_D^{FA} with fluorescence and absorption cell CO₂ and broadener gas partial pressures as shown in Table 3-1 in comparison to the 4.3 μm signal

Table 3-1

Relative Transmission Measurements

Contents Fluorescence Cell (2 cm path length)	Contents Absorption Cell (1.5 cm path length)	The Data R_M
1/2 Torr CO ₂ + 21 Torr AR	5 Torr CO ₂ + 21 1/2 Torr AR	37 ± 8 %
2 Torr CO ₂	2 Torr CO ₂	69 % ± 3 %
2 Torr CO ₂ + 40 Torr He	2 Torr CO ₂ + 40 Torr He	63 % ± 8 %
1 Torr CO ₂ + 20 Torr He	1 Torr CO ₂ + 20 Torr He	71 % ± 8 %
1/2 Torr CO ₂ + 20 Torr He	1/2 Torr CO ₂ + 20 Torr He	79 % ± 3 %
1 Torr CO ₂ + 40 Torr He	5 Torr CO ₂	60 % ± 7 %
1 Torr CO ₂	1 Torr CO ₂	71 % ± 4 %
7.5 Torr CO ₂	7.5 Torr CO ₂	55 % ± 5 %
1 Torr CO ₂ + 40 Torr He	5 Torr CO ₂	49 % ± 9 %
		@ 400 Hz

Data were obtained at 100 Hz chopping frequency except for the last data case which was obtained at 400 Hz.

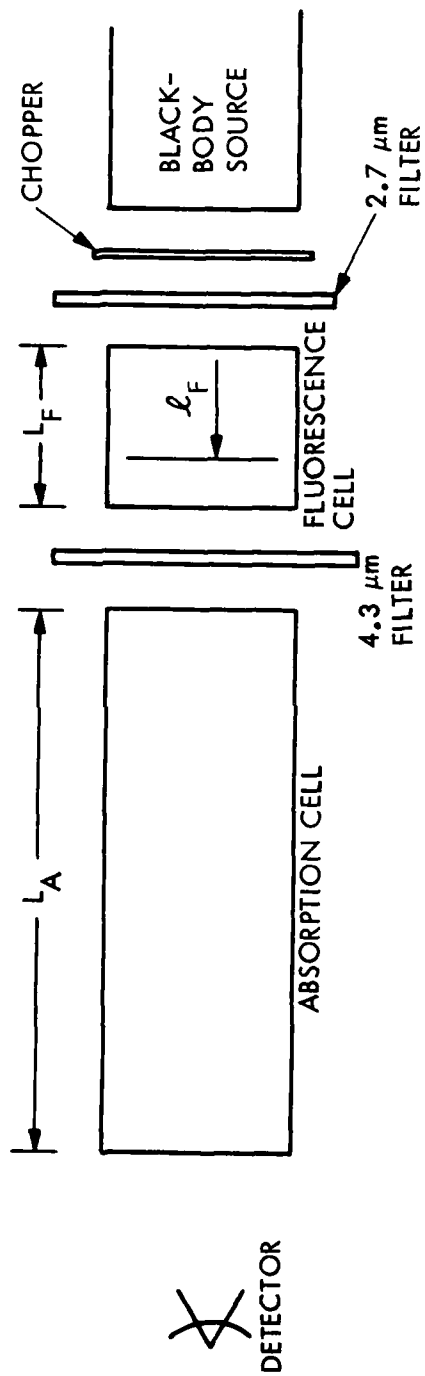


Fig. 3-17 A Schematic of the Apparatus Used in the Initial Laboratory Effort.

S_D^F that is obtained when the absorption cell is evacuated and the partial pressures in the fluorescence cell are again as given in Table 3-1. Earlier analyses of these data (James, DNA 4238F. James and Kumer, DNA 4409F) had employed simple minded radiation transport and the results were quite puzzling in that calculated values of the ratio R_M were consistently smaller than the measured values. This would imply that the process (3-6) was contributing significantly to the signals S_D^{FA} and/or S_D^F . However, this is not consistent with the rapid rate constant ($k \approx 1.1 \times 10^{10} \text{ cm}^3/\text{sec}$) for process (3-4) that has been reported by Finzi and Moore (1975), and furthermore it is not consistent with our analysis (Kumer and James, DNA 4409F) of the variation in signal as a function of chopper frequency that is observed in the initial data.

This effort is aimed at a resolution of these inconsistencies. To this end we

- performed a sophisticated radiation transport analysis of the data that covered the cases of cell wall reflectivity, 0 and 100% (or perfectly black and perfectly reflective)
- investigated the effect of enhanced transmission through the absorption cell that would occur as the result of broadening of the fluorescence cell lines and bands with respect to those in the absorption cell that would occur if the fluorescence cell were hotter than the absorption cell due to its proximity to the hot blackbody source.

- investigated the effects of spatial diffusion within the cell
- considered atmospheric absorption on cell paths external to the cells, and to the evacuated interiors of the blackbody source and of the detector.

On quantitatively accounting for all these effects we still drew a blank in that the calculated values of R_M remained smaller than the measured values. Details of our calculations and some conjecture as to what may remain to be done to resolve the inconsistencies follow.

3.2.2 Detailed Radiation Transport Calculation

Consider the schematic of the apparatus on Figure 3-17, to calculate the 4.3 μm signal at the detector we must calculate the excitation in the fluorescent cell and compute a transmission weighted integral over the resultant 4.3 μm volume emission. The initial excitation $S_o(\ell_F)$ at a point in the fluorescent cell that is designated by ℓ_F is given by

$$S_o = B[\text{CO}_2]_F \sigma_{2.7} T(\ell_F[\text{CO}_2] \sigma_{2.7})$$

where $[CO_2]_F$ is the CO_2 number density in the fluorescent cell. The quantity $\sigma_{2.7}$ is defined in detail by James and Kumer (1973). It is the cross section for absorption of 2.7 μm photons by CO_2 . The transmission function $T(Z)$ is given by

$$T = \sum_{b,j} s_{jb} X_J \int dX e^{-Z s_{Jb} X_J \varphi_F(X, a_F)}$$

where $Z = \ell_F [CO_2] \sigma_{2.7}$, $X_J \cong (2J + 1) e^{-(J/J_0)^2} / \frac{1}{2} J_0^2$ is the fractional rotational population of CO_2 in the state J , $J_0^{-2} = hcB/kT$, $B = 0.4 \text{ cm}^{-1}$ is the rotational constant and $T = 296^\circ K$ the temperature, $s_{Jb} = (J + 1)/(2J + 1)$ and $J/(2J + 1)$ for the 2 branches $b = P$ and Q , X is the photon displacement from line center in units of c fold doppler width, $\varphi_F(X, a)$ is the fluorescent cell Voigt absorption line profile, and $a_F = v_{PF}/v_D$ is the Voigt parameter. The quantity $v_{PF} = (P_{CO_2}^F \gamma_{CO_2} + P_B^F \gamma_B) \times 3 \times 10^{10} \text{ cm/sec}$ the pressure broadened Lorentz $\frac{1}{2}$ line width in units Hz, $P_{CO_2}^F$ and P_B^F the partial pressure in units atm of CO_2 and the broadener gas in the fluorescent cell (either Helium or Argon), $\gamma_{CO_2} = 0.1 \text{ cm}^{-1} \text{ atm}^{-1}$, $\gamma_{He} = 0.04 \text{ cm}^{-1} \text{ atm}^{-1}$ and $\gamma_A = 0.05 \text{ cm}^{-1} \text{ atm}^{-1}$. The quantity B is a constant proportional to the output of the blackbody source. The quantity $\Omega = A_{4,3}/k$ is the branching ratio for emission, the quantity k is the lifetime of the excited CO_2 state, it may be determined as a function of $P_{CO_2}^F$ and P_B^F from data given in our earlier report (Kumer and James, 1977, DNA 4409F).

In case reflection from the cell wall is neglected and the absorption cell evacuated then the signal at the detector N_D^F is given by

$$N_D^F = \int_0^{L_F} dl_F \Omega S_0 (l_F) T((l_F - l_F) [CO_2]_F \sigma_{4,3}) \quad (3-7)$$

AD-A085 724

LOCKHEED MISSILES AND SPACE CO INC PALO ALTO CA PALO --ETC F/G 4/1
FLUORESCENCE EXPERIMENT AND AURORAL DATA EVALUATION TO IMPROVE --ETC(U)
FEB 79 J B KUMER, T C JAMES DNAS001-78-C-0082

UNCLASSIFIED

LMSC/D673384

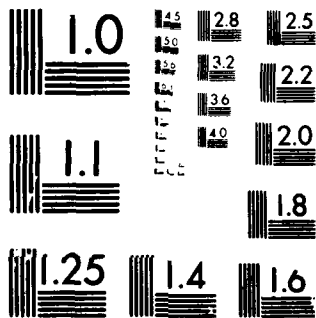
DNA-4906F

NL

2 0 2
AL
2000-00



END
DATE
FILMED
7-80
DTIC



MICROCOPY RESOLUTION TEST CHART
NATIONAL BUREAU OF STANDARDS-1963-A

In case reflection from the walls is neglected and the absorption cell contains concentrations of CO_2 and broadener gas designated by $[\text{CO}_2]_A$ and $[B]_A$, then the signal at the detector is given by

$$N_D^{FA} = \int_0^{l_F} dl_F \Omega S_0(l_F) T_{FA}(l_F) \quad (3-8)$$

where

$$T_{FA} = \sum_{b,J} s_{Jb} X_J \int dx e^{-\tau_{Jb}(x)}$$

where

$$\tau_{Jb}(x) = s_{Jb} X_J (Z_A \varphi_A(x, a_A) + Z_F \varphi_F(x, a_F))$$

where

$$Z_A = L_A [\text{CO}_2]_A \sigma_{4.3}, \quad Z_F = (L_F - l_F) [\text{CO}_2]_F \sigma_{4.3},$$

$$a_A = v_{PA}/v_D \quad \text{and} \quad a_F = v_{PF}/v_D$$

Hence in the case where we assume that reflection of the cell walls is unimportant, we can compute the ratio R of the signal with the absorption empty compared to the signal when the absorption cell is filled via

$$R_N = N_D^{FA}/N_D^F$$

Next we consider the same ratio calculation on the assumption that wall reflection is near unity and cannot be neglected. This assumption is closer to reality and should provide calculated ratio values that are in better agreement with our data than those given by the less realistic calculations (equations (1) and (2)) for N_D^{FA}/N_D^F in which wall reflectivity is neglected.

To account for wall reflectivity calculate the excitation $S(l_F)$ via a plane parallel formulation

$$S(l_F) = S_0 + \int_0^{L_F} dl_F^1 \Omega S(l_F^1) H(|l_F^1 - l_F|) \quad .$$

Since $\Omega \ll 1$ we can safely use the escape function approximation (see Kumer and James, 1974 for a more complete discussion of the escape function approximation) to calculate S , the result is

$$S(l_F) = S_0(l_F) (1 - (1 - E(l_F)) \Omega)^{-1} \quad . \quad (3-9)$$

The escape function $E(l_F)$ is given by

$$E(l_F) = e(l_F) + \epsilon_{FA}(l_F)$$

where

$$e(l_F) = \frac{1}{2} \sum_{b,J} s_{Jb} X_J \int dX E_2(\tau'_{bJ}(X))$$

where

$$\tau'_{bJ}(X) = s_{Jb} X_J l_F [\text{CO}_2]_F \sigma_{4.3} \varphi_F(X, a_F)$$

and

$$\epsilon_{FA} = \frac{1}{2} \sum_{b,J} s_{Jb} X_J \int dX E_2(\tau_{bJ}^{FA}(X))$$

where

$$\tau_{bJ}^{FA} = \tau_{bJ}^F + \tau_{bJ}^A$$

where

$$\tau_{bJ}^F = s_{Jb} X_J (L_F - l_F) [CO_2]_F \sigma_{4.3} \varphi_F (X, a_F)$$

and

$$\tau_{bJ}^A = s_{Jb} X_J L_A [CO_2]_A \sigma_{4.3} \varphi_A (X, a_A)$$

The exponential function E_2 is discussed more completely by Kumer (1977).

In case the absorption cell is evacuated $\tau_{bJ}^A = 0$ and $\epsilon_{FA} = \epsilon_F$. In this case the wall reflection included signal R_D^F is given by

$$R_D^F = \int_0^L dl_F \epsilon_F(l_F) \Omega S(l_F) \quad (3-10)$$

In case wall reflection is included and the absorption cell has CO_2 and broadener gas in it, the signal R_D^{FA} is given by

$$R_D^{FA} = \int_0^{L_F} dl_F \epsilon_{FA}(l_F) \Omega S(l_F) \quad (3-11)$$

The ratio of these wall reflectivity included calculated signals $R_R = R_D^{FA}/R_D^F$ may be compared with the data R_M in Table 3-1.

As mentioned above, the purpose of the measurements R_M was to try to determine if the observed $4.3 \mu m$ radiation was direct fluorescence due to process (I) which is simply

$$\begin{Bmatrix} 101 \\ 021 \end{Bmatrix} \rightarrow \begin{Bmatrix} 100 \\ 020 \end{Bmatrix} + h\nu(4.3 \mu\text{m}) ,$$

or by pure resonance radiation due to the process (II) which is

$$\begin{Bmatrix} 101 \\ 021 \end{Bmatrix} + 000 \rightarrow \begin{Bmatrix} 100 \\ 020 \end{Bmatrix} + 001$$

followed by

$$001 \rightarrow 000 + h\nu(4.3 \mu\text{m}) ,$$

or finally, by process (III)

$$v_1 v_2 1 \rightarrow v_1 v_2 0 + h\nu(4.3 \mu\text{m})$$

summed over all isotopic combinations and over all combinations of CO_2 hot bands. Process (III) requires complete redistribution of the v_3 excitation by the reactions

$$v_1 v_2 1 + v_1' v_2' 0 \rightleftharpoons v_1 v_2 0 + v_1' v_2' 1 .$$

In order to attempt to determine which process is dominant it is necessary to calculate the signals at the detector for the absorption cell evacuated and for the absorption cell containing specified partial pressures $[\text{CO}_2]_A$ and $[B]_A$ of CO_2 and a broadener gas, B, respectively. The ratio of these signals then should tell which of the three processes is dominant. This ratio should be closest to unity for process (I) dominant and it should be smallest for process (III). It is necessary to calculate this ratio for all three processes and then compare these calculated values with the data in order to try to determine which process is dominant.

The results of the calculations R_N and R_R are compared against the data R_M on Table 3-2. It is notable that R_N and R_R are quite similar in all cases, hence reflection and multiple scattering do not appreciably impact the data interpretation. A comparison of the calculations R_R and R_N with the data R_M gives the preliminary indication that a mix between processes I and III provides explanation. As mentioned above, this is inconsistent with the analysis (Kumer and James, Section 2.6 of DNA 4409F, 1978) of the chopper frequency dependence of observed $4.3 \mu\text{m}$ signal. This analysis indicates that process III is completely dominant. It is also not consistent with the very large rate constant ($k \approx 1.1 \times 10^{10} \text{ cm}^3 \text{ sec}^{-1}$) for process (3-4) that was reported by Finzi and Moore (1975), if the rate constant for (3-4) is as large as is claimed by Finzi and Moore, then again, the signal should be dominated by process III.

3.2.3 Other Effects

Since detailed radiation transport and consideration of wall reflectivity did not provide consistency some other effects were examined which might be expected to increase the value of the calculated signal ratio.

Relatively Hot Fluorescent Cell

The first such effect that we considered was a hypothetical case in which the fluorescent cell is assumed to be at a higher temperature than the absorption cell due to its proximity to the hot blackbody source. In this case we might expect the signal ratio to increase due to broadening of the fluorescent cell band and line widths relative to those in the absorption cell. The subroutines to calculate X_j and $\varphi(x,a)$ in the two cells were modified to account for

Table 3-2
DATA COMPARED AGAINST CALCULATIONS

FLUORESCENCE CELL			ABSORPTION CELL			SIGNAL RATIO								
CO ₂	Broadener	L _F	Length	Contents (Torr)		L _A	DATA	Process I		Process II		Process III		Data CASE
				CO ₂	Broadener			R _N	R _R	R _N	R _R	R _N	R _R	
2	0	2	2	0	0	1.5	.69±.03	.957	.899	.341	.354	.463	.466	1
0.5	21(A _R)*	2	5	16.5(A _R)		1.5	.37±.08	.941	.841	.158	.160	.231	.226	2
2	40(H _e)	2	2	40(H _e)		1.5	.63±.08	.981	.942	.460	.446	.550	.531	3
1	20(H _e)	2	1	20(H _e)		1.5	.71±.08	.986	.953	.441	.439	.544	.532	4
0.5	20(H _e)	2	0.5	20(H _e)		1.5	.79±.03	.993	.972	.437	.443	.547	.546	5
1	40(H _e)	2	5	0		1.5	.60±.07	.938	.843	.383	.386	.427	.423	6
1	0	2	1	0		1.5	.71±.04	.976	.936	.279	.298	.453	.455	7
7.5	0	2	7.5	0		1.5	.55±.05	.895	.815	.409	.39	.497	.481	8

*broadener specie indicated inside parenthesis

different cell temperatures and the modified program was run for fluorescent and absorption cell temperatures 373 and 296° K respectively. The modified program was run for data case No. 1 on Table 3-2 and the results are

DATA	SIGNAL RATIO						DATA CASE
	Process I		II		III		
	R_N	R_R	R_N	R_R	R_N	R_R	
R_M							
.37±.08	.962	.921	.318	.336	.471	.484	1

This run against data case 1 showed that the relatively hot fluorescent cell hypothesis would not explain the inconsistency that the measured signal ratios R_M are considerably larger than the predicted ratios R_R and R_N for process III. Based on these results runs against further data cases were not performed in order to reduce computer expense.

Spatial Diffusion Effect

We also tried an approximate approach to include diffusion to the walls. The approach was to modify $S_0(l)$ by multiplying it by the real part of the in phase solution of the time dependent diffusion equation.

$$\frac{\partial n}{\partial t} + kn = e^{i\omega t} + 1 + D \frac{\partial^2 n}{\partial l^2}$$

The real part of the in phase solution (see Kumer and James, DNA 4409F, HAES report No. 70 for terminology and definitions) is given by

$$n_{oR} = (k^2 + w^2)^{-1} \{k G_R + w G_I\}$$

where

$$G = G_R + i G_I = 1 - e^{A(l_F - L_F)} - e^{-Al_F}$$

$$A = A_R + i A_I$$

$$A_R = |A| \cos(\theta/2)$$

$$A_I = |A| \sin(\theta/2)$$

$$|A| = \sqrt{(k^2 + w^2)/D}$$

$$\theta = \tan^{-1}(w/k_v)$$

and where the boundary conditions

$$\lambda \frac{dn}{dl_F} = \alpha f \quad \text{at} \quad l_F = 0$$

$$\lambda \frac{dn}{dl_F} = \alpha f \quad \text{at} \quad l_F = L_F$$

$$\lambda = \sqrt{3} D/v_T \quad .$$

Here $D = .14 \text{ cm}^2 \text{ sec}^{-1}$ at 1 atm Argon partial pressure from Hirschfelder, Curtis and Bird (1954), and $\alpha \approx 0.7$ from Morse and Feschback (1953), and v_T is the molecular velocity at room temperature.

The approximation is to set $S_o \approx \eta_{oR} S_o$, normalization is automatically accounted for in forming the ratios R_R and R_N . Physically the diffusion "rounds off" the steep edge near $l_F = L_F$ in the integrands

$$S_o(l_F) T(|L_F - l_F|)$$

and

$$S(l_F) e_F(|L_F - l_F|)$$

which occur in the denominator of the ratios R_N and R_R , and which tend to reduce the calculated values of R_N and R_R .

The results for data cases 1 and 2 are

SIGNAL RATIO							DATA CASE
DATA	PROCESS I		PROCESS II		PROCESS III		
R_M	R_N	R_R	R_N	R_R	R_N	R_R	
.69±.03	.961	.906	.516	.563	.556	.580	1
.37±.08	.946	.841	.169	.180	.220	.226	2

We see that accounting for the effects of spatial diffusion also does not remove the inconsistency, this is particularly true for cases such as data case 2 where $[CO_2]_F$ is small (0.5 Torr) thus decreasing the steepness of the edge in ST near $l_F = L_F$.

Atmospheric Transmission Effect

We also considered the effects of transmission through the atmosphere external to the cells and the evacuated housings of the detector and the blackbody source.

The elements in Figure 3-17 are backed up against one another tightly enough so that the air paths that the $4.3 \mu m$ radiation traveled across were of the order 1 mm or less. The optical depth in a moderately strong line over this distance for a mixing ratio $X_{CO_2} = 3.2 \times 10^{-4}$ is $\approx .007$ so it is unlikely that this effect could impact the analysis.

3.2.4 Conclusions

The data R_M , the ratio of the fluorescent 4.3 μm signal when the absorption cell is filled to the signal when the absorption cell is evacuated, are larger than predicted values R_R or R_N , perhaps implying the existence of a significant contribution to the signal that is due to the direct fluorescence process (3-6) (or I). The predicted ratios are too small even when detailed radiation transport, wall reflectivity, temperature, diffusion, and atmospheric transmission are accounted for.

The implication that direct fluorescence is contributing significantly to the signal is in contradiction with the large values for the rate constant for process (3-4) that are reported in the literature (Finzi and Moore, 1975) and also in contradiction with our previous analysis (Kumer and James, DNA 4409F, HAES No. 70) of the variations in the signal as a function of blackbody source chopper frequency. Our current laboratory study utilizing the powerful 2.7 μm laser source has confirmed the rapid rate constant for process (3-4) and has also confirmed our previous analysis.

The body of evidence independent of the measurements of R_M which suggest that direct fluorescence does not contribute significantly to the 4.3 μm measurements in our initial blackbody experiments has become firm almost to the point of becoming conclusive. We believe the root of the inconsistency still may be traced to some subtle consideration in the analysis of the data R_M that we have overlooked, however, it is obvious we do not at present know what this consideration might be.

4.0 CONCLUSIONS AND RECOMMENDATIONS

4.1 The Laboratory Effort

In our initial effort to use the tunable 2.7 μm laser source to excite CO_2 fluorescence at 4.3 μm we have shown that the branching ratio for re-emission at 4.3 μm compared to re-emission at 2.7 μm is approximately equal to or greater than 10:1. The precision of this lower limiting measurement could be improved by the use of relatively simple techniques that were not in the scope of our initial effort, namely the use of (1) well documented techniques to improve the laser frequency stability, (2) the mounting of a 2.7 μm filter inside the detector dewar, (3) a multiple pass cell, and (4) the use of faster electronics for recording the 2.7 μm signal.

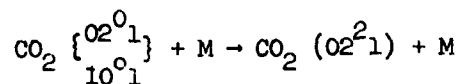
Steps to improve laser frequency stability are detailed by A. Hordvik and P. B. Sackett (Appl. Optics 13, 1060, 1974) and include (i) determination of an optimum OPO tilt angle to obtain uniform mode structure, (ii) the use of an etalon in the OPO cavity to isolate a single output mode, and (iii) the use of an externally controlled piezo-electric crystal to shift the OPO mode structure in either a ramped or a manually controlled way. Hordvik and Sackett describe how they achieved laser frequency stability better than $.001 \text{ cm}^{-3}$ near 2.3 μm for hours at a time with similar equipment. For our purpose we could improve signal/noise (S/N) by at least a factor 4 if we could use the methods of Hordvik and Sackett to improve our pulse to pulse frequency stability to within 0.002 cm^{-3} . Cold filtering at 2.7 μm could improve S/N by at least a factor 10, use of a multiple pass cell by at least a factor 5 and the use of fast, quiet electronics by at least a factor 2

and perhaps by as much as a factor 6. The increase in S/N that can be expected to be achieved by implementing these straightforward techniques then is 2 orders of magnitude or better.

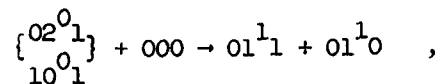
Additionally, the initial effort has demonstrated the applicability of the laser source and peripheral vacuum and electronics equipment for the high precision measurements of quenching and of vibration transfer rate coefficients. In this effort a precise argon quenching rate was determined as was a rate for rapid resonance vibration transfer between the naturally occurring isotopic species of CO_2 and N_2 .

Hence this work demonstrates the applicability of the technique for the measurement of the vibration transfer between N_2 and the important minor CO_2 isotopes 636 ($^{13}\text{C}^{16}\text{O}_2$), 628, and 627. This measurement directly impacts accurate prediction of the time dependence of nuclear induced CO_2 4.3 μm emission at altitudes < 90 km in the atmosphere. Use of a variably cooled fluorescence cell could permit vibration transfer measurements over a temperature range which includes realistic mesopause temperatures. The measurements could be made for all important isotopic species of CO_2 as well as for other species of interest such as NO , N_2O , and CO . It is not inconceivable that some adaptation of the equipment could be used to study quenching and vibration transfer for short lived species such as OH and NO^+ .

Improved laser frequency stability and acquisition of fast, quiet recording electronics will provide a nucleus for the equipment that is required for a laboratory study of the reactions



and



and to obtain the rate of rotational redistribution in CO_2 . The reaction rate measurements directly impact LWIR systems requirements and the measurements of rotational redistribution impact high altitude non-LTE nuclear infrared interference in general.

4.2 THE DATA EVALUATION EFFORT

Field Data Evaluation

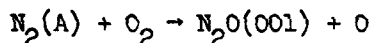
Our evaluation indicated that

a prompt auroral emission by either CO or N_2O can produce the altitude dependence of auroral zenith radiance data in the 4.5 to 4.6 μm band that were recorded by a rocket borne CVF spectrometer on 12 March 1975 provided that these species are abundant enough in the atmosphere to be optically thick below about 100 km for their vibrational resonance radiations near 4.6 and 4.5 μm respectively. Analysis of a spectral scan obtained at 100.6 km altitude weakly suggests that CO is the more likely candidate. Also, there appeared to be a feature in these data near 4.42 μm that was clearly not due to CO_2 , N_2O , or CO.

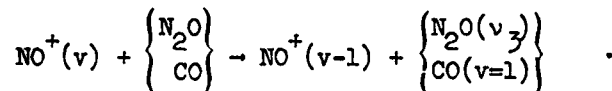
The requirement on optical thickness below 100 km is met by CO on the basis of independent ground based microwave data analyzed and reported by Waters et al (1976), on the other hand the large mixing ratio that is required to achieve appreciable optical depth below 100 km needs to be assumed to exist for N_2O . The required large mixing ratios above 85 km for N_2O and CO are found, necessarily, to be accompanied by large ambient lower altitude components of N_2O and CO radiance as the result of

excitation by collisions, absorption of earthshine, and vibration transfer from N_2^+ that has become excited by tapping the OH airglow via $OH(v) + N_2 \rightarrow OH(v-1) + N_2^+$. The large predicted ambient N_2O and CO radiances impose severe restraints on the number densities of N_2O and CO that could have actually existed on 12 March 1975. Analysis of a comprehensive amount of the 12 March 1975 CVF data is needed to quantify these restraints, however at this point we can say that major modifications in our assumed model for X_{N_2O} are called for. For CO the case, at this point, is not so clear cut.

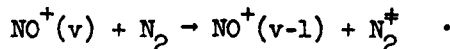
Also, it is somewhat of a puzzle as to what may be a prompt auroral mechanism for producing N_2O or CO emission, candidates are



and



The second mechanism is really very shakey since it must compete with



The vibration transfer process should be more rapid for the molecules N_2O and CO than for N_2 since N_2O and CO have permanent dipole moments while N_2 does not. The question is, can the transfer to N_2O and/or CO be 10^4 times faster than to N_2 so that N_2O and CO can receive a significant fraction of total NO^+ vibration that is available?

Finally, a question that cannot help but come to mind with regard to the series of features at 4.3, 4.42, and 4.6 μm , and some weaker ones which may also be present at longer wavelengths (but shortward of the NO feature); could these features be a temporary instrumental ringing phenomena that degraded the data on just a very short part of the flight, namely when the rocket was between 80 and 110 km altitude on the upleg?

An analysis of the 4.3 μm data was also performed in addition to the analysis of the 4.5 to 4.6 μm data. This analysis was necessary in order to determine the population of vibrationally excited N_2 so that the contribution to N_2O and CO radiance which results from vibration transfer from N_2 could be calculated. The 4.3 μm data proved consistent with our established model for this wavelength region. In particular a column vibration transfer rate of 0.09 ergs/cm² sec from OH(v) to N_2^+ and an efficiency of 16 N_2 vibrations produced per auroral ionization event was required to model the 4.3 μm data. These numbers are consistent with our understanding of other 4.3 μm data as described in our previous reports.

To better understand the 12 March 1975 data in the 4.4 to 4.7 μm region it will be necessary to (1) examine all the 12 March 1975 spectral scans to search for the existence, and if found, to determine the altitude dependence of ambient components of the CO and N_2O radiances in order to quantify the constraints these data place on the N_2O and CO mixing ratios, (2) examine data obtained in other experiments, such as HIRIS and SPIRE for example, in order to determine if the emissions of N_2O and/or CO are present in these data, and if so, to use these data to determine the abundance of N_2O and/or CO in the atmosphere, (3) examine the 12 March 1975

data in more detail in order to see if there is indeed a real feature present in these data near to $4.42 \mu\text{m}$, and finally (4) include emission by NO^+ into the spectral modeling of data in the 4 to $4.8 \mu\text{m}$ region.

Evaluation of Previous Laboratory Absorption Data

Absorption data obtained in our previous laboratory effort had appeared inconsistent with the chopper frequency dependence of data obtained in the same effort and with data reported by other authors. The analysis of this data however had been restricted by the scope of that effort. In this current effort we subjected these data to a more detailed analysis in an attempt to resolve the inconsistency. To this end we quantitatively examined the effects of detailed radiation transport, wall reflectivity, temperature differences between the fluorescence and absorption cell, spatial diffusion of excitation within the fluorescence cell, and finally, atmospheric absorption on exposed optical paths adjoining the system components.

Taken individually each of these effects nudged the interpretation of the absorption data towards consistency, however, the sum of the effects is still not sufficient to resolve the inconsistency. Additionally, the absorption measurements are also inconsistent with our most recent laboratory data obtained with the $2.7 \mu\text{m}$ laser source. We can only conclude that although we have tested every effect that was obvious to us, there is still some key effect, perhaps geometric, that needs to be accounted for to resolve the apparent inconsistency of the absorption data.

5.0 REFERENCES

- Banks, P. M. et al, UARS, NASA JPL Publication 78-54, 15 July 1978
- Bunker, R. P., "Forbidden Transitions in Homopolar Isotopically Unsymmetric Diatomic Molecules and the Dipole Moment of HD." J. Mol. Spectry 46, 119 (1973)
- Caledonia, George, "Proceedings of the HAES Infrared Data Review," Falmouth, Mass., June 1977, AFGL-OP-TM-05
- Condron, Tom, Private communication, 1977
- Finzi, J., and Moore, C. B., J. Chem. Phys. 63, 2285, 1975
- Gordiets, B. F., M. N. Markov and L. A. Shelepin, "Theoretical Study of Upper Atmosphere IR Radiation. Minor Component Concentration and Molecular Band Intensities." Optika i Spektroskopiia. Preprint No. 85, Moscow 1976 (Translated by Irving Kofsky, 1/14/77, for AFGL Research Library, Hancom AFB, MA 01731)
- Hirschfelder, J. O., C. F. Curtiss and R. B. Bird, "Molecular Theory of Gases and Liquids", John Wiley & Sons, New York (1954)
- Hordvik, A. and P. B. Sackett, "Characteristics of the Optical Parametric Oscillator and Its Use for Selective Excitation", Appl. Optics 13, 1060, 1974
- James, T. C., Final Report on Contract DNA001-76-C-0017, HAES Report No. 60, DNA 4238F, 1977
- James, T. C., and J. B. Kumer, J. Geophys. Res., 78, 8320, 1973a
- James, T. C., and J. B. Kumer, Proceedings of the DNA High Altitude Nuclear Phenomenology and Chemistry Meeting, April 1973, San Diego, CA, 1973b.
- Kumer, J. B., Further Evaluation of Icecap Auroral 4.3 μ m Zenith Radiance, Final Report on Contract DNA001-76-C-0015, HAES Rep. 57, Def. Nucl. Agency, Washington, D. C., 1976

- Kumer, J. B., Theory of the CO₂ 4.3μm Aurora and Related Phenomena, J. Geophys. Res., 82, 2203, 1977a
- Kumer, J. B., Atmospheric CO₂ and N₂ Vibrational Temperatures at 40- to 140-km Altitude, J. Geophys. Res., 82, 2195, 1977b
- Kumer, J. B., Proceedings of the HAES Infrared Data Review, Falmouth, Mass., June 1977c, AFGL-OP-TM-05
- Kumer, J. B., and T. C. James, CO₂(001) and N₂ Vibrational Temperatures in the 50 ξ z ξ 130 km Altitude Range, J. Geophys. Res., 79, 638, 1974
- Kumer, J. B., and T. C. James, "Atmospheric CO₂ Infrared Background Investigation. Experimental Confirmation of 4.3μm Fluorescence; Modeling 4.3μm Spectral Structure", DNA 4409F, HAES Report No. 70, 1977
- Kumer, J. B., A. T. Stair, Jr., N. B. Wheeler, K. D. Baker and D. J. Baker, "Evidence for an OH^{±YV} N₂^{±YV} CO₂(V₃) → CO₂ + hν(4.3μm) Mechanism for 4.3 μm Airglow", J. Geophys. Res., 83, 4343, 1978
- Margottin-Maclou, M., L. Doyenette, and L. Henry, Appl. Optics, 10, 1968 (1971)
- Mitchell, Herb, Proceedings of the HAES Infrared Data Review, Falmouth, Mass., June 1977, AFGL-OP-TM-05
- Nadile, R. M., A. T. Stair, Jr., Ned Wheeler, C. L. Wyatt, D. J. Backer and W. F. Grieder, "SPIRE-Spectral Infrared Rocket Experiment (Preliminary Results," presented at the Sixth DARPA sponsored Strategic Space Symposium, SRI, Menlo Park, CA, 14-16 March, 1978
- Sears, R. D., Private Communication, 1976

Sharma, R.D., Private Communication, 1979

Stair, A. T., Jr., Private Communications, 1977a

Stair, A. T., Jr., "Proceedings of the HAES Infrared Data Review, Falmouth, Mass., June 1977b, AFGL-OP-IM-05

Taylor, R. L., "Energy Transfer Processes in the Stratosphere," Can. J. Chem. 52, 1436, 1974

Trinks, J., Offerman, D., and Von Zahn, U., EOS, 58, 455, 1977

Waters, J. W., W. J. Wilson, and F. I. Shimabukuro, "Microwave Measurement of Mesospheric Carbon Monoxide"; Science 191, 1134, 1976

Wheeler, N. B., A. T. Stair, Jr., G. Frodsham, and D. J. Baker, Rocket Borne Spectral Measurements of Atmospheric Infrared Emissions During Quiet Conditions in the Auroral Zone, Rep. AFGL-TR-76-0252, HAES Rep. 32, Air Force Geophys. Lab., Hanscom Air Force Base, Mass., 1976

DISTRIBUTION LIST

DEPARTMENT OF DEFENSE

Assistant to the Secretary of Defense
Atomic Energy
ATTN: Executive Assistant

Defense Advanced Rsch. Proj. Agency
ATTN: TIO

Defense Nuclear Agency
ATTN: RAAE, P. Lunn
ATTN: RAAE, W. McKechney
ATTN: RAAE, H. Fitz, Jr.
4 cy ATTN: TITL

Defense Technical Information Center
12 cy ATTN: DD

Field Command
Defense Nuclear Agency
ATTN: FCPR

Field Command
Defense Nuclear Agency
Livermore Division
ATTN: FCPRL

Undersecretary of Defense for Rsch. & Engrg.
ATTN: Strategic & Space Systems (OS)

DEPARTMENT OF THE ARMY

Atmospheric Sciences Laboratory
U.S. Army Electronics R&D Command
3 cy ATTN: DELAS-EO, F. Niles

BMD Advanced Technology Center
Department of the Army
ATTN: ATC-T, M. Capps

Harry Diamond Laboratories
Department of the Army
ATTN: DELHD-N-P

DEPARTMENT OF THE NAVY

Naval Research Laboratory
ATTN: Code 6709, W. Aii
ATTN: Code 6780, S. Ossakow
ATTN: Code 2627

Naval Surface Weapons Center
ATTN: Code F31

DEPARTMENT OF THE AIR FORCE

Air Force Geophysics Laboratory
2 cy ATTN: LKD, R. Narcisi
2 cy ATTN: LKB, K. Champion
2 cy ATTN: OPR, R. Murphy
2 cy ATTN: LKO, R. Huffman
2 cy ATTN: OPR, J. Kennealy
4 cy ATTN: OPR, A. Stair

Air Force Weapons Laboratory
Air Force Systems Command
ATTN: SUL

DEPARTMENT OF THE AIR FORCE (Continued)

Headquarters Space Division
Air Force Systems Command
ATTN: SZJ, L. Doan

OTHER GOVERNMENT AGENCIES

Department of Commerce
National Bureau of Standards
ATTN: A. Phelps

Department of Commerce
National Oceanic & Atmospheric Admin.
3 cy ATTN: F. Fehsenfeld

DEPARTMENT OF DEFENSE CONTRACTORS

Aerodyne Research, Inc.
ATTN: F. Bien

Concord Sciences
ATTN: E. Sutton

University of Denver, Colorado Seminary
ATTN: D. Murcray

General Electric Co.
ATTN: M. Bortner

General Electric Company—TEMPO
ATTN: T. Stevens
ATTN: W. Knapp
5 cy ATTN: DASIAC

General Research Corp.
ATTN: J. Ise, Jr.

Lockheed Missiles & Space Co., Inc.
ATTN: R. Sears
ATTN: B. McCormac
ATTN: T. James
ATTN: J. Kumer
ATTN: M. Walt

University of Lowell
ATTN: G. Best

University of Minnesota
ATTN: J. Winkler

Mission Research Corp.
ATTN: D. Archer
ATTN: D. Sappenfield
ATTN: M. Scheib

Photometrics, Inc.
ATTN: I. Kofsky

Physical Sciences, Inc.
ATTN: G. Caledonia

University of Pittsburgh
ATTN: F. Kaufman

R & D Associates
ATTN: H. Mitchell

DEPARTMENT OF DEFENSE CONTRACTORS (Continued)

R & D Associates

ATTN: C. MacDonald
ATTN: F. Gilmore

Science Applications, Inc.

ATTN: D. Hamlin

Stewart Radiance Laboratory

ATTN: R. Huppi
ATTN: J. Ulwich

Technology International Corp.

ATTN: W. Boquist

DEPARTMENT OF DEFENSE CONTRACTORS (Continued)

Utah State University

ATTN: Security Office for D. Burt
3 cy ATTN: Security Office for D. Baker
3 cy ATTN: Security Office for K. Baker

Visidyne, Inc.

ATTN: C. Humphrey
ATTN: J. Carpenter
ATTN: W. Reidy
ATTN: H. Smith
ATTN: T. Degges